Towards improving the single grain clinopyroxene geobarometer for garnet peridotites

By

Connor Gregory Elzinga

A thesis submitted in partial fulfillment of the requirements for the degree of

Master of Science

Department of Earth and Atmospheric Sciences

University of Alberta

© Connor Gregory Elzinga, 2023

Abstract

Exploration methods for diamonds often employ the geochemistry of single minerals to identify deposits. Due to the scarcity of diamonds, exploration practices use minerals known as "kimberlite indicator minerals" as these minerals are typically more abundant than diamond and may have equilibrated under conditions where diamond may have been stable. One of these minerals is clinopyroxene from garnet lherzolites, because garnet lherzolites are stable in the diamond stability field. There are multiple published discrimination methods to identify clinopyroxenes from garnet lherzolites such as Ramsay (1992), Nimis (1998), Morris et al. (2002) and Grütter (2009). After applying these discrimination methods to identify garnet lherzolite clinopyroxene, the chemistry of clinopyroxenes can be used with geothermobarometers to calculate pressure and temperature estimates for mantle xenoliths or xenocrysts and thereby identify potentially diamond-bearing kimberlite deposits.

Using published major-element compositions of 678 clinopyroxenes from garnet lherzolites, these clinopyroxene discrimination methods were found to accurately identify clinopyroxenes from garnet lherzolites. Trends between cations were also observed in clinopyroxene. Specifically, with the cations Na and Al+Cr having an approximate 1:1 ratio, suggesting that Na, Al and Cr are substituting dominantly as jadeite ($NaAlSi_2O_6$) and kosmochlor ($NaCrSi_2O_6$) in garnet lherzolite clinopyroxene. Elemental cations are also compared with the calculated pressure and temperature from multiple geothermobarometers with specific focus on the clinopyroxene geothermobarometers. Na, Al and Cr cations were all found to decrease with increasing pressure. Mg and Fe were found to increase with increasing temperature while Ca decreased with increasing temperature.

These natural clinopyroxene samples were compared with clinopyroxenes from high P-T experiments on garnet lherzolites. The experimental clinopyroxenes were noticeably richer in Al and poorer in Na and Cr than natural clinopyroxenes. The differences between natural and experimental clinopyroxenes, specifically with Al, Cr and Na shows a disconnect between the experimental and natural garnet lherzolite clinopyroxenes. The richer Al in experimental samples suggests a higher tschermak component than in the natural clinopyroxenes.

Using the program THERMOCALC, garnet lherzolites were modelled at specific bulk compositions to compare modelled clinopyroxenes to natural clinopyroxenes. The modelled clinopyroxenes, in the garnet lherzolite stability field, did not match well with natural garnet lherzolites as the modelled clinopyroxenes failed garnet lherzolite clinopyroxene discrimination plots. However, the cation trends against pressure and temperature appeared to follow the trends seen in natural samples. Using compositions calculated along geotherms, clinopyroxene appeared more like natural samples based on garnet lherzolite clinopyroxene discrimination methods and followed the cation trends seen in natural samples except for Al cations.

Finally, an updated single-grain clinopyroxene geobarometer was calibrated from natural garnet lherzolites by modifying the Nimis and Taylor (2000) barometer. This barometer was calibrated using the calculated temperature of Taylor's (1998) two pyroxene thermometer and the calculated pressure of the Nickel and Green (1985) barometer, with Al calculated after Carswell and Gibb (1987) (the recommend thermometer and barometer of Nimis and Grütter 2010). Through multiple linear regression an expression was developed to calculate P (kbar) as a function of T(K), $Cr/(Cr+Al_{M1})$, Cr/Al, Cr+Al-0.86(Na+K) and Ca/(Ca+Mg+Fe) in clinopyroxene. The expression is:

$$P(kbar) = 1239.28 - 0.0076 \cdot T(K) \cdot \ln(Cr/(Cr+Al_{M1})) + 9.2988 \cdot \ln(Cr/Al) + 0.2056 \cdot T(K) - 0.0051 \cdot T(K) \cdot \ln(Cr+Al-0.86(Na+K)) - 201.2262 \cdot \ln(T(K)) + 56.8249 \cdot \ln(Ca/(Ca+Mg+Fe))$$

With Al_{M1} calculated as:

$$Al_{M1} = Al - 0.5(Al + Cr + 2Ti - Na - K)$$

Application of this updated barometer was applied to xenoliths from four localities. These localities are Chidliak kimberlite field, Diavik-Ekati kimberlites, Finsch diamond mine and Jagersfontein diamond mine. The updated barometer performs well as pressures calculated from xenoliths from the four localities using the updated barometer are in good agreement with the Nickel and Green (1985) barometer, with Al calculated after Carswell and Gibb (1987).

Preface

This thesis is an original work by Connor Elzinga. No part of this thesis has been previously published.

Acknowledgements

I would firstly like to thank my supervisor Bob Luth for being an exceptional mentor during my graduate studies. Bob met with me weekly to answer my questions, was always available when I needed advice or for general day to day chats. Bob greatly supported my career opportunities every summer and I'm tremendously grateful for the opportunities he allowed me to take part in

I am grateful to my committee members Bob Luth, Graham Pearson and Thomas Stachel. Your comments and insight have helped improved this final product and will aid in any future publications from this research.

This project was funded through the DERTS program at the University of Alberta and NSERC Discovery grants from Bob Luth.

My time at the University of Alberta was immensely enjoyable thanks to the friendships and experiences I made. Finally, thank you to my family and Joan for supporting me from start to finish.

Table of Contents

List of Tables

List of Figures

List of abbreviations and symbols

~	Approximately
a_{CrTs}	Activity of CaCr-Tschermak ($Ca^{M2}Cr^{M1}Al^{T}Si^{T}O_6$) component in clinopyroxene
Al_{M1}	M1 site aluminum
Alm	Almandine ($Fe_3Al_2Si_3O_{12}$)
Andr	Andradite ($Ca_3Fe_2Si_3O_{12}$)
Al_T	Tetrahedral site aluminum
apfu	Atoms per formula unit
°C	Degrees Celsius
Ca#	Molar calcium number, $Ca/(Ca+Mg+Fe^{2+})$
Cats	Ca-tschermaks ($CaAl_2SiO_6$)
Cbuf	Ca-buffonite ($CaMg_{1/2}Ti_{1/2}AlSiO_6$)
Cen	Clinoenstatite ($Mg_2Si_2O_6$)
Cess	Ca-esseneite ($CaFeAlSiO_6$)
CFMAS	$CaO-FeO-MgO-Al_2O_3-SiO_2$
Cfm	($FeMgSi_2O_6$)
Cfs	clinoferrosilite ($Fe_2Si_2O_6$)
CMS	$CaO-MgO-SiO_2$
CMAS	$CaO-MgO-Al_2O_3-SiO_2$
CMAS-Cr	$CaO-MgO-Al_2O_3-SiO_2-Cr_2O_3$
Cpx	Clinopyroxene
Cr#	Molar chromium number, Cr/(Cr+Al)
Crdi	Cr-diopside ($CaCrAlSiO_6$)

Cren	Cr-enstatite ($MgCrAlSiO_6$)
Di	Diopside ($CaMgSi_2O_6$)
En	Enstatite ($Mg_2Si_2O_6$)
e.g.	For example
Fa	Fayalite (Fe_2SiO_4)
Fm	($FeMgSi_2O_6$)
FMAS	FeO-MgO-Al_2O_3-SiO_2
Fo	Forsterite (Mg_2SiO_4)
Fs	Ferrosilite ($Fe_2Si_2O_6$)
f_{O_2}	Oxygen fugacity
Grt	Garnet
Gr	Grossular ($Ca_3Al_2Si_3O_{12}$)
Gpa	Gigapascals
Hd	Hedenbergite ($CaFeSi_2O_6$)
i.e.	that is
Jd	Jadeite ($NaAlSi_2O_6$)
K	Kelvin
Kbar	kilobar
Kjd	K-jadeite ($KAlSi_2O_6$)
KNCFMASHTOCr	K_2O–Na_2O–CaO–FeO–MgO–Al_2O_3–SiO_2–H_2O–TiO_2–Fe_2O_3–Cr_2O_3
Knr	Knorringite ($Mg_3Cr_2Si_3O_{12}$)
Kos	Kosmochlor ($NaCrSi_2O_6$)
Mg#	Molar magnesium number Mg/(Mg+Fe)

Mess	Mg-esseneite ($MgFeAlSiO_6$)
Mgts	Mg-tschermak ($MgAl_2SiO_6$)
Mo	Monticellite ($CaMgSiO_4$)
NCMAS	Na_2O-CaO-MgO-Al_2O_3-SiO_2
NCMAS-Cr	Na_2O-CaO-MgO-Al_2O_3-SiO_2
NCFMASOCr	Na_2O–CaO–FeO–MgO–Al_2O_3–SiO_2–Fe_2O_3–Cr_2O_3
Obuf	Ortho-buffonite ($Mg(Mg_{1/2}Ti_{1/2})AlSiO_6$)
Ocfm	Ordered cfm ($MgFeSiO_4$)
Odi	Ortho-diopside ($CaMgSi_2O_6$)
Ojd	Ortho-jadeite ($NaAlSi_2O_6$ component in orthopyroxene)
Opx	Orthopyroxene
P	Pressure
P_{calc}	Calculated Pressure
P_{exp}	Experimental Pressure
P-T	Pressure-Temperature
Py	Pyrope ($Mg_3Al_2Si_3O_{12}$)
Spl	Spinel
T	Temperature
Tig	Ti endmember garnet ($Mg_{3.5}AlTi_{0.5}Si_3O_{12}$)
Uv	Uvarovite ($Ca_3Cr_2Si_3O_{12}$)
WDS	Wavelength dispersive spectroscopy
Wo	Wollastonite ($CaSiO_3$)
wt%	Weight percent

Chapter 1 Introduction and Background

1.1 Introduction

Thermobarometry of garnet-bearing ultramafic rocks has provided valuable information on the nature, depth, and evolution of mantle xenoliths and high-grade metamorphic rocks. Since the pioneering work of Boyd (1973), mineral chemistry has been used to give estimates of pressure and temperature of equilibrium. Boyd (1973) developed a pyroxene geotherm using ultramafic rocks containing the assemblage enstatite + diopside + garnet. The thermometer was developed using an enstatite-in-diopside thermometer because the solid solution is sensitive to temperature in the range 900-1400 °C and is relatively insensitive to pressure. The barometer was developed using an Al-in-enstatite barometer based on the aluminum exchange between orthopyroxene and garnet. Since Boyd's work a large number of geothermobarometers have been developed, tested, and implemented (e.g. O' Neill and Wood 1979, Harley 1984, Nickel and Green 1985, Krogh 1988, Brey and Köhler 1990, Taylor 1998, Nimis and Taylor 2000, Brey et al. 2008, Nimis and Grütter 2010, Sudholz et al 2021). At present, the most widely used geothermometers for peridotites are based on Ca-Mg equilibria between clinopyroxene and orthopyroxene, and Mg-Fe equilibria between garnet and olivine, orthopyroxene or clinopyroxene (Nimis and Grütter 2010). One of the most widely used suites of geothermobarometers is that of Brey and Köhler (1990), which has become a de facto standard in mantle xenolith studies (Nimis and Grütter 2010). Brey and Köhler (1990) considered elemental exchange between minerals in four-phase peridotites (olivine, clinopyroxene, orthopyroxene and garnet) with the enstatite exchange between orthopyroxene and clinopyroxene the most widely used. The two pyroxene thermometer formulation was calibrated on experiments in synthetic and natural systems. They also calibrated an alternative geothermometer, the Ca-in-orthopyroxene thermometer, which uses the diopside

component in orthopyroxene to calculate the equilibrium temperature. Additionally, Brey and Köhler (1990) provided an update to the geobarometer based on Al-exchange between orthopyroxene and garnet.

Nimis and Grütter (2010) provide a comprehensive evaluation of extant geothermometers and geobarometers applicable to garnet peridotites, particularly those from diamond-stable depths. Nimis and Grütter (2010) recommended the geothermometer of Taylor (1998), which is based on the enstatite exchange between orthopyroxene and clinopyroxene with a formulation incorporating corrections for the minor elements Na, Ti, and Fe (Nimis and Grütter 2010). The recommended geobarometer of Nimis and Grütter (2010) is that of Al-in-orthopyroxene of Nickel and Green (1985) based on Al-exchange between orthopyroxene and garnet.

Constraining the pressure and temperature conditions sampled by kimberlite magmas is fundamental for both academic and exploration purposes. In many cases, the samples available are xenocrysts (single minerals) rather than xenoliths that may contain multiple minerals amenable to use for geothermometry and geobarometry. Exploiting the mineral chemistry of single mineral grains to constrain the P-T of their origin is required to use these xenocryst populations for either academic or exploration purposes.

Therefore, considerable effort has been directed at developing single-mineral geothermometers and geobarometers such as the single-grain clinopyroxene geothermobarometer. The single-grain clinopyroxene thermometer and barometer of Nimis and Taylor (2000) are widely used in diamond exploration and mantle xenolith and xenocryst studies (Grütter 2009). Clinopyroxene is a common kimberlite indicator mineral occurring as xenocrysts. Constraining the P,T of origin of such xenocrysts can provide insight into the thickness and thermal evolution of the lithospheric mantle (e.g Read et al. 2004, Grütter 2009) as well.

1.2 Existing Single Grain Clinopyroxene Geothermobarometers for Mantle Conditions

Nimis and Taylor (2000) calibrated a Cr-in-clinopyroxene barometer and an enstatite-in-clinopyroxene thermometer using experimental clinopyroxenes synthesized at 850-1500 °C and 0-60 kbar in the CMS and CMAS-Cr systems and complex, natural, lherzolitic systems. This geothermobarometer's initial development began with Nimis (1998), with a barometer based on the exchange of aluminum between garnet and clinopyroxene as expressed by the reaction 2/3 $Ca_3Al_2Si_3O_{12}$ (grossular) + 1/3 $Mg_3Al_2Si_3O_{12}$ (pyrope) = $CaMgSi_2O_6$ (diopside) + $CaAl_2SiO_6$ (Ca-Tschermak) and a thermometer based on enstatite-in-clinopyroxene ($CaMgSi_2O_6$ (clinopyroxene) + $Mg_2Si_2O_6$ (orthopyroxene) = $Mg_2Si_2O_6$ (clinopyroxene) + $CaMgSi_2O_6$ (orthopyroxene)). The Al-exchange barometer is strongly pressure-sensitive because of a large, positive molar volume change with the reaction written as above. The reaction gives rise to less aluminous clinopyroxenes as pressure increases (Nimis 1998). The enstatite-in-clinopyroxene thermometer is based on the two-pyroxene geothermometer as discussed earlier. Nimis (1998) found the elemental combination that is the most sensitive to pressure variations was a plot of Ca vs. Al content after compositional filtering for garnet peridotite clinopyroxenes, where the Ca content is negatively correlated with temperature and the Al content is negatively correlated with pressure. These Ca and Al plots are useful for distinguishing between high and low pressure clinopyroxenes and therefore can be used to separate graphite- and diamond-facies clinopyroxenes (Nimis 1998).

Nimis and Taylor (2000) built upon the geothermobarometer of Nimis (1998) by modifying the barometer to consider Cr-exchange between garnet and diopside ($CaMgSi_2O_6$ (diopside) + $CaCrAlSiO_6$ (CaCr-Tschermak) = 1/2 $(Ca_2Mg)Cr_2Si_3O_{12}$ ($uvarovite_2knorringite_1$) + 1/2

(Ca_2Mg)$Al_2Si_3O_{12}$ ($grossular_2pyrope_1$)[1]). This reaction differed from the Nimis (1998) barometer, which was based on Al-exchange between clinopyroxene and garnet. The geobarometric expression developed (equation 9 of Nimis and Taylor 2000) uses temperature (K), a term they define as the activity of CaCr-Tschermak (a_{CrTs} = Cr – 0.81Cr#(Na+K)) in clinopyroxene and the Cr# (Cr/(Cr+Al)) of clinopyroxene to calculate the pressure in kbar. The temperature dependency of the geobarometer is reasonably low and ranges from 1.2-2.4 kbar/50 °C (dependant on composition) and only four chemical parameters (Cr, Al, Na, and K) need to be analyzed to obtain pressure estimates. The Cr-in-clinopyroxene barometer tends to underestimate pressures above 50 kbar, such that the barometer fails in many high pressure and temperature samples (Nimis 2002). Their formulation has no explicit dependence on either the Ca content of the clinopyroxene or the composition of the coexisting garnet.

The geothermometer of Nimis and Taylor (2000) is based on the Ca-Mg exchange between clinopyroxene and orthopyroxene. The geothermometer developed uses the enstatite activity in clinopyroxene and has corrections for minor components Fe, Ti, Al, and Cr (equation 17 of Nimis and Taylor 2000). The single grain clinopyroxene thermometer yields similar estimates to the Taylor (1998) thermometer as both thermometers use similar expressions for the enstatite activity in clinopyroxene and similar corrections for minor components (Nimis and Grütter 2010).

Nimis et al. (2020) provided an empirical correction to the Nimis and Taylor (2000) geobarometer to correct the high-pressure underestimation. An empirical correction was calculated by comparing the pressures calculated with the Nimis and Taylor (2000) barometer

[1] The barometer uses Cr partitioning between clinopyroxene and garnet and the chemical formula is expressed this way to maintain elemental balance. The reaction for this barometer can be traced back to the classic Al partitioning between orthopyroxene and garnet that is written $MgAl_2SiO_6 + Mg_2Si_2O_6 = Mg_3Al_2Si_3O_{12}$

and those from the Nickel and Green (1985) barometer (as modified by Carswell 1991) for clinopyroxene-orthopyroxene-garnet bearing mantle xenoliths. Both barometers were calculated using the Taylor (1998) thermometer with pressure and temperature calculated by iteration. The correction was determined on a second-polynomial fit through the xenolith data. The formula for the correction is:

$$P_{Correction} = 0.05024P_{NT}^2 + 0.7633P_{NT} + 0.1257$$

The correction improves the consistency between the Nimis and Taylor (2000) and Nickel and Green (1985) (as modified by Carswell 1991), barometers in mantle xenoliths (Nimis et al. 2020). This correction was described as a "band aid measure" by Nimis et al. (2020) in the absence of new experimental data.

An experimental recalibration of the Cr-in-clinopyroxene geobarometer was undertaken by Sudholz et al. (2021) where they performed 29 experiments between 3-7 GPa and 1100-1400 °C. They re-examined the exchange reaction over an extended pressure, temperature, and compositional range relative to Nimis and Taylor (2000) to attempt to improve the performance of the barometer at high pressure. Sudholz et al. (2021) developed a new geobarometric expression (equation 5 of Sudholz et al. 2021) based on Cr-exchange between garnet and diopside (same reaction exchange as Nimis and Taylor 2000), using the same variables as Nimis and Taylor (2000) which are temperature (K), CaCr-Tschermak activity (a_{CrTs}) in clinopyroxene and Cr# (Cr/(Cr + Al)).

1.3 Mantle Clinopyroxene Compositional Filtering and Error Sources

The application of the single grain clinopyroxene thermobarometer requires careful compositional filtering, as well as evaluation of analytical errors and associated temperature and

pressure estimation errors. Filtering attempts to ensure that clinopyroxenes are from garnet lherzolites, essentially because of the implicit requirements that the clinopyroxenes be in equilibrium with both garnet and orthopyroxene for Nimis and Taylor's (2000) thermobarometer. Nimis (1998) and Nimis and Taylor (2000) used Ramsay's (1992) Cr_2O_3 vs. Al_2O_3 classification diagram (following methods of Ramsay and Tompkins 1994) (Figure 1.1) to separate clinopyroxenes from garnet lherzolites, spinel lherzolites, eclogites and megacrysts. Nimis (1998) found more than 90% of clinopyroxenes from garnet peridotite xenoliths plot within Ramsay's (1992) garnet peridotite field. Nimis (1998) and Nimis and Taylor (2000) also applied an Al_2O_3 vs. MgO diagram to clinopyroxenes that plotted in the Cr_2O_3 vs. Al_2O_3 garnet peridotite field in the Ramsay diagram, to separate clinopyroxenes from garnet peridotites and low Al_2O_3, low MgO, metasomatized, garnet-free peridotites (Figure 1. 2). Nimis and Taylor (2000) also applied a quality-control filter, restricting the analyses to cation sums > 3.98 and < 4.02 on a six-oxygen basis. Finally, they further restricted the compositional range of clinopyroxenes to less than 5 wt% Cr_2O_3 and $a_{CrTs} \geq 0.003$.

Grütter (2009) endorsed and refined the filtering process of Nimis and Taylor (2000). His filters include:

1) The Cr_2O_3 vs. Al_2O_3 garnet peridotite field of Ramsay and Tompkins (1994)

2) The Cr_2O_3 vs. Al_2O_3 diagram can be supplemented by a plot of Na+K vs. Cr+Al to assess the tschermak vs jadeite/kosmochlor component of clinopyroxene

3) Reject low Al clinopyroxenes using the Al_2O_3 vs. MgO diagram of Nimis (1998)

4) Cation sums > 3.96 and < 4.04 on a six-oxygen basis, this is less restrictive than the Nimis and Taylor (2000) sums of > 3.98 and < 4.02

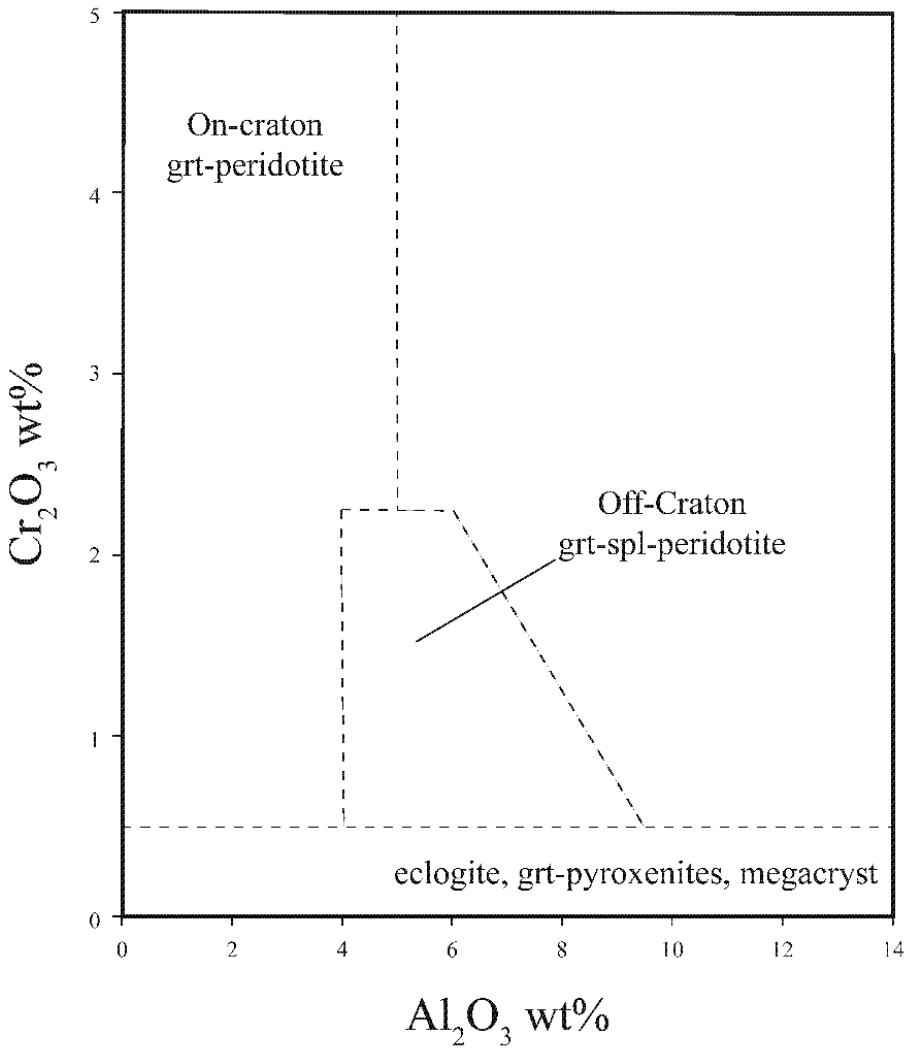

Figure 1.1 Al_2O_3 vs Cr_2O_3 classification diagram of Ramsay (1992) for distinguishing mantle clinopyroxene sources

5) Cr_2O_3 less than 5 wt%, matching Nimis and Taylor (2000)

6) Cr# ranging from 0.06 to 0.50

7) $a_{CrTs} \geq 0.003$ matching Nimis and Taylor's (2000) filter.

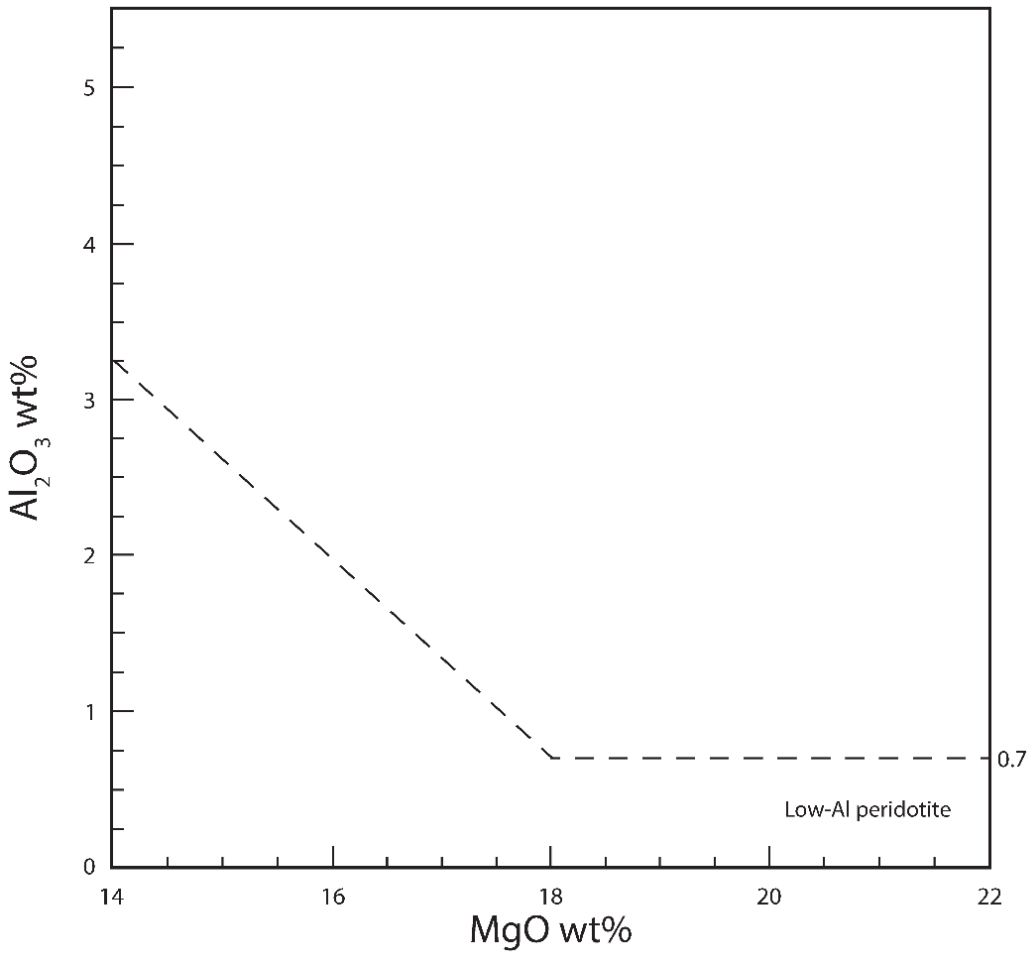

Figure 1.2 MgO vs Al_2O_3 for discriminating chromian diopsides from garnet-free peridotites that are unusually low in Al (modified after Nimis 1998). Used with clinopyroxenes that plot in Ramsay's (1992) On-craton garnet-peridotite field. The upper field identifies clinopyroxenes from garnet peridotites and the lower field identifies clinopyroxenes from garnet-free peridotites

Ziberna et al. (2016) proposed partially revised compositional filters based on decreased reliability of the single grain clinopyroxene thermobarometer for particular compositions and various sources of error. They found that compositions characterized by low CaCr-Tschermak activity values decreased the reliability of the Cr-in-clinopyroxene barometer.

Ziberna et al. (2016) filters include:

1) Total cations ranging > 3.98 and < 4.02 on a six-oxygen basis, matching the filter used by Nimis and Taylor (2000)

2) Grains must plot within the Cr_2O_3 vs. Al_2O_3 garnet peridotite field of Ramsay and Tompkins (1994)

3) Plot grains within the high-Al field of Nimis' (1998) Al_2O_3 vs. MgO diagram

4) Cr# compositions in the range 0.10-0.65. Cr# values in the range of 0.50-0.65 should be used with caution. This differs from Grütter's (2009) Cr# range of 0.06 to 0.50.

5) Recognize compositions sensitive to analytical uncertainties using a_{CrTs}/Cr# > x where x is a function of analytical conditions. This replaces the filter $a_{CrTs} \geq 0.003$ of Nimis and Taylor (2000) and Grütter (2009). If a_{CrTs}/Cr# ≤ 0.011 the clinopyroxenes should be discarded, if $0.011 < a_{CrTs}$/Cr# ≤ 0.024 high-quality analyses are recommended, values above 0.024 can be used safely. The range for a_{CrTs}/Cr# in experiments used by Nimis and Taylor (2000) was 0.016-0.393, values larger or smaller than experimental compositions will lie outside the calibration range

6) Verify equilibrium with orthopyroxene. This verification cannot be obtained with simple compositional filters. Generally, Ca/(Ca+Mg) > 0.5 should be considered suspicious as a very small proportion of orthopyroxene saturated clinopyroxenes are above this value. In addition, a very low temperature estimate from the enstatite-in-clinopyroxene thermometer (< 600 °C) would also be a strong indication the clinopyroxene was not in equilibrium with orthopyroxene.

Although the single grain clinopyroxene thermobarometer is an extremely useful and widely used geothermobarometer, there are still associated uncertainties. The enstatite-in-clinopyroxene thermometer has been proven to be an excellent geothermometer when compared with other geothermometers (as discussed before) (Nimis and Grütter 2010) and significant errors are only

expected at low temperature (< 900 °C) in response to large (relative) errors in CaO, SiO_2 and Na_2O measurements (Nimis 2002).

The Cr-in-clinopyroxene barometer of Nimis and Taylor (2000) suffers from underestimation at high pressure and temperature conditions, as the barometer tends to underestimate at equilibrium pressures above 50 kbar (Nimis 2002). The most compelling evidence for errors in the pressure estimates are the discrepancies between the single-grain clinopyroxene and the orthopyroxene-garnet barometers on xenolith samples. The differences can be very large for clinopyroxenes with low values of a_{CrTs}, one of the main variables in the barometer (Ziberna et al. 2016). Ziberna et al. (2016) found the decreased precision in the Cr-in-clinopyroxene barometer for clinopyroxenes with low a_{CrTs} values is related to propagation of analytical errors. These analytical errors increase with decreasing beam current and counting times and the propagated pressure uncertainties are negatively correlated with the clinopyroxene a_{CrTs} and positively correlated with clinopyroxene Cr#. The analytical errors on Al, Cr and Na are specifically focused on, as they are used to calculate a_{CrTs} (equation 7 of Nimis and Taylor 2000). The analytical conditions are used to calculate the analytical errors on Al, Cr and Na to calculate pressure uncertainties through error propagation (Ziberna et al. 2016). Ziberna et al. (2016) suggest using high-quality analyses for reducing analytical errors on Al, Cr and Na, which decreases propagated errors.

Sudholz et al. (2021) attempted to correct the underestimation of Nimis and Taylor's (2000) barometer by recalibrating the Cr-in-clinopyroxene geobarometer as discussed earlier. They filtered major and minor elemental data according to the protocol of Ziberna et al. (2016). Both analytical and experimental uncertainties are propagated by Sudholz et al. (2021) to accurately describe uncertainties on estimated pressure.

This previously discussed propagation of uncertainties results in P-T estimation uncertainties, and this effects geotherm estimations. Mather et al. (2011) compared the Nimis and Taylor (2000) geothermobarometer using clinopyroxene xenocrysts to multimineral geothermobarometers using garnet lherzolites. Mather et al. (2011) discusses errors in P-T estimation on these geothermobarometers from uncertainties on electron microprobe analyses such as counting statistics, instrumental drift, and noise and the effects on estimating palaeogeotherms. These are considered external errors and average uncertainties from these external errors are used to calculate a range of mineral compositions from an average value. This range of mineral compositions gives modified mineral compositions which are used to calculate P-T (Mather et al. 2011). Mather et al. (2011) varied oxide composition up or down by 1, 1.5 and 2 standard deviations away from the mean composition and created a range of mineral compositions which in turn create different P-T results and palaeogeotherms for each range of mineral compositions.

1.4 Objectives

The objectives of this thesis are summarised as follows:

i. The compilation of mantle clinopyroxene geochemical data from garnet lherzolites. This database is compiled from high quality analyses of garnet peridotite from published literature. The geochemical data from natural garnet lherzolites will be compared with pressure and temperature geobarometer calculations, experimental garnet lherzolites and current discrimination methods for garnet lherzolite clinopyroxenes.

ii. Evaluating thermodynamic models for clinopyroxene from modelled garnet lherzolites and comparing the models to natural garnet lherzolite data

iii. Revise the geobarometer for Cr-diopside using natural garnet lherzolite samples, either through thermodynamic modelling or refining the previous geobarometer formulation

Chapter 2 Chemistry of Clinopyroxenes from Mantle-derived Garnet Lherzolites

2.1 Introduction

2.1.1 Overview

Pyroxenes are a group of rock forming silicates that occur in various igneous and metamorphic rocks. Pyroxenes crystallize in the orthorhombic and monoclinic systems to form orthopyroxene and clinopyroxene, respectively. Pyroxenes contain single SiO_3 chains of linked SiO_4 tetrahedra and are represented by a general chemical formula $(M2)(M1)(T)_2O_6$. The M2 site represents cations in distorted 6 to 8 coordination, M1 cations are in regular octahedral coordination and T cations are tetrahedrally coordinated (Morimoto 1988). The M2 site typically accommodates Na, Ca, Mn^{2+}, Fe^{2+}, Mg, and Li. M1 accommodates Mg, Fe^{2+}, Mn^{2+}, Al, Cr, Ti, and Fe^{3+}. Cr usually occurs as Cr^{3+} and Ti as Ti^{4+} in terrestrial pyroxenes. In more reducing environments Cr and Ti can occur as Cr^{2+} and Ti^{3+}. The T site is occupied by Si and Al, dominantly Si. The cations mentioned are the most common ones in the rock-forming pyroxenes; however, others do occur in trace amounts (Cameron and Papike 1981).

Morimoto (1988) proposed allocating cations to obtain a pyroxene formula following these steps:

1) Sum T to 2.000 using Si^{4+}, then Al^{3+}, then Fe^{3+}.

2) Sum M1 to 1.000 using all remaining excess Al^{3+} and Fe^{3+}. If there is insufficient Al^{3+} and Fe^{3+} to sum to 1.000 add Ti^{4+} first, then Cr^{3+}, then V^{3+}, then Ti^{3+}, then Zr^{4+}, then Sc^{3+}, then Zn^{2+}, then Mg^{2+}, then Fe^{2+} and finally Mn^{2+} until the sum is 1.000.
3) Sum M2 using all Mg^{2+}, Fe^{2+} and Mn^{2+} in excess of that used to fill the M1 site. Then add Li^{+}, Ca^{2+} and Na^{+} so that sum becomes 1.000 or close to it.

The pyroxene group includes twenty minerals accepted by the Subcommittee on Pyroxenes established by the Commission of New Minerals and Mineral Names of the International Mineralogical Association (Morimoto 1988). Pyroxenes form extensive solid solution and are subdivided into ranges with specified compositions and names. Pyroxenes are generally divided into three chemical groups: Ca-Mg-Fe pyroxenes, Ca-Na and Na pyroxenes, and other pyroxenes (Morimoto 1988). The Ca-Mg-Fe pyroxenes are the most common rock forming pyroxenes. These are represented in the pyroxene quadrilateral, which is a ternary diagram of the system $CaSiO_3$ (the pyroxenoid wollastonite), $Mg_2Si_2O_6$ (enstatite), and $Fe_2Si_2O_6$ (ferrosilite) (Figure 2.1).

Sodic pyroxenes are represented by the minerals jadeite ($NaAlSi_2O_6$), aegirine ($NaFe^{3+}Si_2O_6$), kosmochlor ($NaCrSi_2O_6$) and jervisite ($NaScSi_2O_6$). The Na pyroxenes show extensive solid solution with the Ca-Mg-Fe pyroxenes giving rise to Ca-Na pyroxenes such as omphacite ((Ca, Na)(Mg, Fe^{2+}, Fe^{3+}, Al)Si_2O_6). Na and Ca-Na pyroxenes are classified using the Ca-Mg-Fe pyroxenes-jadeite-aegirine diagram in crustal settings (Morimoto 1988). In mantle lithologies, clinopyroxene is rich in Cr so mantle pyroxenes are better represented by the diagram Ca-Mg-Fe pyroxenes-jadeite-kosmochlor (Figure 2.2). Nimis and Taylor (2000) describe mantle clinopyroxene as chromian diopside, which is defined as $CaMgSi_2O_6$-rich clinopyroxene with >0.5 wt% Cr_2O_3.

2.1.2 Dataset

A reference dataset for chemical analyses and testing of discrimination schemes for garnet lherzolite clinopyroxenes has been compiled for this study. This dataset contains major-element compositions of 678 clinopyroxenes drawn from literature sources, with a focus on kimberlite-hosted garnet lherzolite clinopyroxenes recovered during diamond exploration. For literature analyses, only samples with oxide totals between 98.5 and 101.5 wt% are used. The dataset covers a wide range of cratons including the Slave, Superior, North Atlantic, Wyoming, Kaapvaal and Siberia cratons. During the later stages of this thesis, a complementary dataset was kindly provided by Thomas Stachel which was used to supplement this database. All compiled data are included in the Supplementary Online Dataset (Appendix A) for this study.

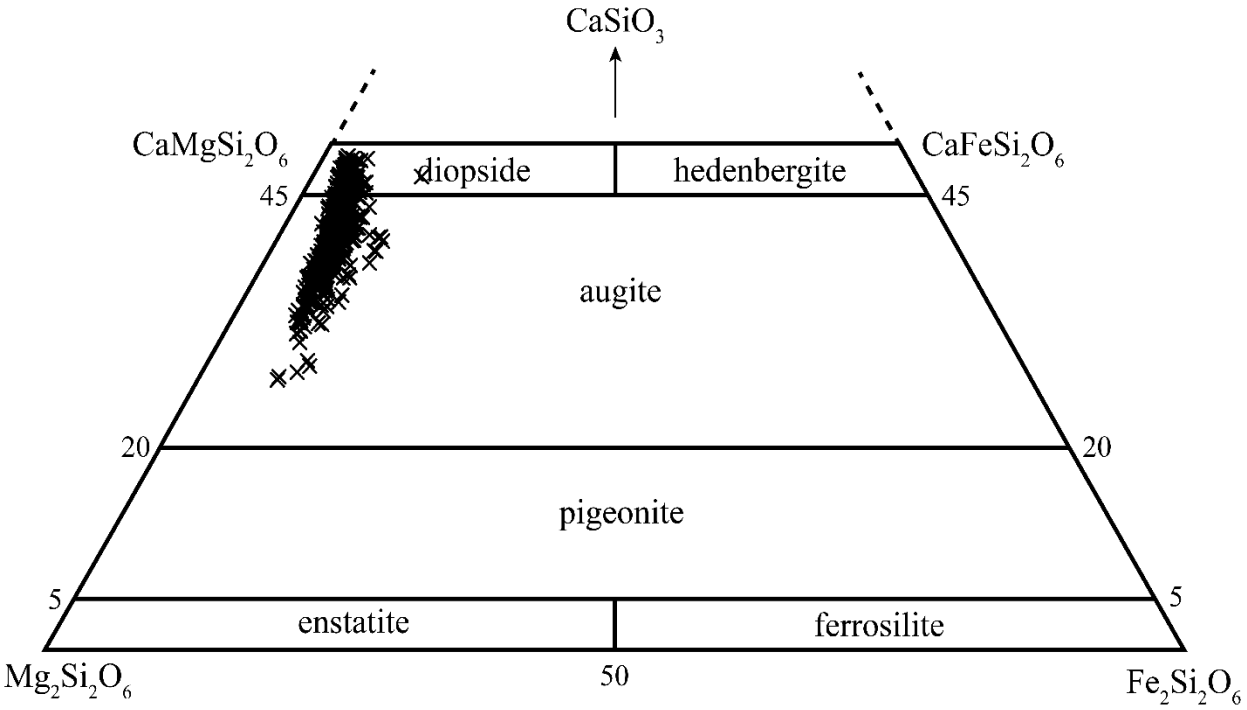

Figure 2.1 Modified pyroxene quadrilateral after Morimoto (1998) with clinopyroxenes from dataset of mantle garnet lherzolites for this study.

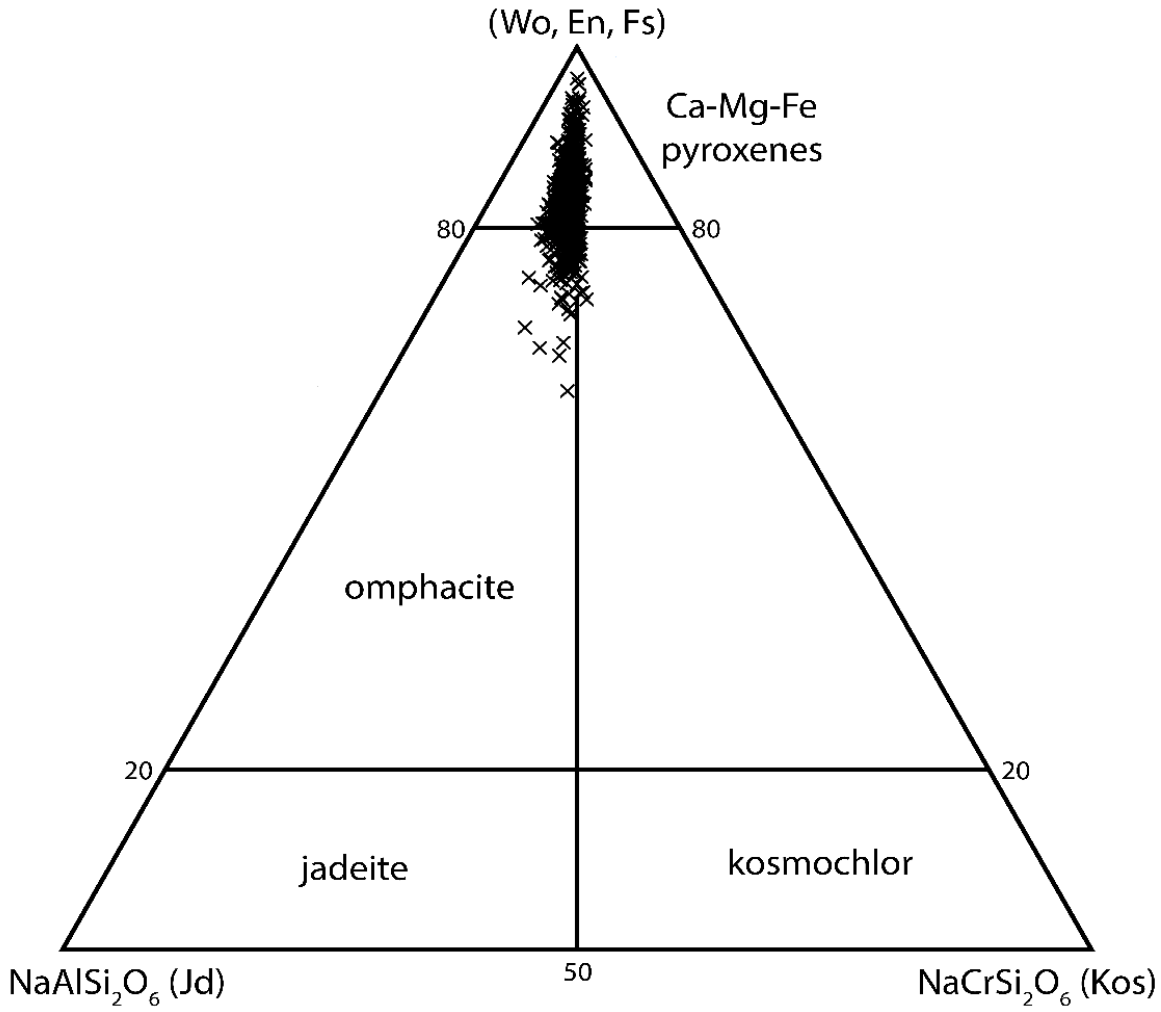

Figure 2.2 Ca-Na clinopyroxene plot for clinopyroxenes from dataset of mantle garnet lherzolites. The diagram is modified after Morimoto (1988) with kosmochlor replacing aegirine due to the Cr-rich nature of mantle clinopyroxenes.

2.1.3 Goals

The goal of this chapter is to provide an overview of the chemistry of mantle-derived clinopyroxenes from garnet lherzolites over a broad range of pressure and temperature settings. Published discrimination methods will be applied to the dataset of garnet lherzolite clinopyroxenes to see if current chemical discriminations apply to the majority of the dataset

samples. The compositional variability of the clinopyroxenes as functions of pressure and temperature will be presented to explore the relationships of cation exchange with pressure and temperature of garnet lherzolite in mantle settings. Natural clinopyroxenes will also be compared with synthesized experimental garnet lherzolite clinopyroxenes to analyze the relationship between cations and pressure and temperature. This comparison will illustrate the differences and similarities between natural and experimental clinopyroxenes.

2.2 Mantle Clinopyroxene Background

2.2.1 Historical Discrimination

Discrimination between clinopyroxene from on-craton garnet peridotite, off-craton garnet peridotite, spinel peridotite, eclogite, pyroxenite and megacryst is possible using Ramsay's (1992) Cr_2O_3 vs. Al_2O_3 classification diagram (following methods of Ramsay and Tompkins 1994) (Figure 2.3). On this diagram, the 0.5 wt% Cr_2O_3 boundary separates clinopyroxenes from peridotitic and non-peridotitic sources. The Al_2O_3 content is useful for separating clinopyroxenes from garnet peridotites and from spinel/garnet-spinel peridotites (Nimis 1998). An additional discrimination plot that is used in conjunction with Ramsay and Tompkins' (1994) plot is Nimis' (1998) MgO vs Al_2O_3 plot. Clinopyroxene that plots in Ramsay and Tompkins' (1994) garnet peridotite field are plotted onto the MgO vs Al_2O_3 wt% diagram to separate clinopyroxenes from garnet peridotites and low Al_2O_3, low MgO, metasomatized, garnet-free peridotites (Figure 2.4). If low Al_2O_3 clinopyroxenes from garnet free peridotites are included in a dataset under consideration, equilibration pressures are overestimated, yielding incorrect pressure estimates (Nimis 2002).

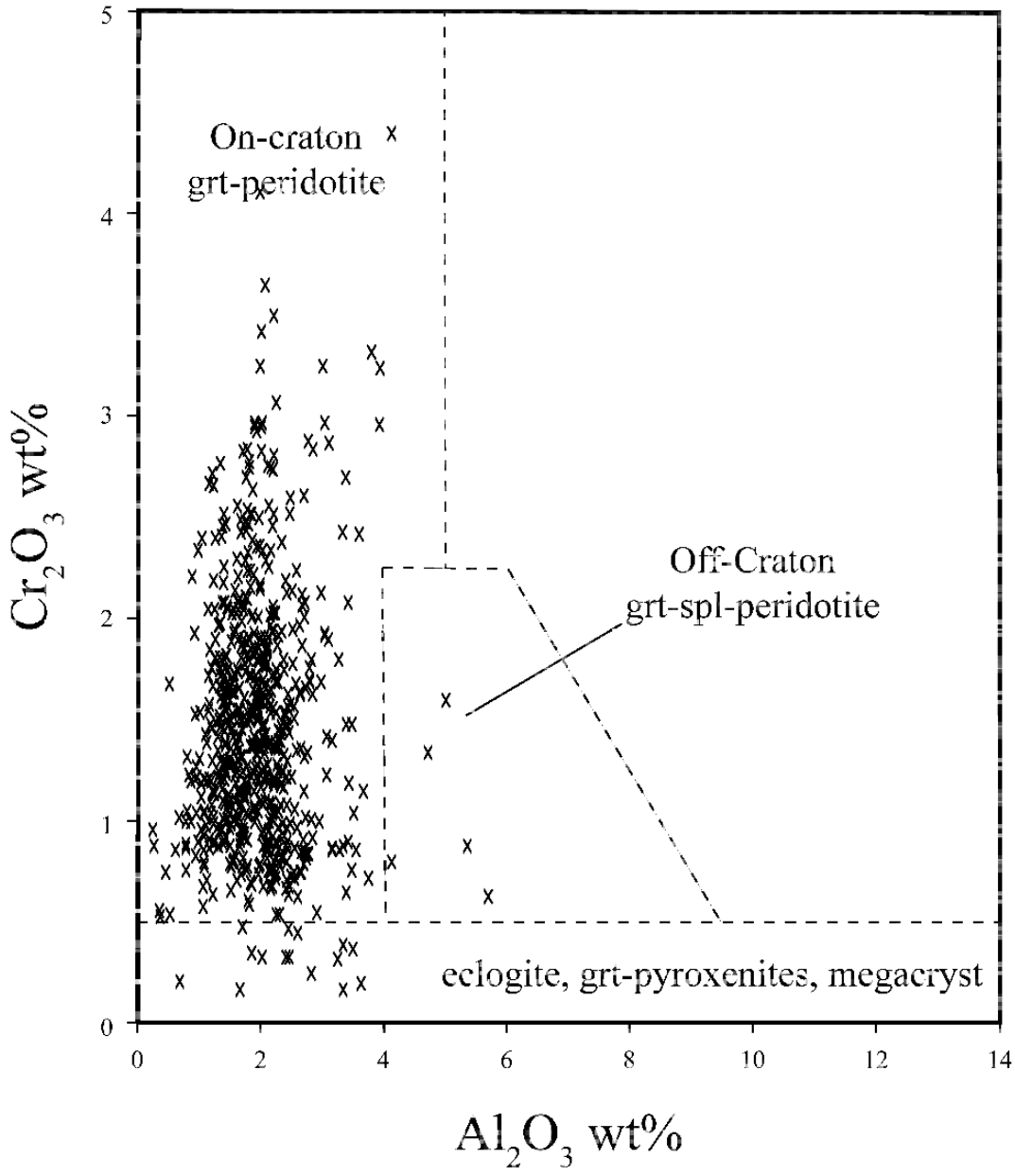

Figure 2.3 Cr_2O_3 vs Al_2O_3 wt% clinopyroxene classification of Ramsay (1992) with dataset clinopyroxenes from garnet lherzolites

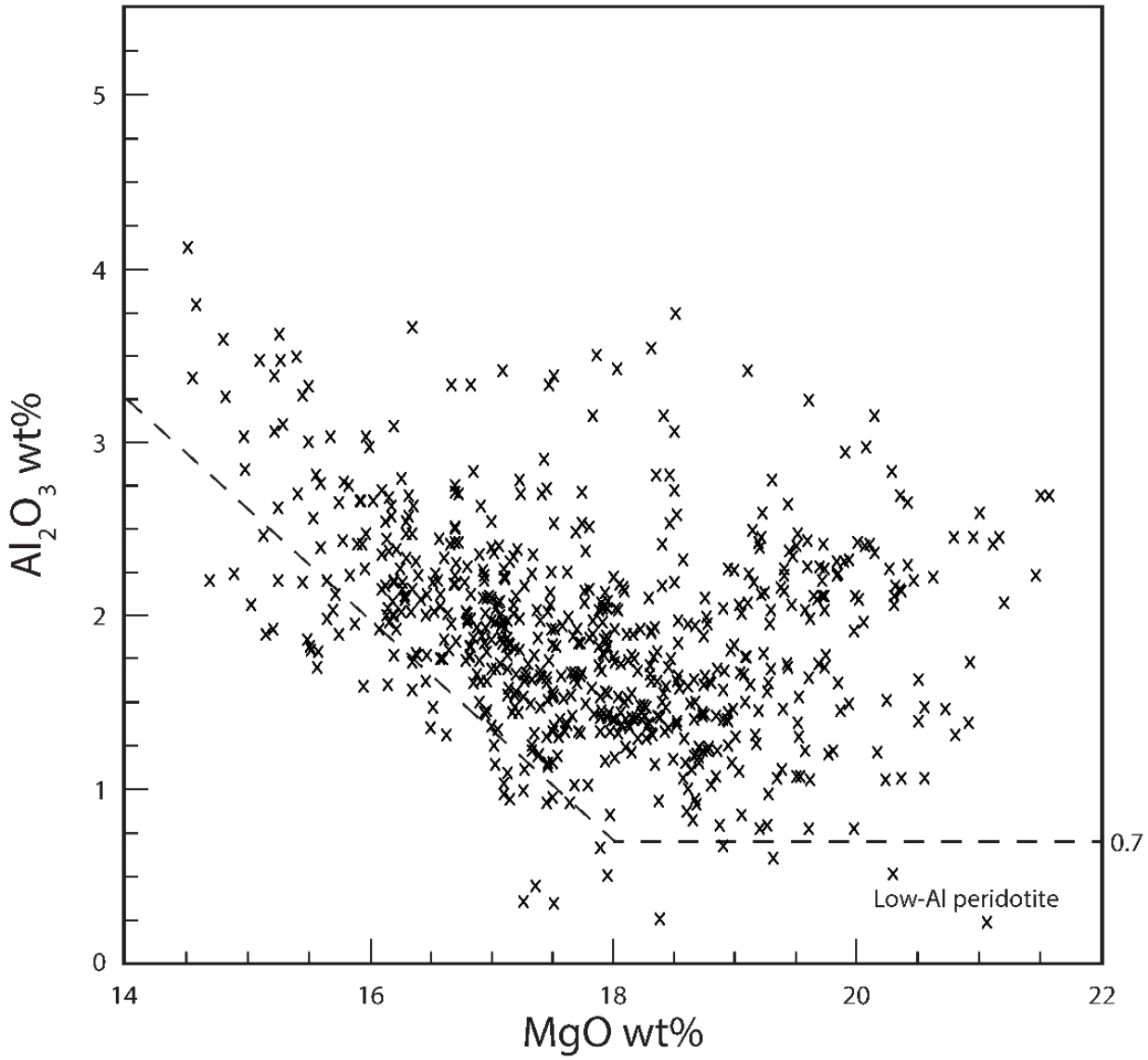

Figure 2.4 MgO vs Al_2O_3 wt% clinopyroxene discrimination of Nimis (1998) with dataset clinopyroxenes from garnet lherzolites

An additional screen is the Al-Na-Cr ternary of Morris et al. (2002). Morris et al. (2002) developed this screening because they find that the cut-off of 0.5 Cr_2O_3 wt% of Ramsay (1992) overlapped with clinopyroxenes from other rock types. This ternary is applied to clinopyroxenes because the atomic proportions of Al, Cr and Na in mantle clinopyroxenes recovered from kimberlites have ~1:1 ratios of (Al+Cr):Na (Figure 2.5). This indicates jadeite and kosmochlor

components of the clinopyroxenes dominate in controlling the distribution of these elements in the mineral structures in mantle settings. Rocks from crustal settings typically are low in Na and Cr so they will plot in the Al corner of the ternary (Morris et al. 2002).

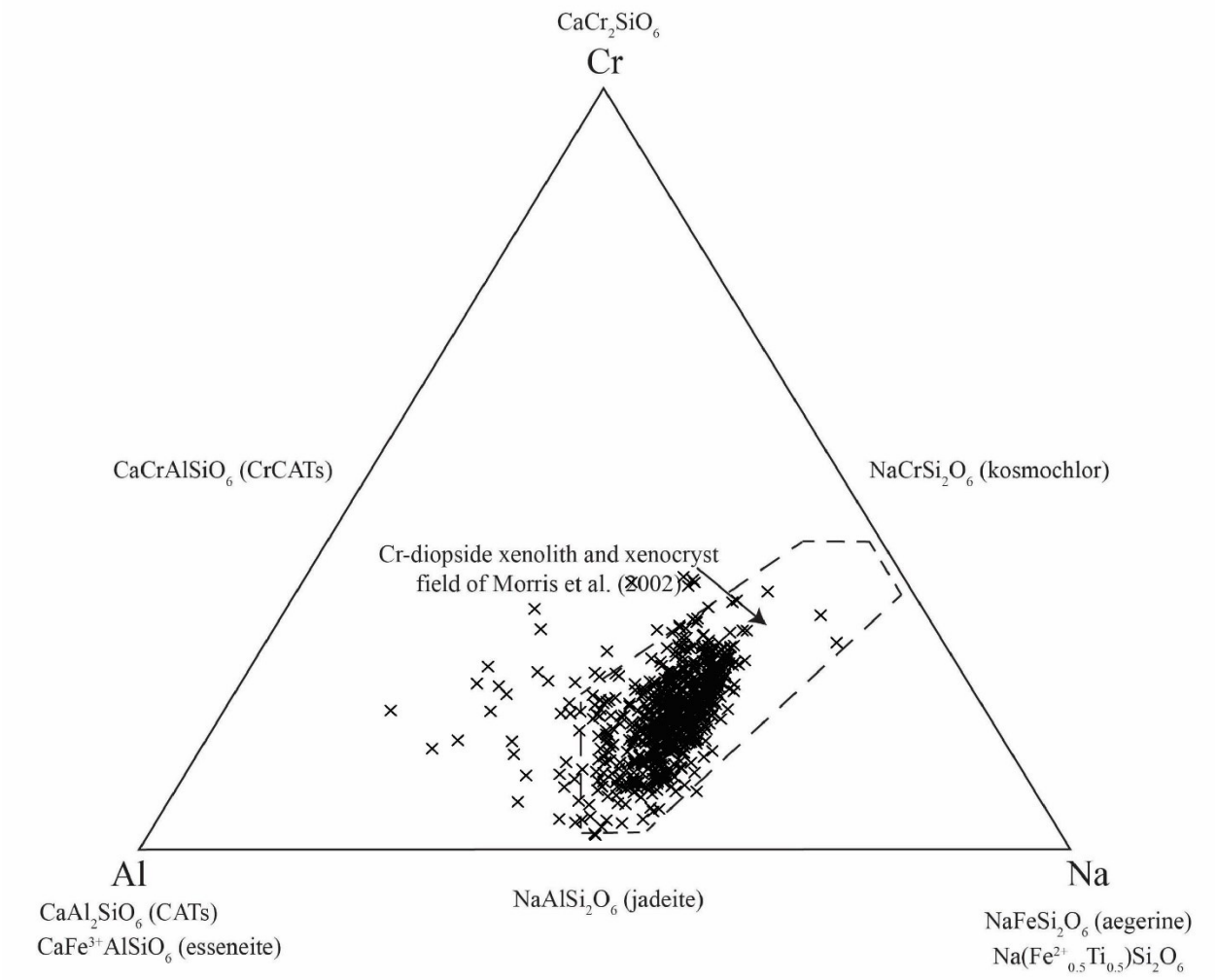

Figure 2.5 Al-Na-Cr ternary clinopyroxene discrimination of Morris et al. (2002) with dataset clinopyroxenes from garnet lherzolites. The ternary includes a field for mantle derived clinopyroxenes and key mineral endmembers for Al, Na and Cr clinopyroxenes.

2.4 Dataset Clinopyroxene Chemistry

Clinopyroxenes from garnet lherzolites are described as chromian diopside, which is defined as $CaMgSi_2O_6$-rich clinopyroxene with >0.5 wt% Cr_2O_3 by Nimis and Taylor (2000) and is a major

host for sodium, calcium, chromium, and titanium in mantle peridotites (Pearson et al. 2014). Clinopyroxene shows extensive solid solution with orthopyroxene and/or garnet at high P and T in the mantle and most samples in the database can be described as augite in the pyroxene quadrilateral (Figure 2.1). The Mg# of the database clinopyroxene range from 0.819 to 0.959 with an average value of 0.920. The Ca# of clinopyroxene is strongly T-dependant and ranges from 0.267-0.488. This temperature dependence reflects the miscibility gap between clinopyroxene and orthopyroxene represented by Ca-Mg-Fe^{2+} equilibria, with the lower Ca# indicating higher temperatures of equilibrium (Lindsley 1983). The Al_2O_3 content of the clinopyroxene varies from 0.24 wt% and 5.70 wt%, corresponding to 0.010 to 0.240 Al cations per 6 oxygens. Cr_2O_3 content varies from 0.17 wt% and 4.40 wt% with the majority of the samples having >0.5 wt% (Figure 2.3). Corresponding calculated Cr cations range from 0.005 apfu to 0.125 apfu. Na_2O content varies from 0.22 wt% to 4.22 wt% with corresponding Na cations ranging from 0.015 apfu to 0.295 apfu. K_2O content varies from 0.00 to 0.31 wt% with corresponding K cations ranging from 0.000 apfu to 0.014 apfu. Na+K and Al+Cr are positively correlated in clinopyroxenes from garnet lherzolites (Figure 2.6).

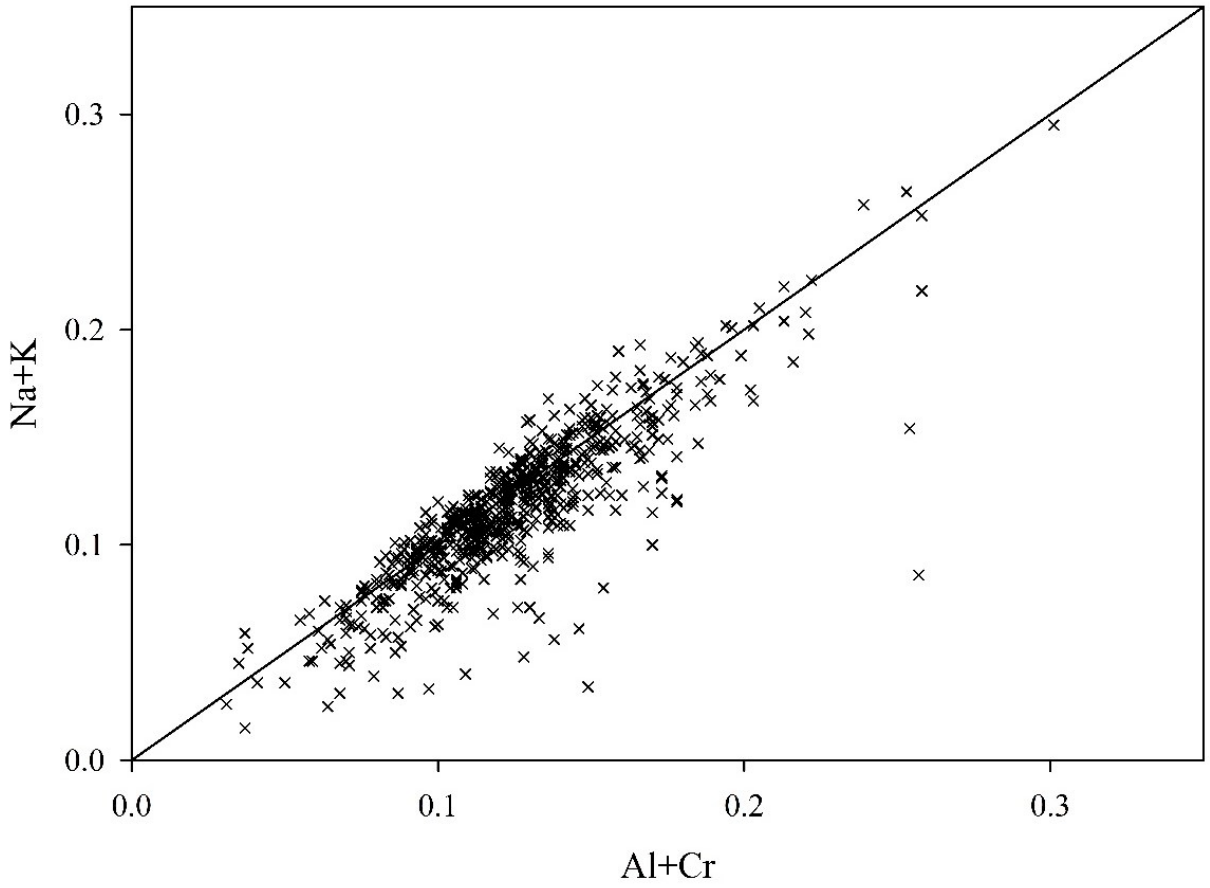

Figure 2.6 Plot of Al+Cr vs Na+K of database clinopyroxene from garnet lherzolites. There is a strong positive correlation between Al+Cr and Na+K with ~1:1 ratio seen from the one to one line in the image.

Samples above the one-to-one line in Figure 2.6 require Na+K to charge balance with other 3+ or 4+ cations, such as Fe^{3+} or Ti^{4+}. The samples below the one-to-one line are richer in Al+Cr and this suggests a Tschermak-type substitution as Al+Cr is not completely charge balanced with Na+K. This observation is in agreement with Morris et al. (2002) with the observed (Al+Cr):Na ratio of ~1. Read et al. (2004) uses the formula Al+Cr-Na-K to distinguish clinopyroxenes from garnet lherzolites (<0.05 (per 6 oxygen)) from those of spinel lherzolites (>0.05) (which reflect the higher tschermak component in clinopyroxenes in spinel lherzolites) (Read et al. 2004) (Figure 2.7).

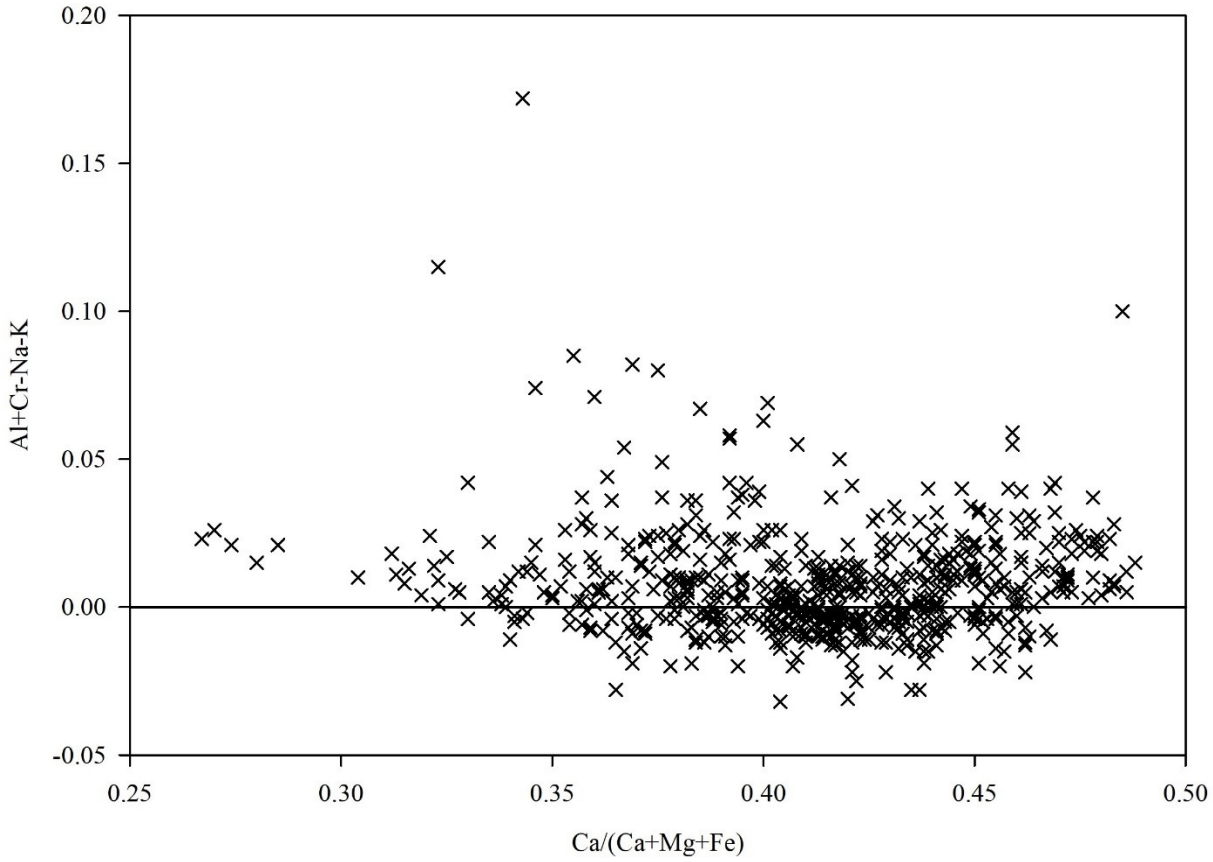

Figure 2.7 Tschermak vs Ca-number of database clinopyroxene from garnet lherzolites. Modified after Grütter (2009)

Clinopyroxene contains both ferrous and ferric iron in garnet lherzolites. Total iron is typically analyzed as FeO in electron microprobe analyses as most iron occurs in a ferrous state. Ferric iron concentrations can be quantified using Mössbauer spectroscopy (e.g. Canil and O'Neill 1996, Woodland and Peltonen 1999, Woodland 2009) with up to 36.7% of all iron in the Mössbauer analyzed clinopyroxene being Fe^{3+}. The partitioning of Fe^{3+} between clinopyroxene and garnet varies with temperature, f_{O_2}, chemistry of the individual minerals and bulk rock composition (Woodland 2009). For the subset of samples in the dataset with Fe^{3+} data, Na and Fe^{3+} are positively correlated, in agreement with the observations of Woodland (2009). Woodland (2009) concluded that the dominant mechanism for incorporating Fe^{3+} in

clinopyroxenes in garnet lherzolites was the aegirine component ($NaFe^{3+}Si_2O_6$) due to low tetrahedral Al. The partitioning of Fe^{3+} between clinopyroxene and garnet can be considered in terms of two different Fe^{3+}-Al exchange reactions, one involving Na-bearing endmembers ($NaAlSi_2O_6$ and $NaFe^{3+}Si_2O_6$) in clinopyroxene and Ca-bearing or Fe^{2+}-bearing components in garnet (Reaction 1 and 2 in Woodland 2009). Mg# increases when Fe^{3+} is taken into consideration as Mg# is typically calculated with FeO_T (Mg# calculation becomes $Mg/(Mg+Fe^{2+})$). The change in Mg# can affect interpretations on depletion, as Mg# is related to the degree of melt depletion or enrichment in iron (Pearson et al. 2014). However, consideration of Fe^{3+} remains problematic in the absence of routine Fe^{3+} analyses. For mantle clinopyroxenes, with low FeO_{total}, attempting to constrain Fe^{3+} by stoichiometry does not work (see Canil and O'Neill 1996).

2.5 Geothermobarometry of Dataset Clinopyroxene

2.5.1 Applied Geothermobarometers

Multiple experimentally calibrated thermobarometers are available to estimate the P and T of polymineralic mantle xenoliths and single grain mantle xenocrysts. The geothermobarometers that are applied to the current database are the Nimis and Taylor (2000) single grain clinopyroxene thermobarometer (NT2000), Sudholz et al. (2021) single grain clinopyroxene barometer (SUD2021) used with the Nimis and Taylor (2000) thermometer, Nimis et al. (2020) corrected barometer (NT2020 Corrected) used with the Nimis and Taylor (2000) thermometer, Brey and Köhler (1990) two-pyroxene thermometer and the garnet-orthopyroxene barometer (BK1990) and the Nickel and Green (1985) garnet-orthopyroxene barometer with Al in M1 calculated after Carlswell & Gibb (1987) (NG1985) with the Taylor (1998) two-pyroxene

thermometer (TA1998) (as recommended by Nimis and Grütter 2010). Specific focus will be given to the Nimis and Taylor (2000) thermobarometer and the Sudholz et al. (2021) barometer.

All data were screened for quality using the following criteria, similar to Nimis and Grütter (2010): oxide totals between 98.5 and 101.5 wt%; cation sums for pyroxene ≥ 3.990 apfu (6-oxygen basis), olivine ≥ 2.990 apfu (4-oxygen basis), garnet ≥ 7.990 apfu (12-oxygen basis). The Nimis and Taylor (2000) thermobarometer and Sudholz et al. (2021) barometer require further compositional filtering as discussed in Section 1.3. The Grütter (2009) and Ziberna et al (2016) filters result in the rejection of 126 and 186 xenoliths from the database, respectively. Equilibrium between clinopyroxene and orthopyroxene in peridotite xenoliths was verified using the recommendations of Nimis and Grütter (2010), where disequilibrium between both pyroxenes is defined as the difference in calculated temperature between the Taylor (1998) two-pyroxene thermometer and corrected Ca-in-opx thermometer of Brey and Köhler (1990) larger than 90°C at TA98 < 900°C, 70°C at TA98 = 900-1200°C, or 50°C at TA98 > 1200°C.

2.5.2 Chemical changes with Pressure and Temperature changes

Clinopyroxene shows extensive solid solution toward orthopyroxene and/or garnet at high P and T in the mantle. This solid solution forms the basis for geothermobarometers using mantle clinopyroxenes. The extent of solid solution depends on bulk composition of the peridotite as well as the P and T of equilibration. However, experimental geothermobarometer calibrations typically use a variety of bulk compositions which range from fertile to depleted mantle (e.g. Brey and Köhler 1990, Taylor 1998, Nimis and Taylor 2000, Sudholz et al. 2021) to calibrate the effects of composition. The change in clinopyroxene chemistry with a change in pressure and temperature (i.e. depth) will be the focus of this section. Specific focus will be given to endmember clinopyroxene chemistry and individual cations in the clinopyroxene structure.

For the dataset clinopyroxenes, Al, Cr and Na all decrease with increasing pressure and temperature and the trends are obvious on a local scale. For the whole dataset the trend for Al is still visible. However, with the whole dataset the trends are harder to see with Cr and Na due to scatter from bulk composition (Figures 2.8, 2.9 and 2.10). This agrees with the previously discussed correlation of (Al+Cr):Na ratio of ~1, as Na and Al+Cr decrease sympathetically with increasing pressure and temperature. If all Al and Cr are charge-balanced with Na in garnet lherzolite clinopyroxenes, these can be treated as jadeite and kosmochlor components. This in turn means jadeite and kosmochlor decrease in individual clinopyroxene grains with depth. Aluminum can occupy the M1 site (as in jadeite), but also the tetrahedral site if Si does not completely fill that site. Tetrahedral site Al (Al_T) can be calculated as $Al_T=2–Si$, although this calculation of Al_T using Si can be prone to propagation errors because of analytical errors or poor analyses (Nimis and Taylor 2000). By mass balance, Al_{M1} would be $Al_{M1}=Al–Al_T$. Al_T is incorporated as Ca-Tschermak ($CaAlAlSiO_6$), CaCr-Tschermak ($CaCrAlSiO_6$) (as with Nimis 1998 and Nimis and Taylor 2000 barometers), esseneite ($CaFeAlSiO_6$), grossmanite ($CaTiAlSiO_6$) and Ca-buffonite ($CaMg_{0.5}Ti_{0.5}AlSiO_6$) endmembers (Morimoto 1988). Al_{M1} decreases with increasing pressure and temperature following the general trend of total Al (Figure 2.11). Al_T remains low (<0.06 apfu) in garnet lherzolite clinopyroxene due to the higher silica content on the tetrahedral site. There does not appear to be a clear correlation with pressure or temperature for Al_T in natural garnet lherzolite clinopyroxenes (Figure 2.12).

Mg and Fe^{total} increase with increasing temperature and pressure, with a corresponding decrease in Ca in the dataset clinopyroxenes (Figures 2.13, 2.14, 2.15). Ca# represents all these cations and the Ca# of clinopyroxene is strongly T-dependent because of the enstatite-diopside exchange

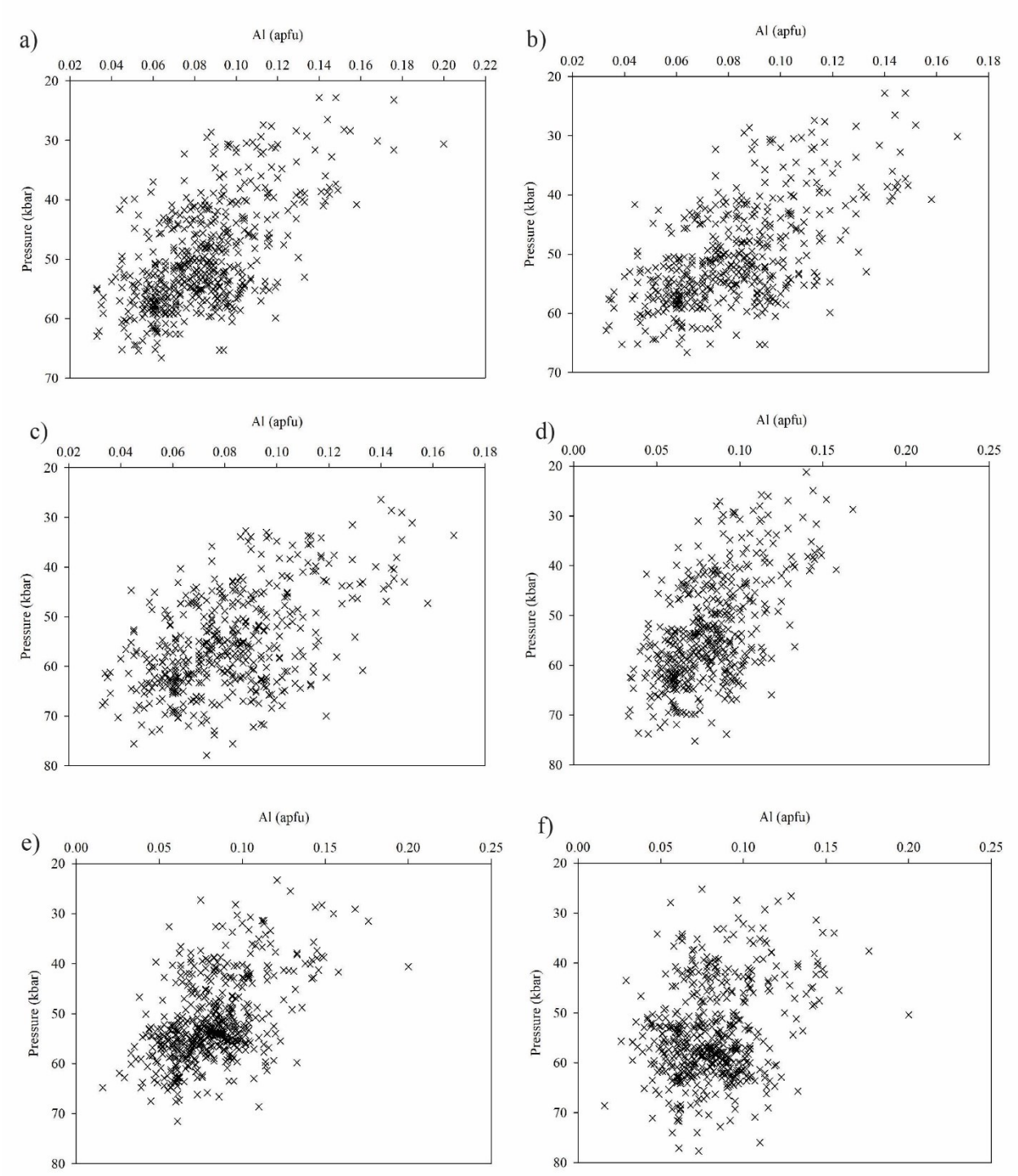

Figure 2.8 Al cations vs pressure from clinopyroxenes with barometers a) NT2000 barometer with Grütter (2009) filtering methodology, b) NT2000 barometer with Ziberna et al. (2016) filtering methodology, c) SUD2021 barometer, d) NT2020 Corrected barometer, e) NG1985 barometer and f) BK1990 barometer

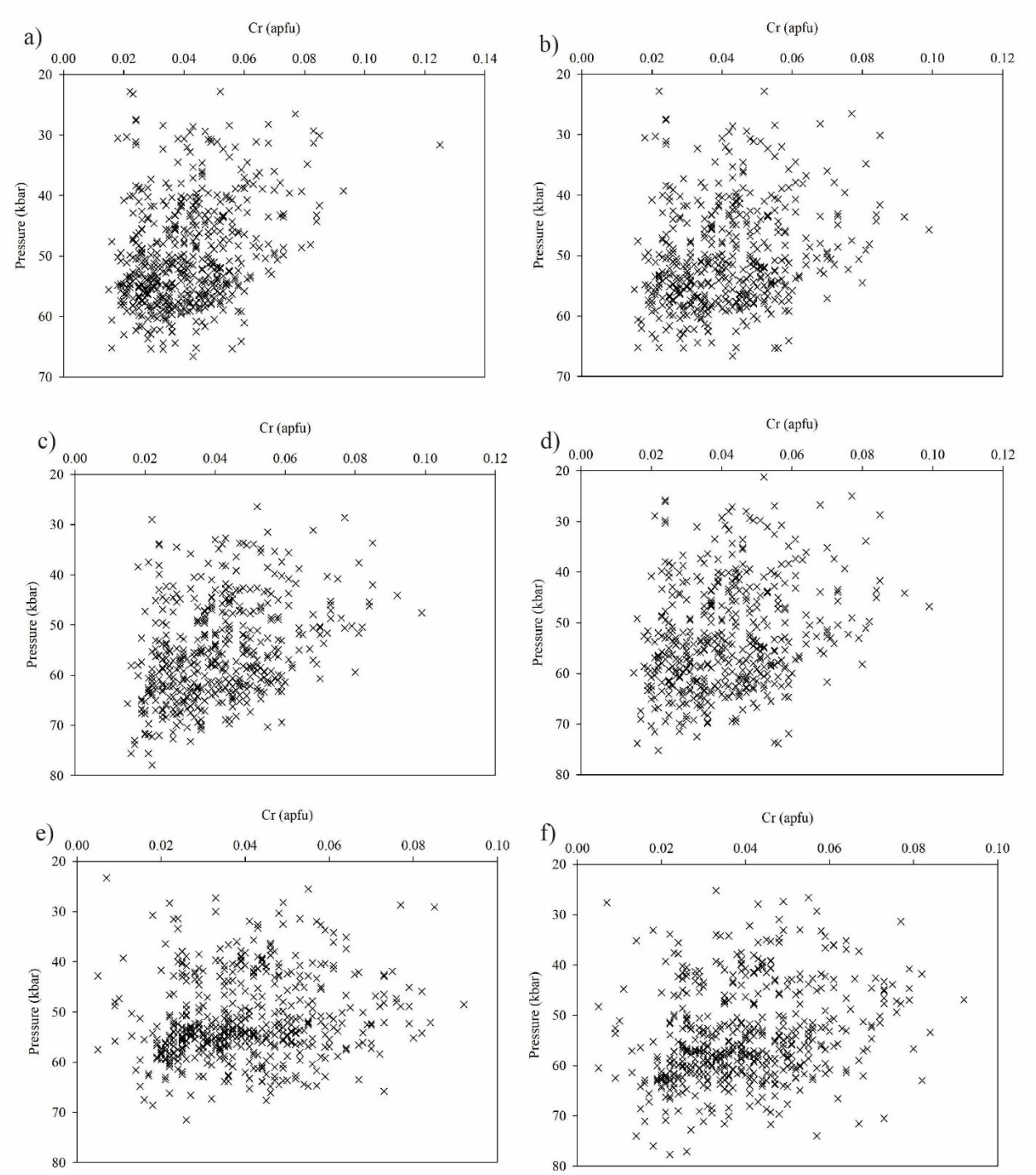

Figure 2.9 Cr cations vs pressure from clinopyroxenes with barometers a) NT2000 barometer with Grütter (2009) filtering methodology, b) NT2000 barometer with Ziberna et al. (2016) filtering methodology, c) SUD2021 barometer, d) NT2020 Corrected barometer, e) NG1985 barometer and f) BK1990 barometer

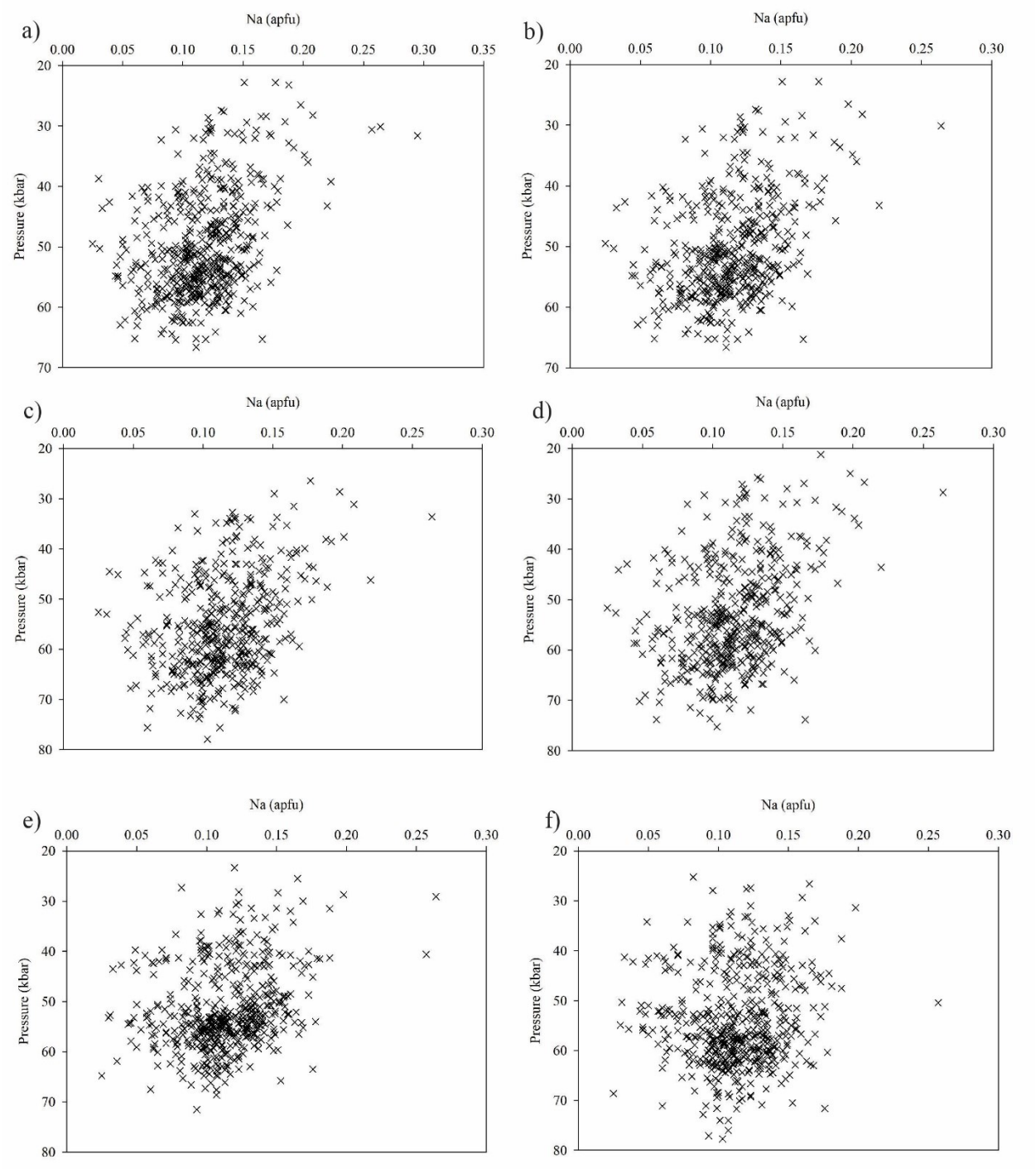

Figure 2.10 Na cations vs pressure from clinopyroxenes with barometers a) NT2000 barometer with Grütter (2009) filtering methodology, b) NT2000 barometer with Ziberna et al. (2016) filtering methodology, c) SUD2021 barometer, d) NT2020 Corrected barometer, e) NG1985 barometer and f) BK1990 barometer

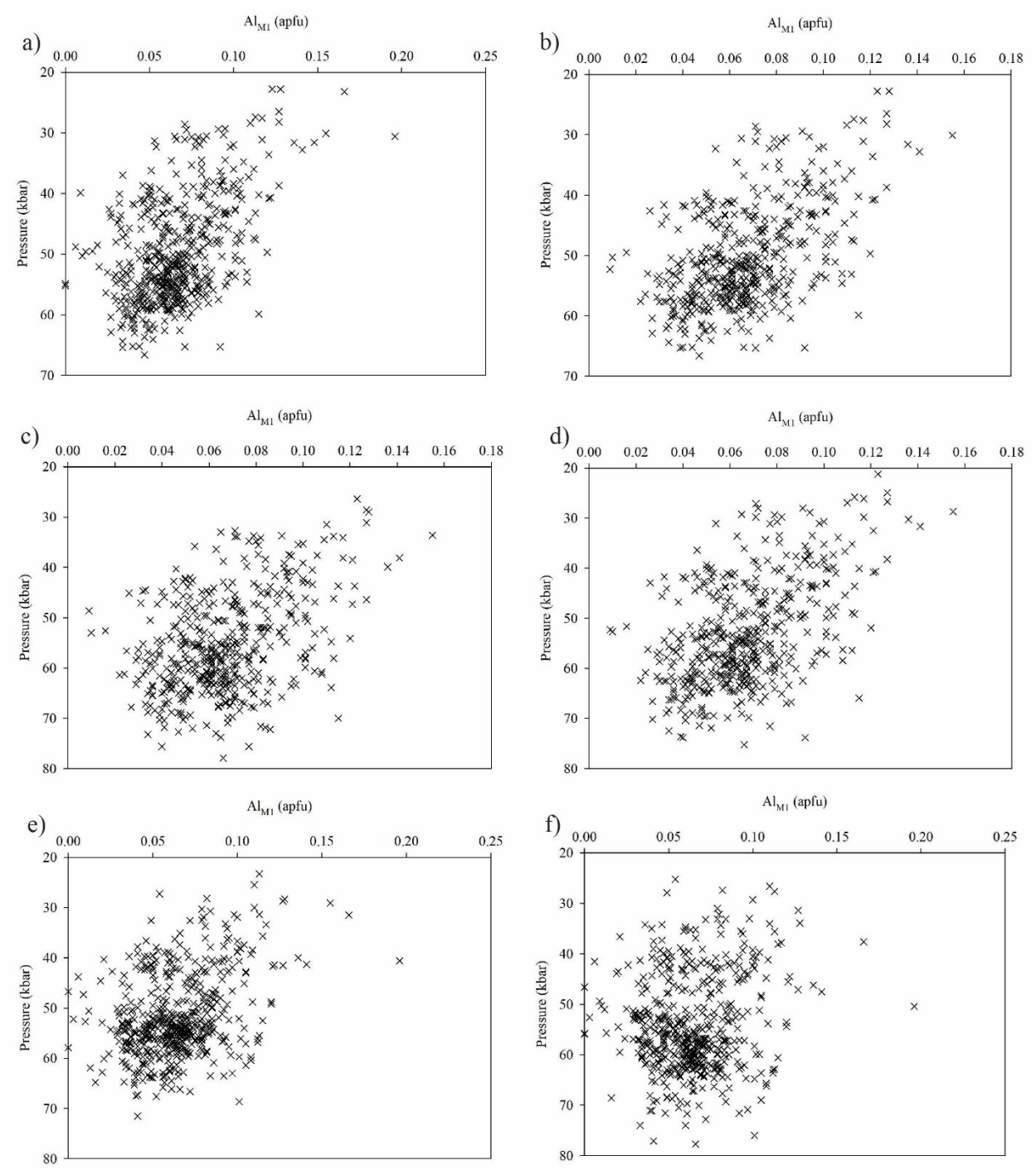

Figure 2.11 Al_{M1} cations vs pressure from clinopyroxenes with barometers a) NT2000 barometer with Grütter (2009) filtering methodology, b) NT2000 barometer with Ziberna et al. (2016) filtering methodology, c) SUD2021 barometer, d) NT2020 Corrected barometer, e) NG1985 barometer and f) BK1990 barometer

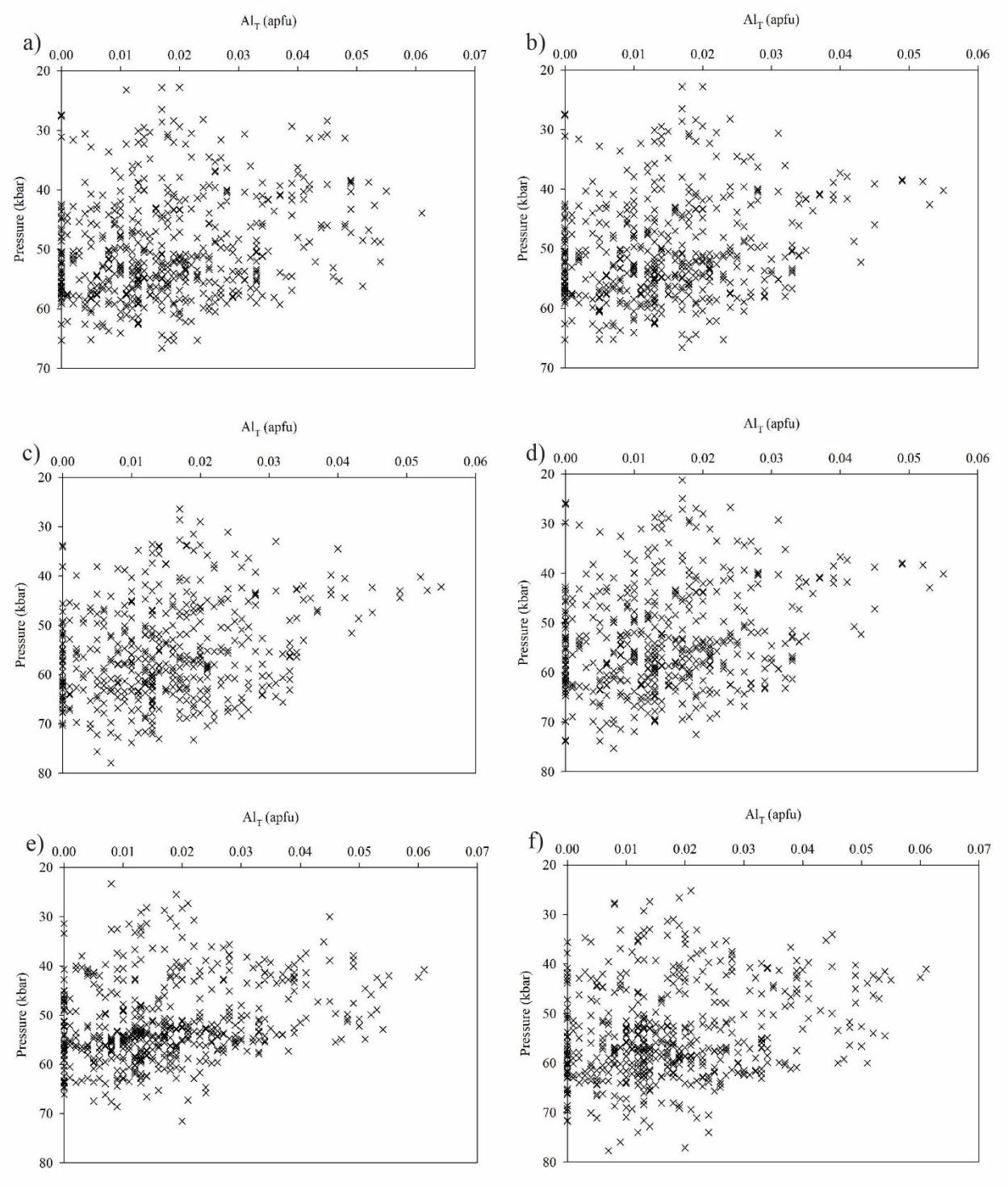

Figure 2.12 Al_T cations vs pressure from clinopyroxenes with barometers a) NT2000 barometer with Grütter (2009) filtering methodology, b) NT2000 barometer with Ziberna et al. (2016) filtering methodology, c) SUD2021 barometer, d) NT2020 Corrected barometer, e) NG1985 barometer and f) BK1990 barometer

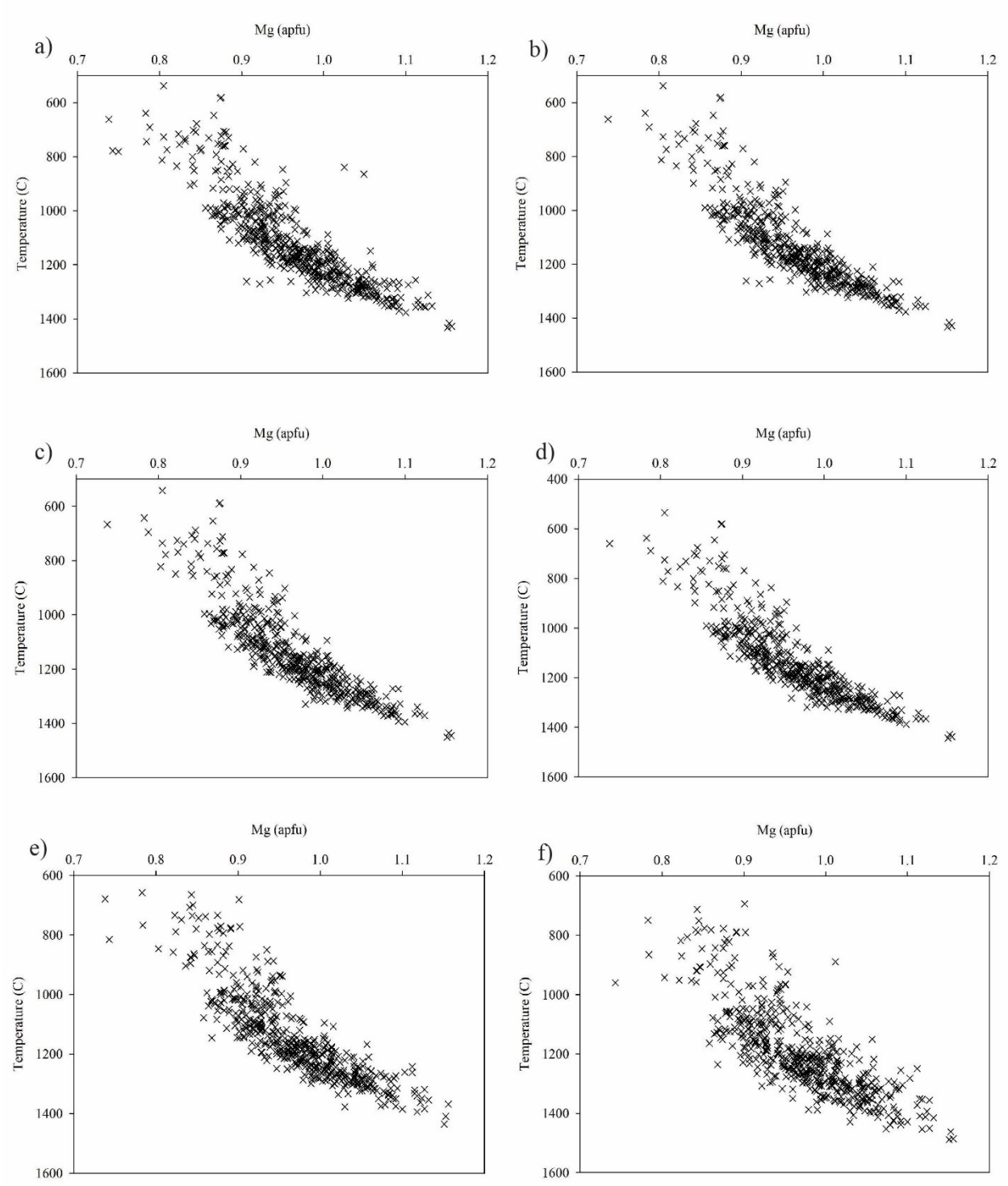

Figure 2.13 Mg cations vs temperature from clinopyroxenes with thermometers a) NT2000 thermometer with Grütter (2009) filtering methodology, b) NT2000 thermometer with Ziberna et al. (2016) filtering methodology, c) NT2000 thermometer using SUD2021 barometer, d) NT2000 thermometer using NT2020 Corrected barometer, e) TA1998 thermometer and f) BK1990 thermometer

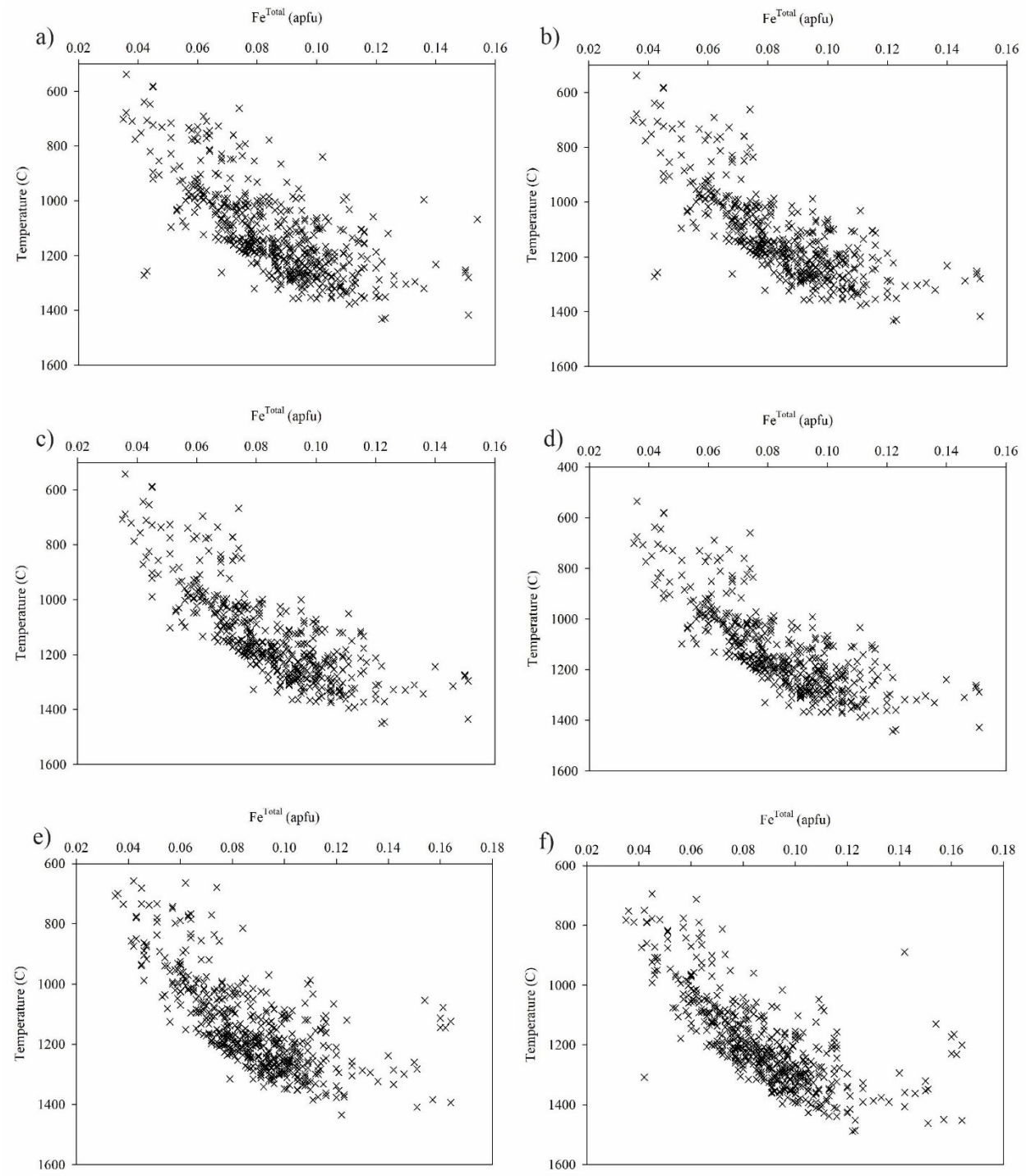

Figure 2.14 Fe^{2+} cations vs temperature from clinopyroxenes with thermometers a) NT2000 thermometer with Grütter (2009) filtering methodology, b) NT2000 thermometer with Ziberna et al. (2016) filtering methodology, c) NT2000 thermometer using SUD2021 barometer, d) NT2000 thermometer using NT2020 Corrected barometer, e) TA1998 thermometer and f) BK1990 thermometer

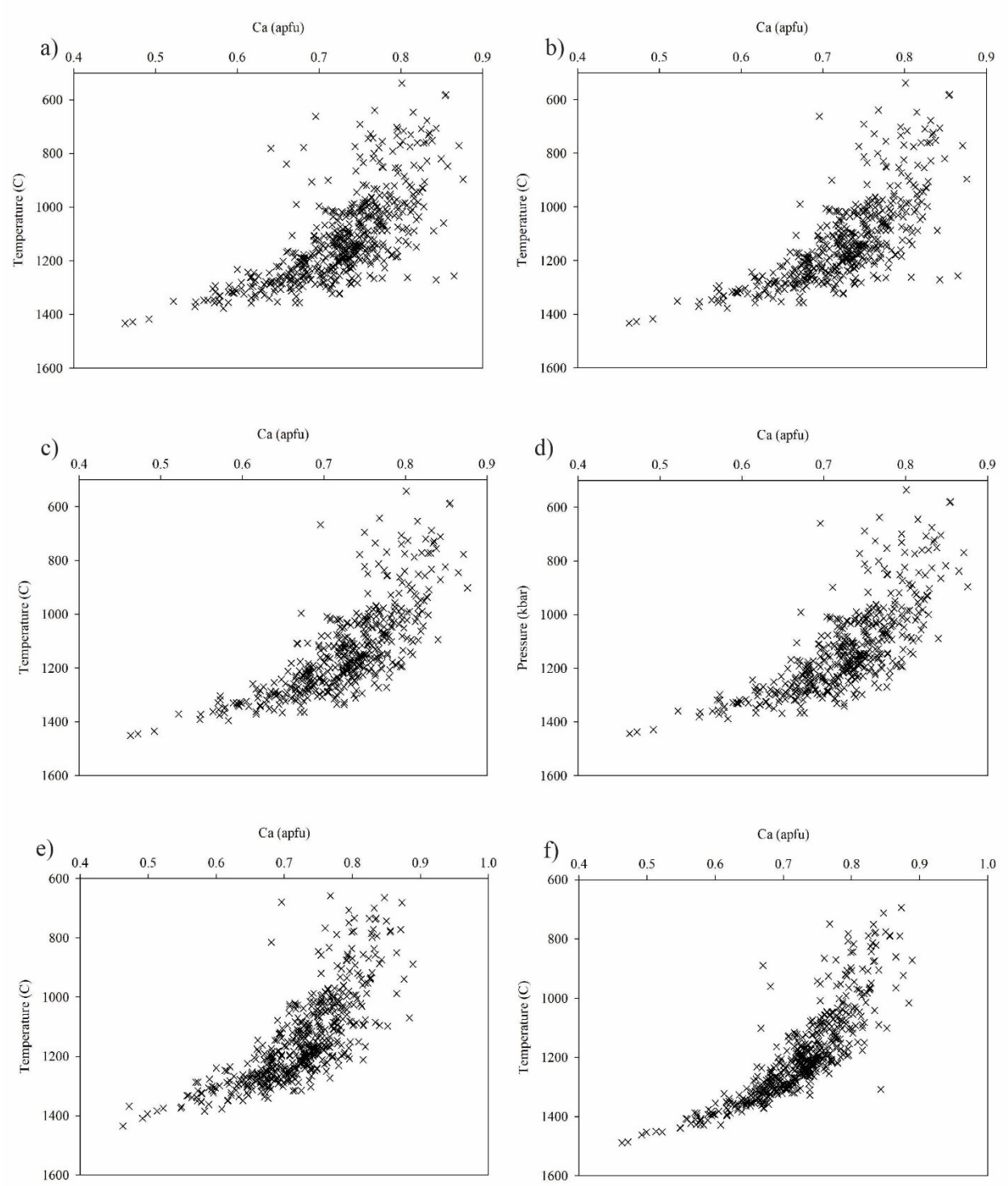

Figure 2.15 Ca cations vs temperature from clinopyroxenes with thermometers a) NT2000 thermometer with Grütter (2009) filtering methodology, b) NT2000 thermometer with Ziberna et al. (2016) filtering methodology, c) NT2000 thermometer using SUD2021 barometer, d) NT2000 thermometer using NT2020 Corrected barometer, e) TA1998 thermometer and f) BK1990 thermometer

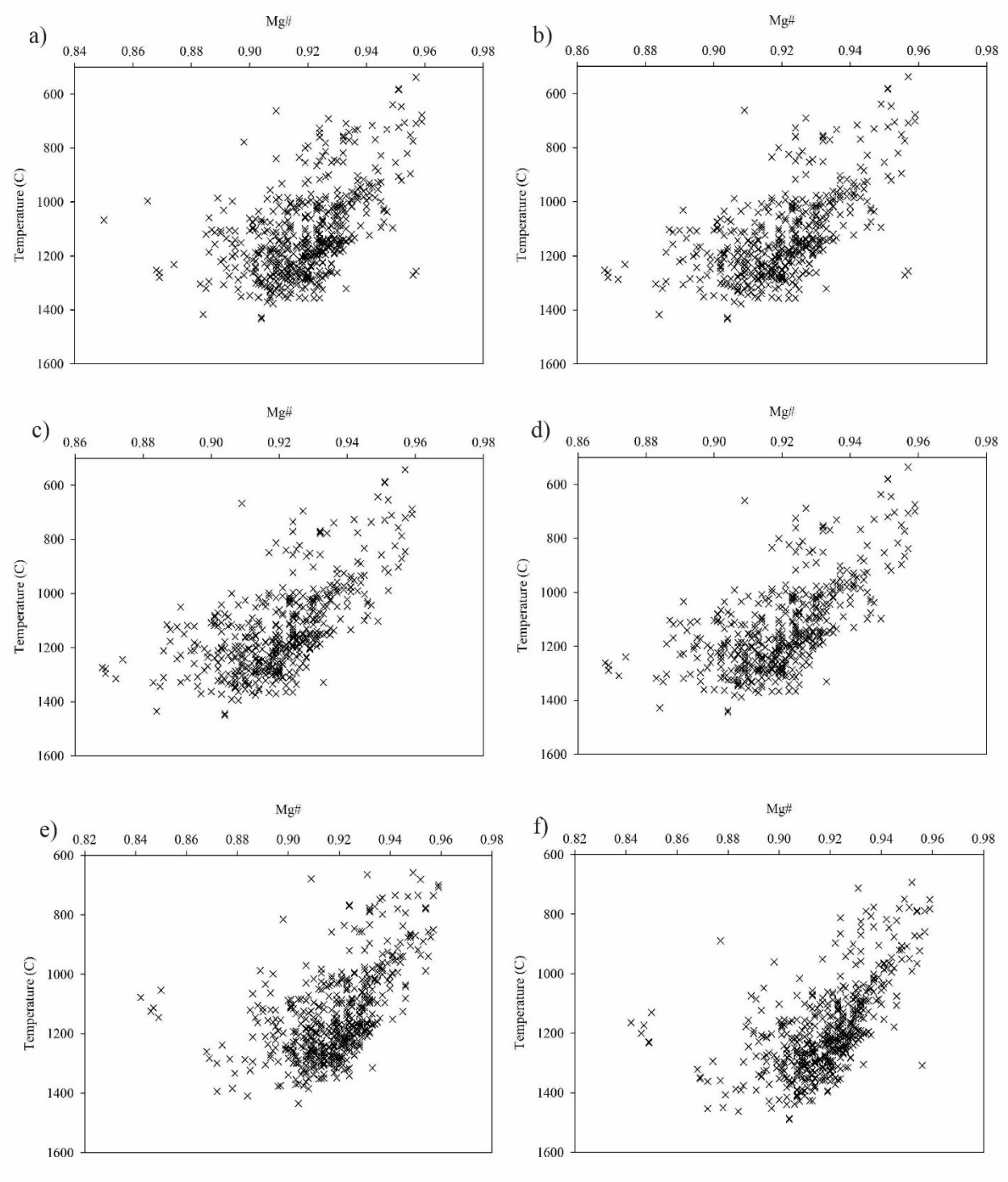

Figure 2.16 Mg# vs temperature from clinopyroxenes with thermometers a) NT2000 thermometer with Grütter (2009) filtering methodology, b) NT2000 thermometer with Ziberna et al. (2016) filtering methodology, c) NT2000 thermometer using SUD2021 barometer, d) NT2000 thermometer using NT2020 Corrected barometer, e) TA1998 thermometer and f) BK1990 thermometer

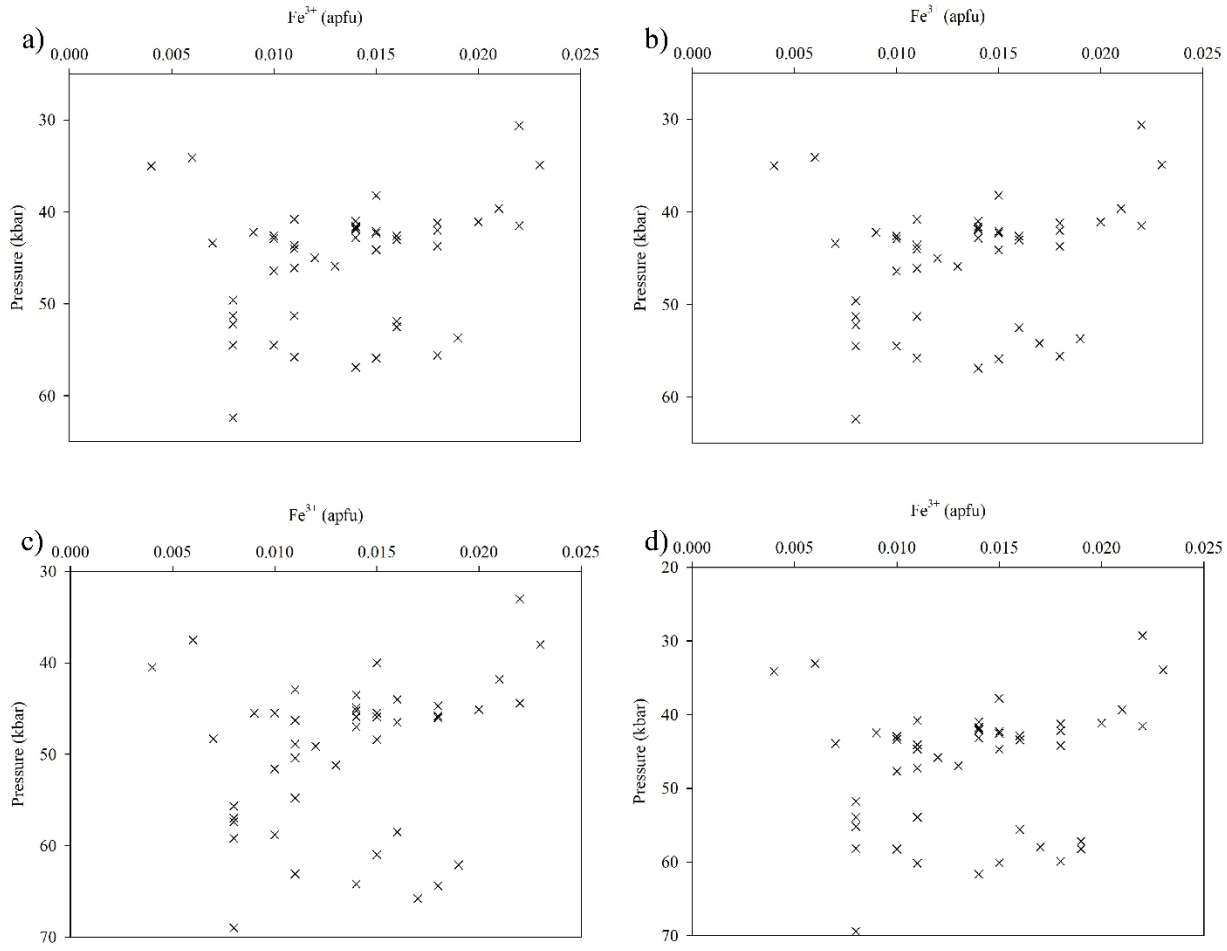

Figure 2.17 Fe^{3+} cations vs pressure from clinopyroxenes with thermometers a) NT2000 barometer with Grütter (2009) filtering methodology, b) NT2000 barometer with Ziberna et al. (2016) filtering methodology, c) SUD2021 barometer, d) NT2020 Corrected barometer

between orthopyroxene and clinopyroxene (Brey and Köhler 1990, Pearson et al. 2014). Ca# decreases with increasing temperature, representing the increase of Mg and Fe^{total} and decrease of Ca as previously discussed. Mg# decreases with increasing temperature and pressure (Figure 2.16).

Ferric iron cations determined by Mössbauer spectroscopy do not appear to have a clear correlation with temperature or pressure (Figure 2.17). Ferric iron in clinopyroxene varies with temperature, fO_2, chemistry of the individual minerals and bulk rock composition so a clear correlation with pressure is not expected (Woodland 2009). The presence of unquantified (in

routine analyses) Fe^{3+} is problematic because it can charge balance with Na in aegirine ($NaFeSi_2O_6$) and with Al_T in esseneite ($CaFe^{3+}AlSiO_6$). Ferric iron in the latter substitution will decrease the Cr-tschermak and Ca-tschermak because Fe^{3+} competes with Al^{M1} and Cr for Al_T. This affects the amount of Al_T available for Cr-tschermak and Ca-tschermak components which in turn will affect barometer calculations (e.g. Nimis 1998, Nimis and Taylor 2000, Sudholz et al. 2021). Ferric iron charge balanced with Na will affect the jadeite and kosmochlor components as less Na will be available for Al and Cr but would not affect the Al_T.

2.6 Comparing Natural Clinopyroxene to Experimental Clinopyroxene

Experimental garnet lherzolites are designed to simulate natural garnet lherzolites in melting experiments and geothermobarometer calibrations (e.g. Nickel and Green 1985, Brey and Köhler 1990, Taylor 1998, Walter 1998, Nimis and Taylor 2000, Yaxley 2000, Brey et al. 2008a, Brey et al. 2008b, Brey et al. 2009, Brey et al. 2011, Davis et al. 2011, Sudholz et al 2021). In this section, clinopyroxenes from these experiments are compared to the natural samples.

Historically, experiments were initially conducted in the CMAS, FMAS and CFMAS systems (e.g. Boyd 1973, O' Neill and Wood 1979, Perkins and Newton 1981, Gasparik 1984, Harley 1984, Nickel et al. 1985, Nickel and Green 1985, Brey et al. 1986, Krogh 1988). Building on these experiments, additional components were added to systems such as CMAS-Cr, NCMAS, NCMAS-Cr. In addition, natural samples were used in experiments to better simulate the natural environment (e.g. Brey, Köhler and Nickel 1990, Taylor 1998, Yaxley 2000, Brey et al. 2008a, Brey et al. 2008b, Brey et al. 2009, Brey et al. 2011, Davis et al. 2011, Sudholz et al. 2021). Comparisons will be made with experimental samples that contain sodium, as natural samples of mantle clinopyroxene are a major host of sodium as discussed previously.

The experiments in these studies ranged in temperature from 1050 °C to 1755 °C and pressure from 22 kbar to 100 kbar. The Mg# ranged from 0.853 to 0.949 with an average value of 0.900. This range is narrower than the range of the natural database clinopyroxenes of 0.819 to 0.959. The Ca# of experimental clinopyroxene ranges from 0.139 to 0.451 with an average of 0.333. Natural clinopyroxene Ca# ranges from 0.267-0.488 with an average value of 0.415. Experimental clinopyroxene goes to lower Ca# with a noticeably lower average than natural clinopyroxenes.

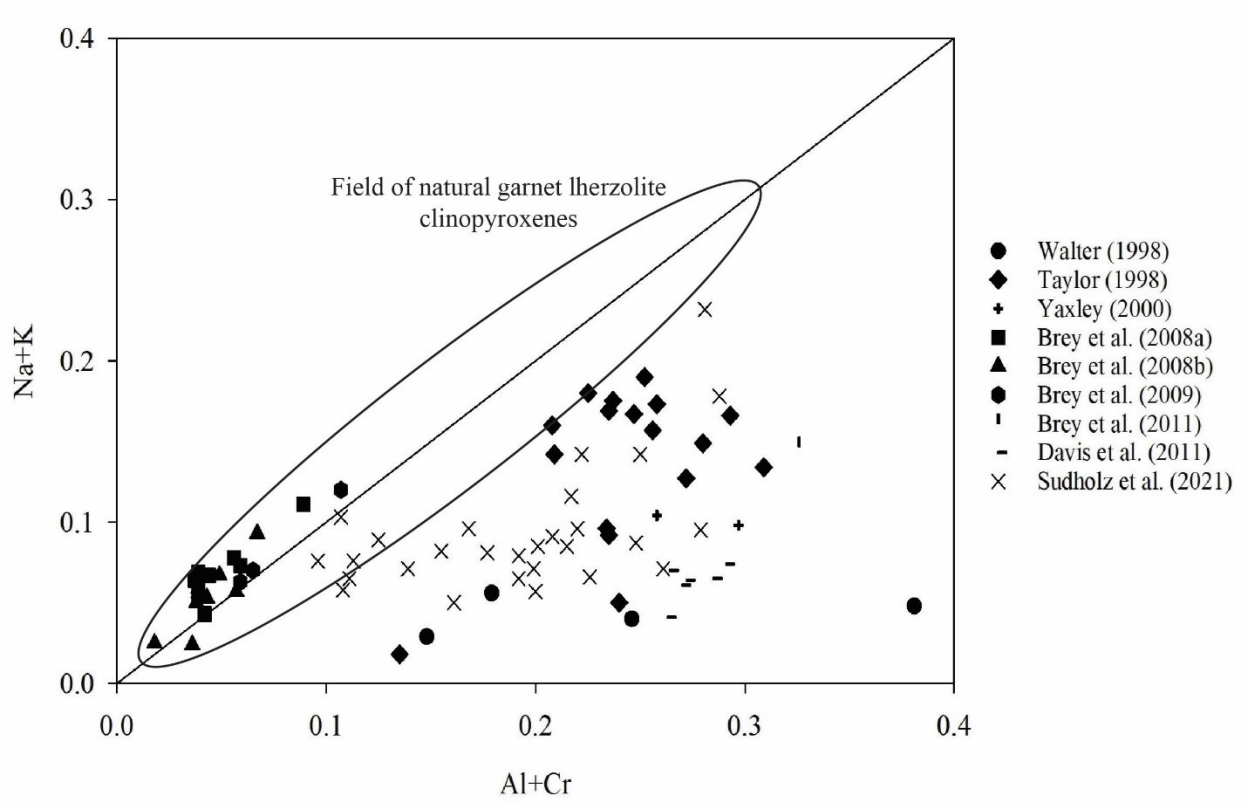

Figure 2.18 Plot of Al+Cr vs Na of clinopyroxene from experimental garnet lherzolites with overlay of natural garnet lherzolite clinopyroxene field from Fig 2.6. There is a one-to-one correlation at Al+Cr and Na values <0.1. At higher values Al+Cr>Na and there is not a one-to-one correlation as seen with natural clinopyroxenes

The experimental clinopyroxenes range from 0.32 wt% to 8.70 wt% Al_2O_3, corresponding to 0.014 to 0.360 Al apfu with an average value of 0.155 apfu. Natural clinopyroxene Al_2O_3 content

varies from 0.24 wt% and 5.70 wt% (0.010 apfu to 0.240 apfu) with an average value of 0.081 apfu. Natural clinopyroxenes have a noticeably lower maximum Al content than the experimental clinopyroxenes. This is most noticeable with tetrahedral Al as the average

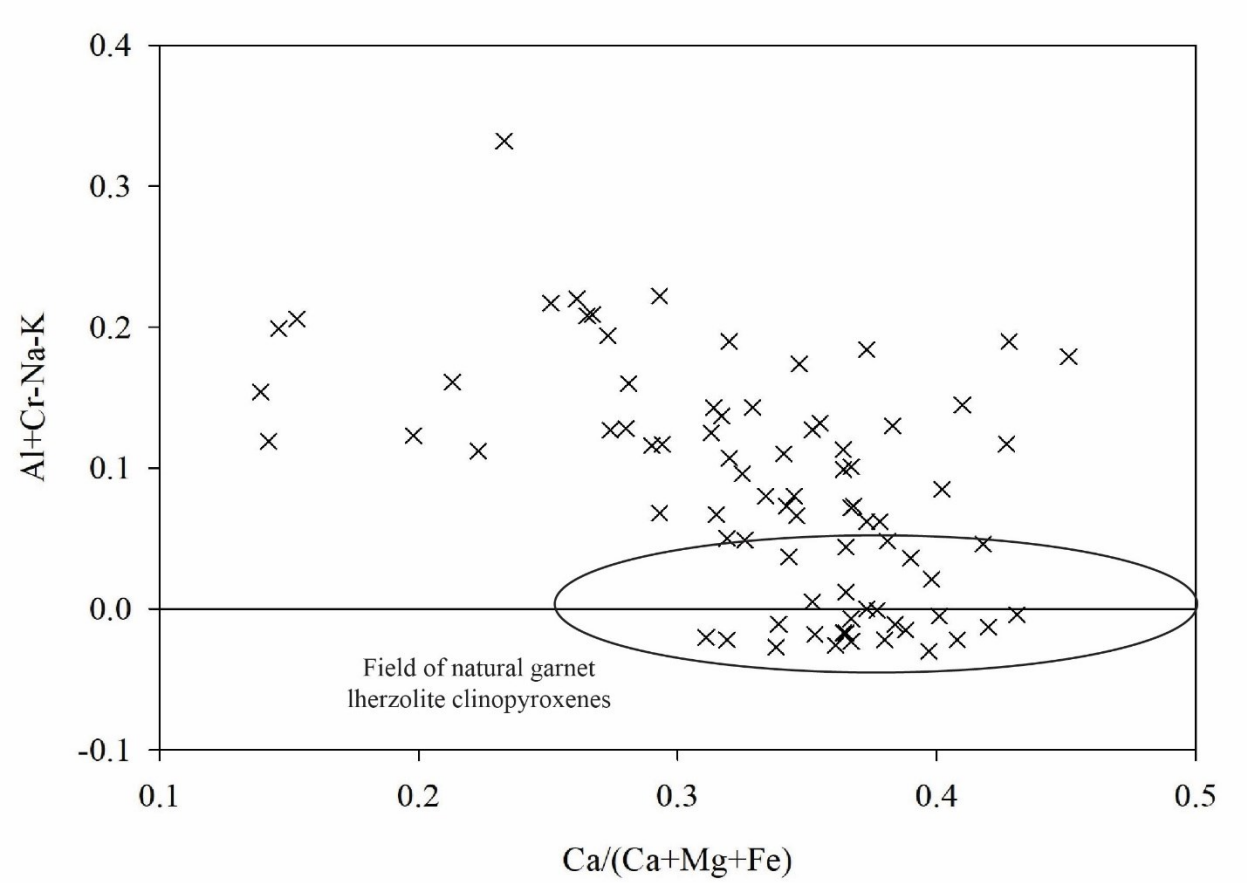

Figure 2.19 Tschermak vs Ca-number of clinopyroxene from experimental garnet lherzolites with field for natural garnet lherzolite clinopyroxenes. Modified after Grütter (2009). When compared with natural samples Al+Cr-Na-K reaches higher values and the majority of the samples are above 0.05. The majority of natural samples are <0.05 Al+Cr-Na-K

value in the experimental clinopyroxenes is 0.059 apfu and natural clinopyroxene has an average value of 0.015 apfu (calculated from Al_T=2-Si). Al_{M1} in experimental samples are also higher than in natural samples (average experimental Al_{M1}=0.096 vs average natural Al_{M1}=0.063). Experimental clinopyroxene Cr_2O_3 varies from 0.05 wt% to 2.19 wt% (0.001 to 0.064 Cr apfu). Natural Cr_2O_3 content varies from 0.17 wt% and 4.40 wt% (0.005 to 0.125 Cr apfu). The

experimental clinopyroxenes do not cover the full range of Cr seen in natural samples. Experimental Na_2O varies from 0.26 wt% to 3.32 wt% (0.018 to 0.232 Na apfu) with an average of 0.091 apfu. Natural Na_2O content varies from 0.22 wt% and 4.22 wt% (0.015 to 0.295 Na apfu) and an average of 0.114 apfu. Natural samples can have higher Na when compared to experimental clinopyroxenes.

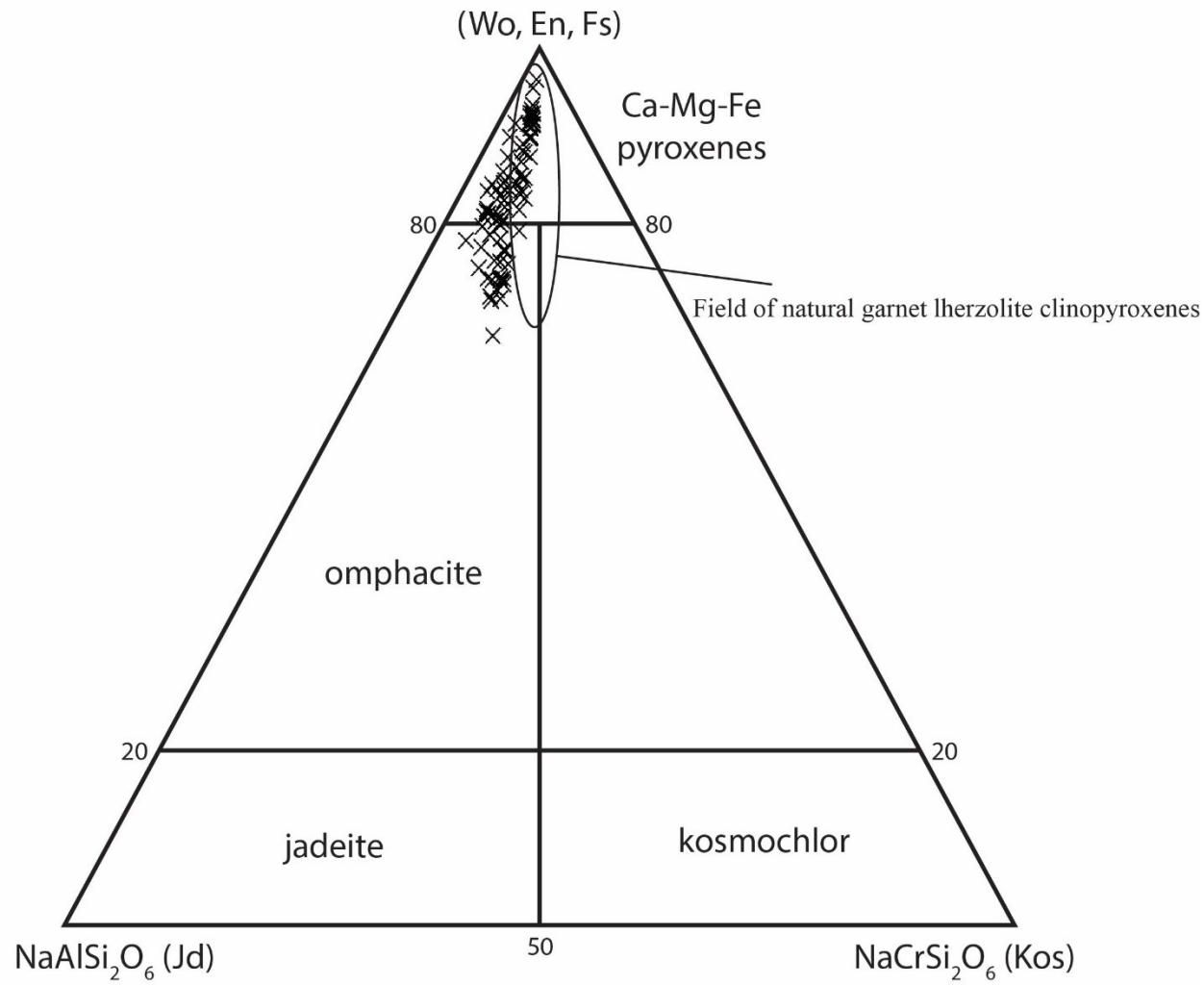

Figure 2.20 Ca-Na clinopyroxene plot for clinopyroxenes from experimental garnet lherzolites with field for natural garnet lherzolite clinopyroxenes. The diagram is modified after Morimoto (1988) with kosmochlor replacing aegirine due to the Cr-rich nature of mantle clinopyroxenes.

Na and Al+Cr have a positive correlation at values ≤0.100 apfu Al+Cr in experimental clinopyroxenes. More aluminous experimental clinopyroxenes have Al+Cr>Na (Figure 2.18). This differs from natural samples, which have a strong positive ~1:1 correlation (Figure 2.6). In contrast, the average (Al+Cr):Na ratio of experimental samples is 2.197, reflecting their higher Al content. Al+Cr-Na-K<0.05 is another criterion of garnet lherzolite clinopyroxene, as discussed previously (Read et al. 2004). Experimental clinopyroxenes have Al+Cr-Na-K ranging from -0.030 to 0.332, with 81.7% >0.05 (Figure 2.19). In the Ca-Mg-Fe pyroxenes-jadeite-kosmochlor diagram, experimental clinopyroxenes are noticeably richer in aluminum and poorer in chromium compared with clinopyroxenes from natural garnet lherzolites (Figure 2.20). In conclusion, much of the experimental composition space overemphasizes high Al, low Cr, low Na compositions that are not consistent with natural garnet lherzolite clinopyroxenes.

2.7 Experimental Clinopyroxene Chemical Changes with Changes in Pressure and Temperature

Both Al and Cr decrease with increasing pressure and temperature in the experimental clinopyroxenes. They differ from natural samples as from 20 to 40 kbar there is a plateau in Al and Cr where pressure approximately remains constant with changing Al (0.150 apfu to 0.400 apfu) and Cr (0.030 apfu to 0.070 apfu) values (Figure 2.21 and 2.22). Al and Cr in natural clinopyroxene decrease in a linear fashion with increasing pressure and temperature (Figures 2.8, 2.9). Na in experimental samples does not appear correlated with pressure or temperature (Figure 2.23). This differs from natural samples where Na correlates with pressure and temperature (Figure 2.10). Al_T and Al_{M1} follow the same trend as total Al, with a plateau Al_T (0.060 apfu to 0.170 apfu) and Al_{M1} (0.100 apfu to 0.200 apfu) at lower pressures (20 to 40 kbar) and a decrease of with increasing Al_T and Al_{M1} pressures (Figure 2.24 and 2.25). Experimental clinopyroxene

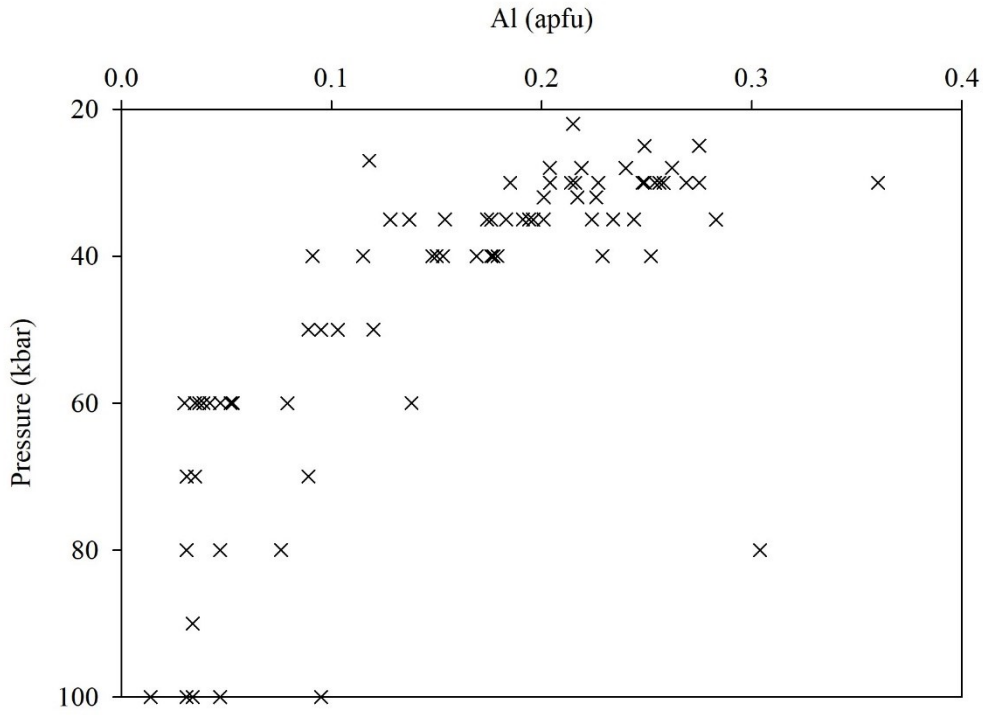

Figure 2.21 Al cations vs experimental pressure for experimental clinopyroxenes

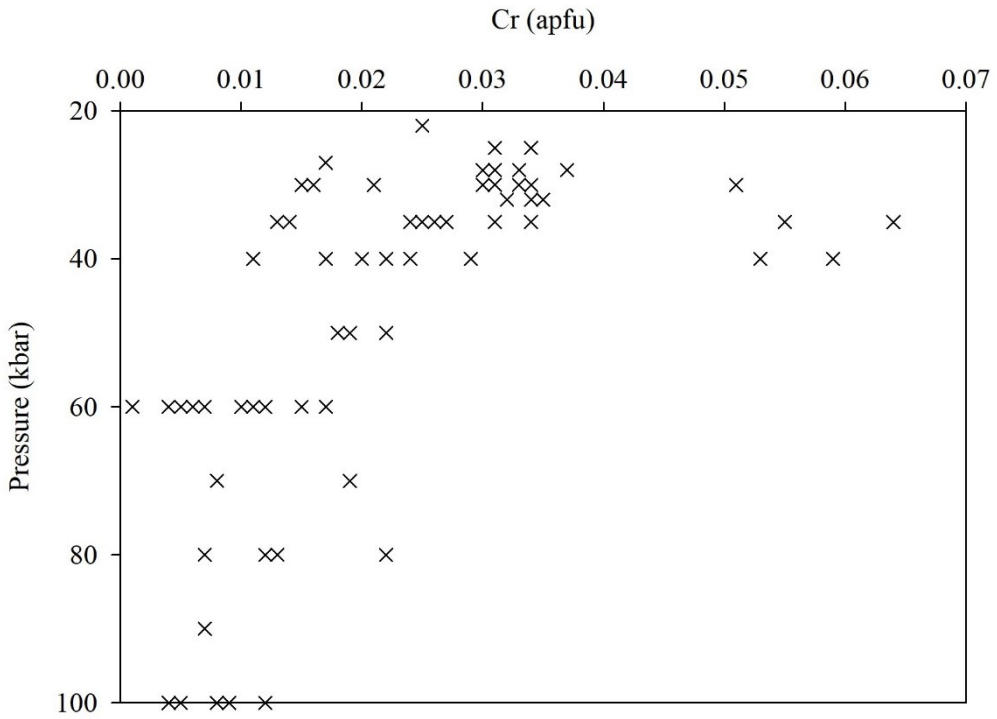

Figure 2.22 Cr cations vs experimental pressure for experimental clinopyroxenes

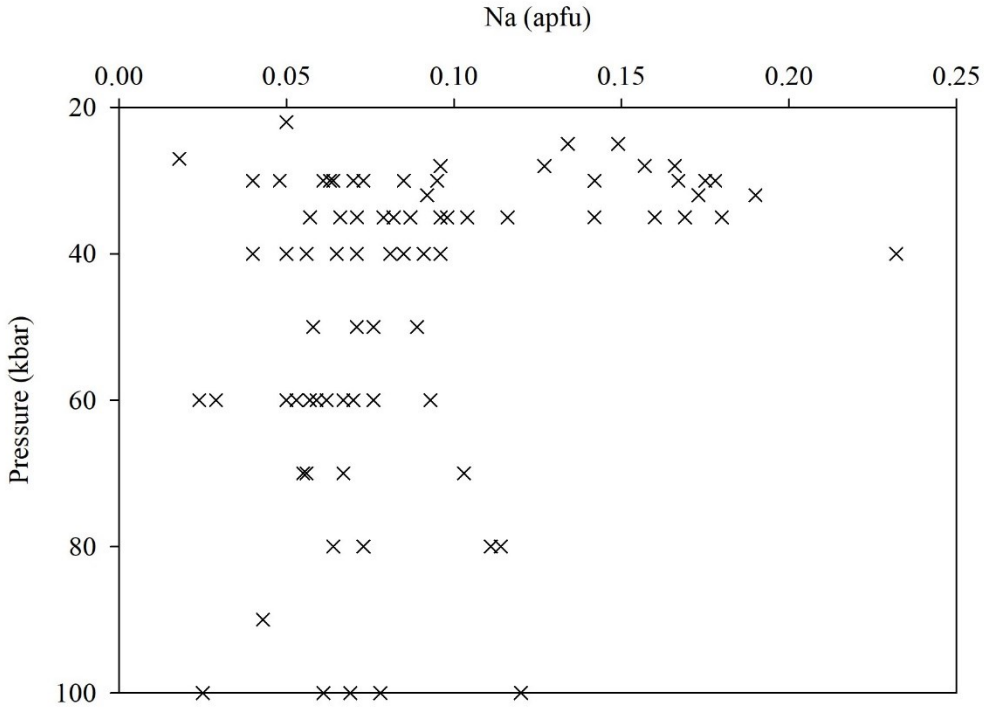

Figure 2.23 Na cations vs experimental pressure for experimental clinopyroxenes

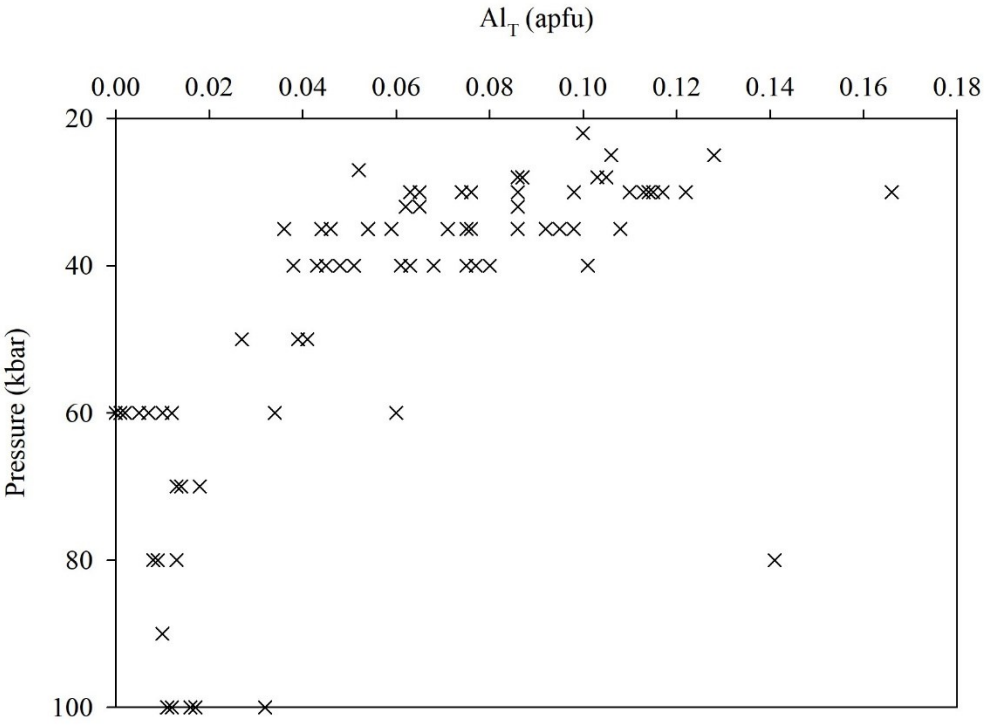

Figure 2.24 Tetrahedral Al cations vs experimental pressure for experimental clinopyroxenes

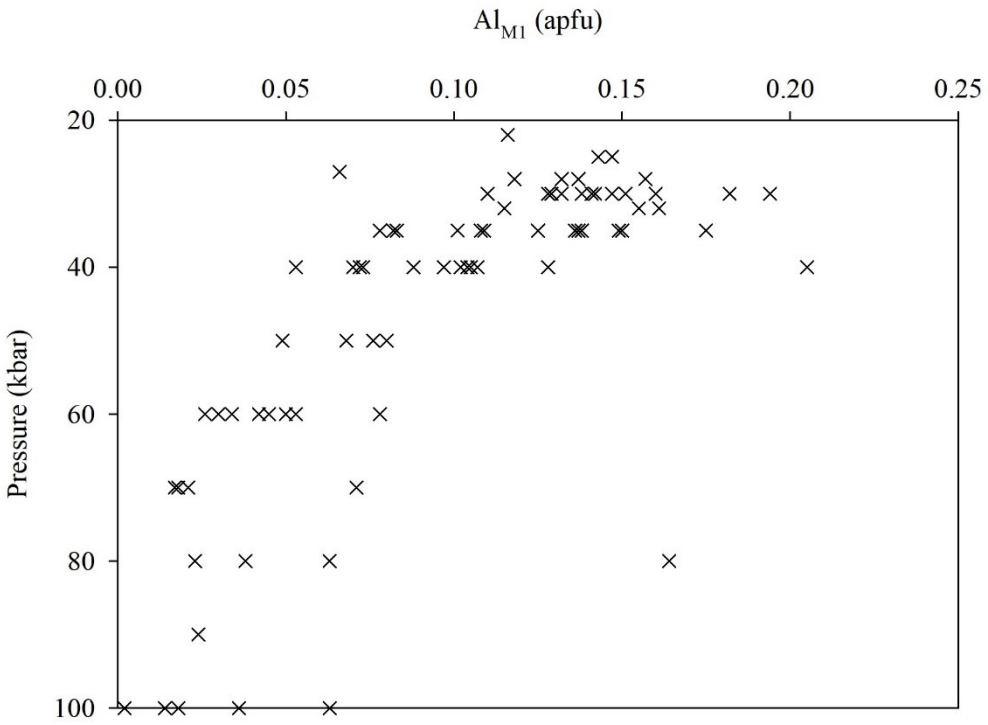

Figure 2.25 M1 Al cations vs experimental pressure for experimental clinopyroxenes

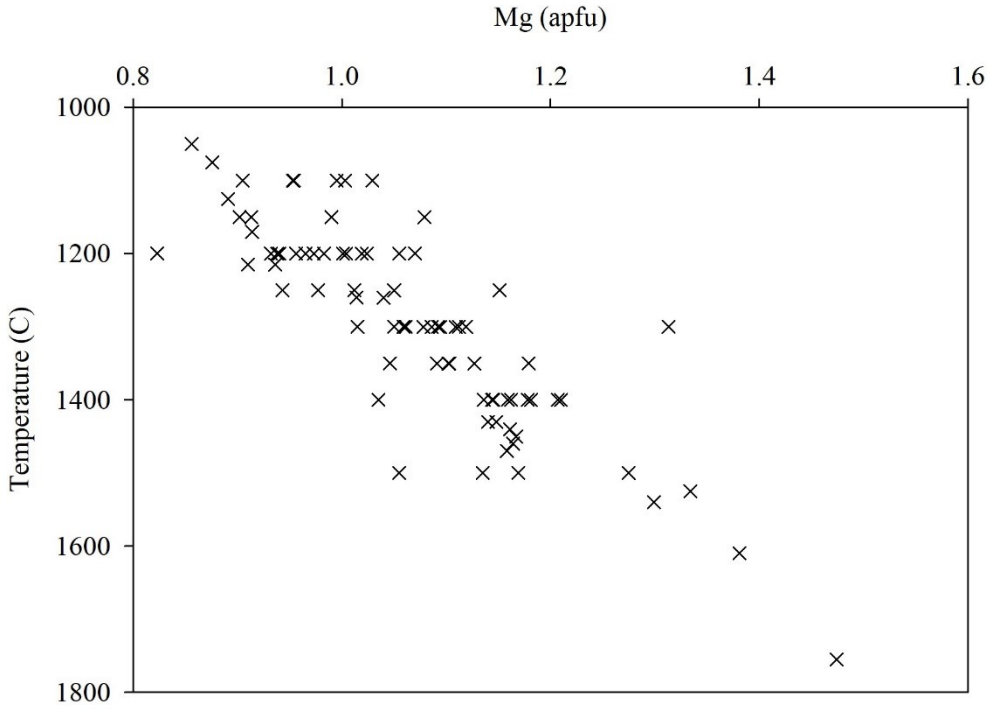

Figure 2.26 Mg cations vs experimental temperature for experimental clinopyroxenes

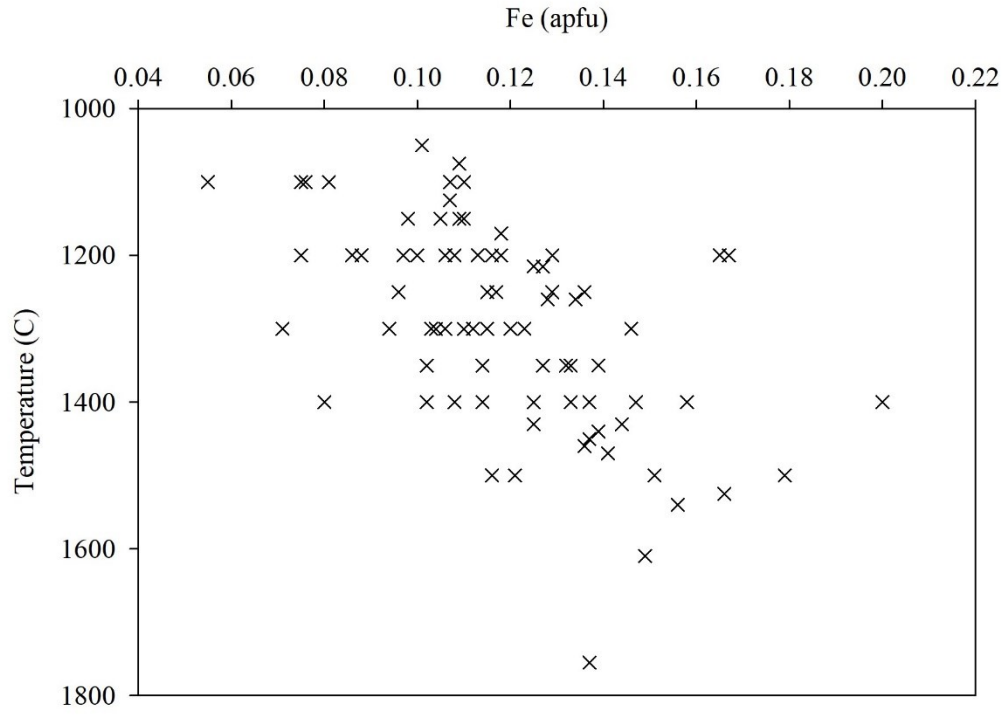

Figure 2.27 Fe^{2+} cations vs experimental temperature for experimental clinopyroxenes

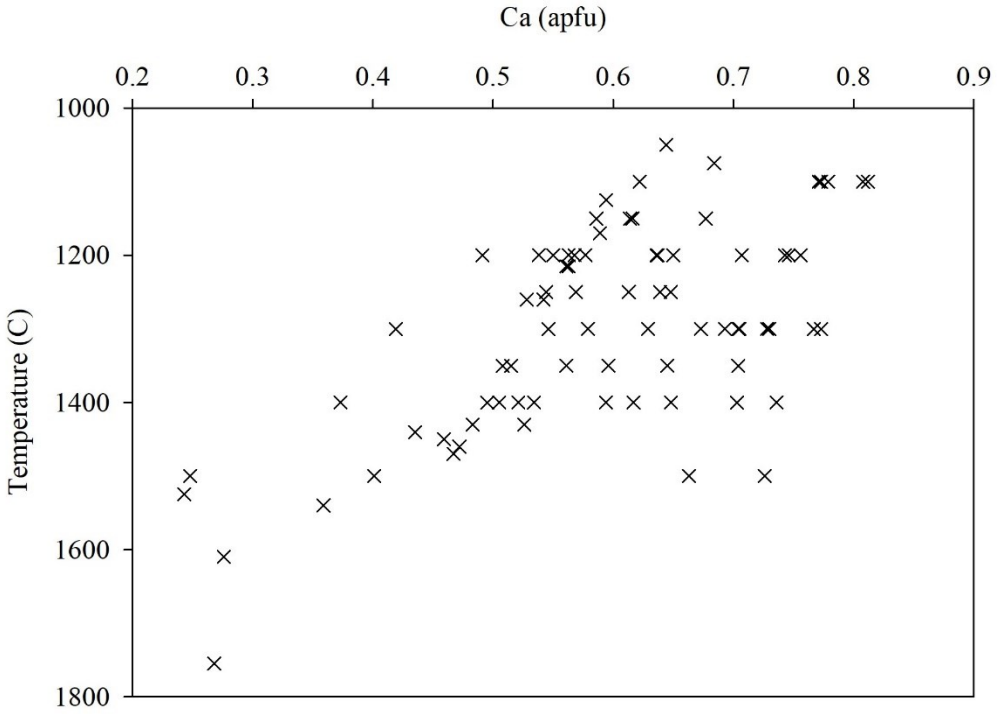

Figure 2.28 Ca cations vs experimental temperature for experimental clinopyroxenes

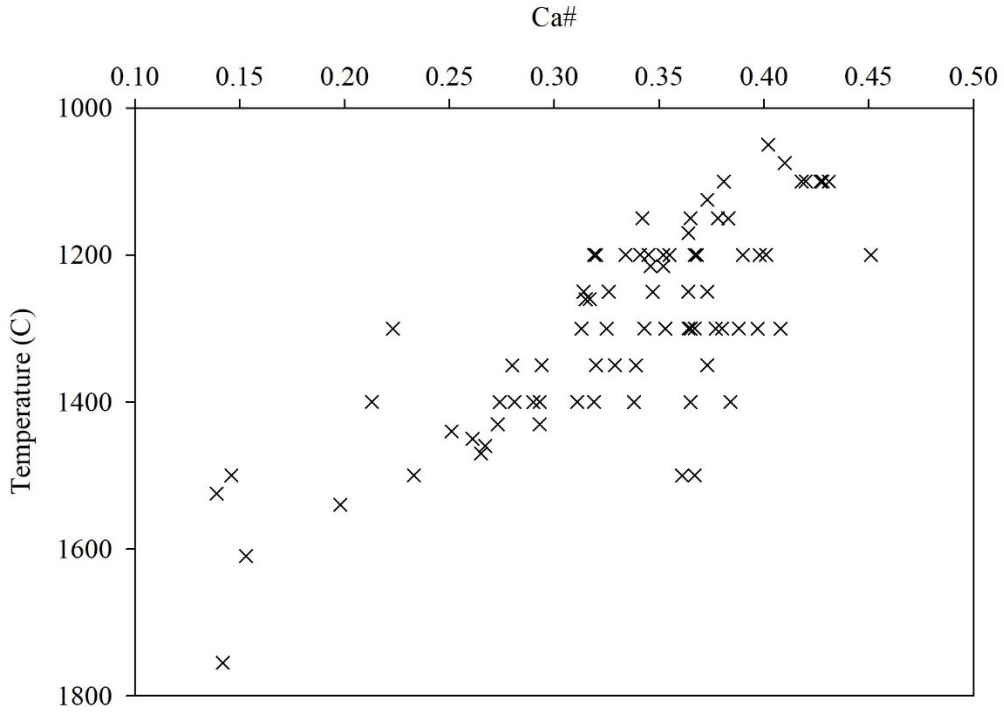

Figure 2.29 Ca# vs experimental temperature for experimental clinopyroxenes

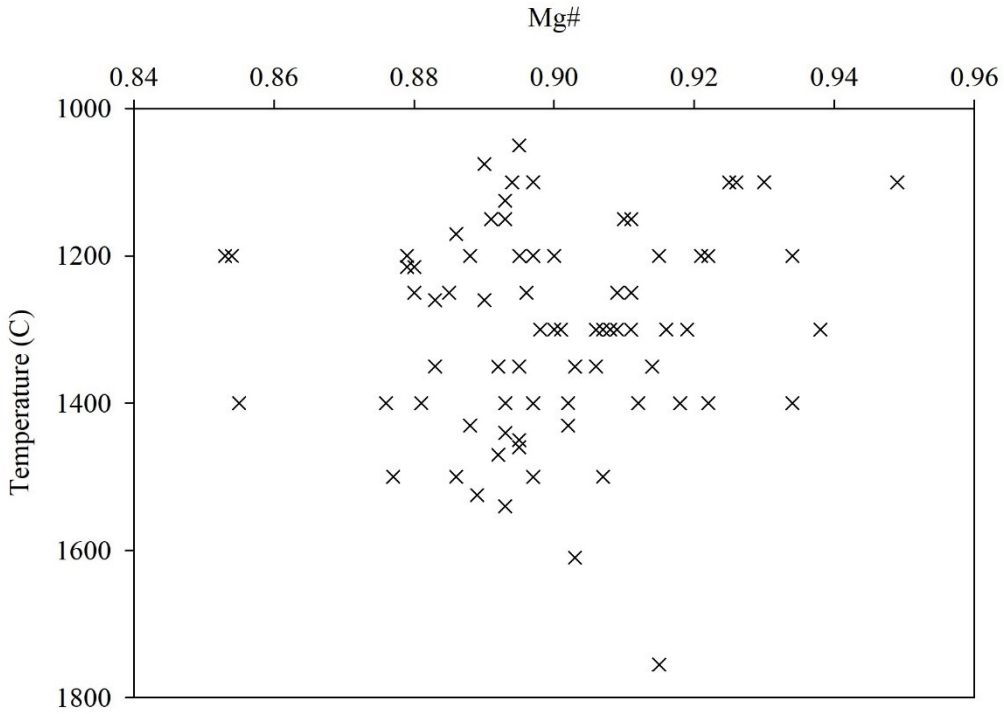

Figure 2.30 Mg# vs experimental temperature for experimental clinopyroxenes

Al_T greatly differs from natural samples as there is a correlation with pressure and temperature in experimental Al_T, as well as Al_T having much higher apfu values as discussed earlier. Experimental clinopyroxene Mg and Fe^{total} increase with temperature and pressure, Ca decreases with increasing temperature and pressure (Figures 2.26, 2.27, 2.28), consistent with natural samples (Figures 2.13, 2.14, 2.15). Experimental Ca# decreases with increasing temperature, matching natural samples (Figure 2.29). Mg# in experimental clinopyroxene does not have a clear correlation with temperature or pressure (Figure 2.30). This differs from natural clinopyroxenes where Mg# decreases with increasing temperature and pressure (Figure 2.16).

2.8 Discussion and Conclusions

There is a clear disconnect between natural and experimental samples in their Al, Cr and Na contents. Ca, Mg and Fe^{2+} are more similar between natural and experimental samples as experimental clinopyroxenes Ca, Mg and Fe^{2+} are within the range of natural samples. The elevated Al in experimental samples give rise to a higher Al_T, which incorporated as endmembers such as Ca-Tschermak, CaCr-Tschermak and esseneite. Natural samples have low Al_T with the majority of Al located on the M1 site. Natural samples have higher Na than experimental samples, which charge balances with Al located on the M1 site giving rise to a jadeite component in natural clinopyroxenes. Cr is higher in natural samples and correlates with Na in natural samples, along with Al, which represents the kosmochlor component. The lower Na and higher Al_T in experimental samples means experimental clinopyroxene has a higher CaCr-Tschermak component than do natural samples.

This disconnect between natural and experimental clinopyroxenes may explain why the Cr in clinopyroxene barometer of Nimis and Taylor (2000) underestimates at higher pressures as the basis of this barometer is the activity of CaCr-Tschermak. Natural samples have a lower CaCr-

Tschermak components due to the lower Al_T. Experimental samples by comparison will have larger CaCr-Tschermak component due to the higher Al_T. This disconnect will be discussed in the next chapter of this thesis.

Chapter 3 Thermodynamic Modelling of Clinopyroxene

3.1 Introduction

At the present time, thermodynamic modelling is a useful tool that uses thermodynamic data to model phase diagrams, multiple-reaction thermobarometry and mineral compositions for a given bulk composition at specified P-T conditions. Examples of software that undertake this modelling includes THERMOCALC, Perple_X and THERIAK-DOMINO (Powell and Holland 1988, Connolly 2005, de Capitani & Petrakakis 2010, respectively). Specific focus will be given to THERMOCALC in this study, as recent developments in THERMOCALC have provided thermodynamic models for mantle peridotites. THERMOCALC was first provided in 1988 as a software tool for addressing thermobarometry problems (Powell and Holland 1988). Since then, there has been many thermodynamic dataset and activity-compositions model updates for THERMOCALC.

The first thermodynamic model to deal with calculating phase relations in peridotite is Jennings and Holland (2015). Jennings and Holland (2015) model the system NCFMASOCr from 0.001 to 60 kbar and from 800 °C to liquidus temperatures. This model is built upon the model of Green et al. (2012a) which modelled orthopyroxene, clinopyroxene and garnet in the system CMAS. The next updated model is Holland et al. (2018) which builds upon Jennings and Holland (2015) in the system KNCFMASHTOCr. The model calculates phase relations in bulk compositions ranging from peridotite to granite, from 0.001 to 70 kbar and from 650 °C to peridotite liquidus

temperatures. The most recent model is Tomlinson and Holland's (2021) model which is based on model of Holland et al. (2018). Tomlinson and Holland's (2021) updated model is specifically for calculating peridotite phase relations and melt compositions from 0.01 to 60 kbar and from 600 °C to the peridotite liquidus in the KNCFMASTOCr system.

These recent updates in THERMOCALC provide the ability to model multiple-reaction thermobarometry and mineral compositions for garnet lherzolites from different bulk compositions and these will be related to the single grain clinopyroxene thermobarometer. These models will also be compared with natural and experimental samples along with the geothermobarometer calculations from these samples to explore recalibrating the existing single grain clinopyroxene barometer.

3.2 Clinopyroxene in THERMOCALC

3.2.1 Clinopyroxene endmembers in THERMOCALC database and models

Clinopyroxene has been modelled in numerous studies (Green et al. 2012, Green et al. 2016, Jennings and Holland 2015, Holland et al. 2018 and references therein). Holland and Powell (2011) provide thermodynamic data for the clinopyroxene endmembers diopside, hedenbergite, Ca-Tschermak pyroxene, Ca-Eskola pyroxene, clinoenstatite, clinoferrosilite, jadeite and kosmochlor (Pyroxenes and pyroxenoid group in their Appendix 1). Through their subsequent papers, the clinopyroxene solution model has been updated in Green et al. (2012a) and Jennings and Holland (2015). Green et al. (2012a) specifically updated the model Ca-Tschermak's clinopyroxenes (Al substitution), Jennings and Holland (2015) state clinopyroxene is modelled after Green et al. (2012a) and updated the model by adding data for Fe^{2+}, Na, Cr and Fe^{3+} substitution. The most recent version of clinopyroxene thermodynamic data and models comes

from Holland et al. (2018), with clinopyroxene being modelled after Green et al. (2012a) and Jennings and Holland (2015), with additions for Ti and K-jadeite.

3.2.2 Ca-Tschermak Substitution in THERMOCALC

The Ca-Tschermak component in clinopyroxene can be used as a geobarometer (e.g. Nimis 1998), however, its use as a geobarometer depends on the quality of thermodynamic data as well as diopside-cats solid solution. The Al-Si distribution between tetrahedral sites is separated between disordered and ordered (Green et al. 2012a) based on a degree of short-range ordering (Cohen 1986, Benisek et al. 2007). Short-range order is defined as the probability of finding Al-Si next nearest neighbour pairs in the tetrahedral (T) site. Each T site is surrounded by four nearest-neighbour T-sites, with two of these four sharing common oxygens with the regarding T site and belong to the same tetrahedral chain. In completely ordered cats, nearest neighbour pairs are Al and Si (Cohen and Burnham 1985). In disorder cats, nearest neighbour pairs are Al-Al and Si-Si (Cohen and Burnham 1985).

To account for this ordered and disordered cats, Green et al. (2012a) split the tetrahedral site into T1 and T2 and adopted an order parameter ($Q = x_{Al}^{T2} – x_{Al}^{T1}$) in THERMOCALC. Two endmember compositions were then added:

1) an ordered Ca-Tschermak's pyroxene (catso in Green et al. 2012a appendix), where Al is only partitioned on T2 and Si is only partitioned on T1.

2) a disordered Ca-Tschermak's pyroxene (catsd in Green et al. 2012a appendix), where Al and Si are partitioned between T1 and T2 ($Si_{T1}=1/2$, $Al_{T1}=1/2$ and $Si_{T2}=1/2$, $Al_{T2}=1/2$).

To facilitate later expansion of the THERMOCALC dataset, the Al-Si ordering in cats pyroxene was calculated using the symmetric formalism of Holland and Powell (1996a and 1996b) (Green et al. 2012a).

In the most recent versions of THERMOCALC (Jennings and Holland 2015 and Holland et al. 2018) they state clinopyroxene is modelled after Green et al. (2012a), with further elemental additions. However, Jennings and Holland (2015) and Holland et al. (2018) both did not consider the ordered and disorder cats as they only have one tetrahedral site in their data, treating the Ca-tschermak component as ordered cats (e.g. Table A3 Holland et al. 2018).

3.2.3 Fe^{2+}, Na, Fe^{3+}, Cr, Ti and K Substitution in THERMOCALC

Fe^{2+}, Na, Fe^{3+} and Cr were added to the clinopyroxene model by Jennings and Holland (2015). Fe^{3+} and Cr were added to the model using a cats-like components, with Fe^{3+} and Cr substituting on the M1 site in place of Al. The endmembers used are Ca-esseneite and Cr-diopside (Table A3 in Jennings and Holland 2015). Cr-diopside is used as a geobarometer (Nimis and Taylor 2000) and it's use as a geobarometer depends on the quality of thermodynamic data.

Na and K were added to the model by Jennings and Holland (2015) and Holland et al. (2018), respectively. The endmembers added were jadeite and K-jadeite, to accommodate for Na, K and excess Al on the M1 site relative to the T site (Jennings and Holland 2015, Green et al. 2016, Holland et al. 2018). Ti was added to the model by Holland et al. (2018), as Ca-buffonite (Table A3 in Holland et al. 2018).

3.3 Modelling of Garnet Lherzolites in THERMOCALC

3.3.1 Model, Dataset and Bulk Compositions

Phase relationships and mineral chemistry for garnet lherzolites were modelled in THERMOCALC after the model of Holland et al. (2018) using the updated dataset ds634 from Tomlinson and Holland (2021). Fertile lherzolite compositions KLB-1 and KR4003 are used in the modelling. One depleted bulk composition is used, modified after Workman and Hart (2005) (Table 3.1).

Table 3.1 Bulk compositions used in THERMOCALC modelling. All bulk compositions are normalized to 100 for use in THERMOCALC

		SiO_2	TiO_2	Al_2O_3	Cr_2O_3	FeO	MgO	CaO	Na_2O	K_2O	O	SUM	Reference
KLB-1	mol%	38.46	0.07	1.77	0.11	5.88	50.53	2.82	0.25	0.01	0.10	100	Takahashi 1986
KR4003	mol%	39.38	0.11	2.20	0.14	5.89	48.75	3.24	0.19	0.05	0.06	100	Walter 1998
Depleted	mol%	38.68	0.08	2.03	0.19	5.92	49.95	2.94	0.11	0.003	0.10	100	Workman and Hart 2005

THERMOCALC produces an output based on the scripts the user chooses. This includes thermodynamic data such as Gibbs free energy and activity for endmembers at specific pressures and temperatures. THERMOCALC can also calculate the mode percentages of minerals along with the chemistry of said minerals at specific PT. The P-T space explored in this study was 20 to 70 kbar and 1000 °C to 1700 °C, with pressure and temperature increments varied by 5 kbar and 100 °C, respectively.

3.3.2 Model Mineral Chemistry and Chemical Changes with Pressure and Temperature

THERMOCALC calculates the compositions of minerals at a given PT for a predetermined bulk composition. This section will focus on the calculated mineral compositions as they evolve with changing PT conditions.

The majority of modelled clinopyroxenes from the bulk compositions KLB-1, KR4003 and Workman and Hart (2005) depleted are below the 0.5 wt% Cr_2O_3 cut off in Ramsay's (1992) diagram (Figure 3.1), which is one of the filters used for natural clinopyroxene data (Chapter 2). Therefore, these clinopyroxenes would not be considered to be from garnet lherzolites. This highlights a concern in terms of the clinopyroxene solution model. Al_2O_3 in Ramsay's (1992) diagram ranges from 0 wt% to 4 wt% for Cr_2O_3 from 0.5 wt% to 2.25 wt% and from 0 wt% to 5 wt% Al_2O_3 for Cr_2O_3 values >2.25 wt% for garnet peridotites. The majority of modelled clinopyroxenes have less than 4 wt% Al_2O_3 (Figure 3.1). The other discrimination plot used by Nimis and Taylor (2000) is Nimis' (1998) MgO vs Al_2O_3 wt%. Natural clinopyroxene that plots in Ramsay and Tompkins' (1994) garnet peridotite field are plotted onto the MgO vs Al_2O_3 wt% diagram to separate clinopyroxenes from garnet peridotites and low Al_2O_3, low MgO, metasomatized, garnet-free peridotites. All the modelled clinopyroxenes plot on the high Al_2O_3 side of Nimis' (1998) plot. The modelled MgO wt% and Al_2O_3 wt% both go to higher values than the values used by Nimis' (1998) diagram (Figure 3 in Nimis 1998).

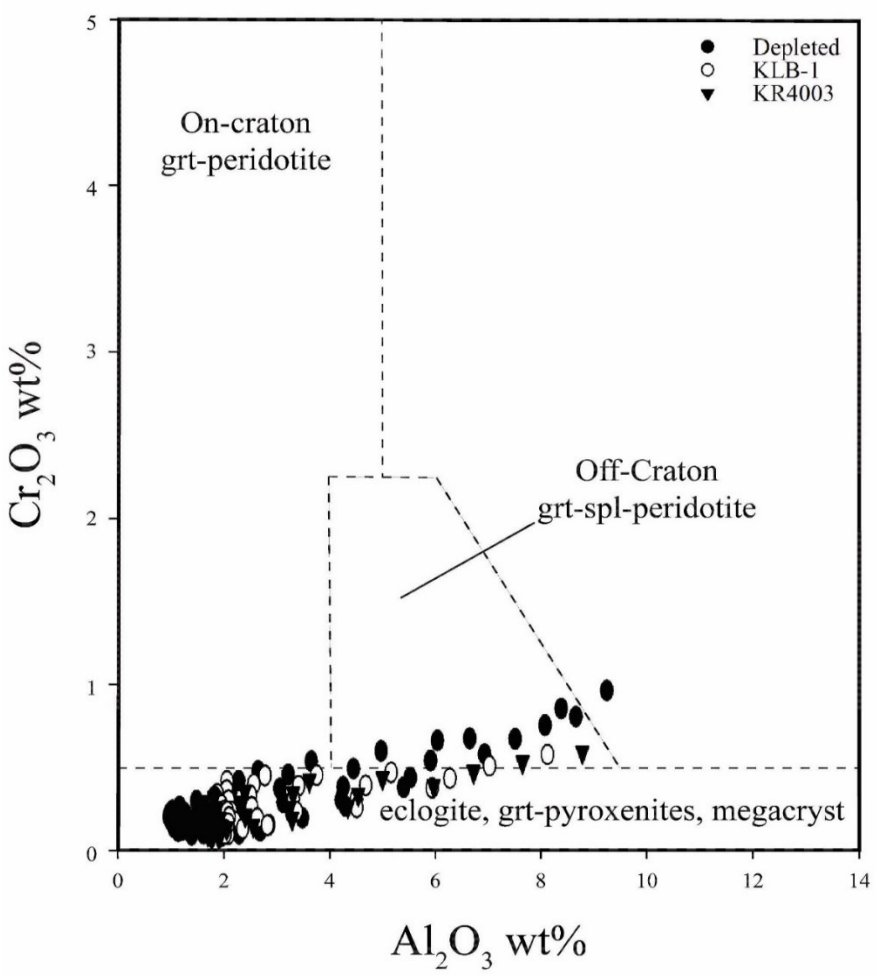

Figure 3.1 Cr_2O_3 vs Al_2O_3 wt% clinopyroxene classification of Ramsay (1992) with modelled garnet lherzolite clinopyroxene from three different bulk compositions from 20-70 kbar and 1000-1700 °C

3.3.3 Cation variation with P and T

Ca# in modelled clinopyroxene ranges from 0.155-0.427 with the compositions being similar between all three used bulk compositions. Ca# decreases with increasing T in the modelled samples (Figure 3.2), consistent with trends for both natural and experimental samples.

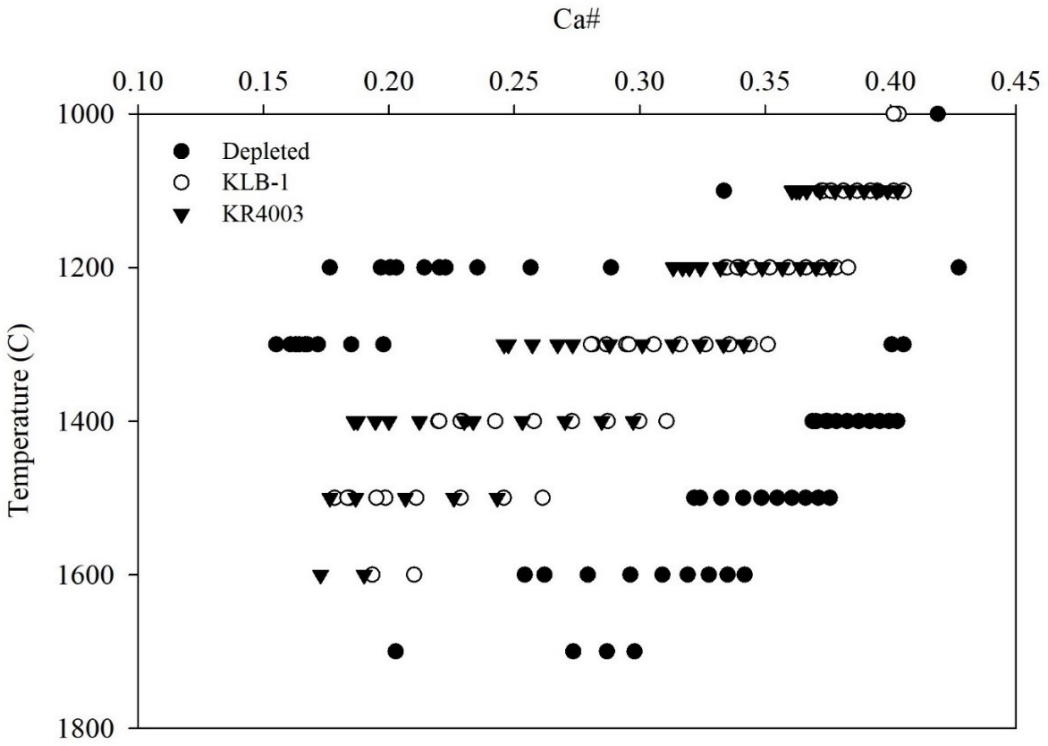

Figure 3.2 Ca# vs temperature for PT modelled garnet lherzolite clinopyroxenes. The variation in Ca# at constant temperature is due to different pressures

Al+Cr-Na-K of modelled samples range from -0.060 to 0.383 with an average value of 0.032 between the three bulk compositions (Figure 3.3). Al+Cr-Na-K values <0.05 (per 6 oxygen) are assessed as being derived from garnet lherzolites. Al+Cr-Na-K clinopyroxene values >0.05 are assessed as being derived from spinel lherzolites (Read et al. 2004). A large proportion of the modelled clinopyroxene have Al+Cr-Na-K>0.050, unlike the natural data where almost all the natural samples were between 0.050 and -0.050 (Figure 2.7).

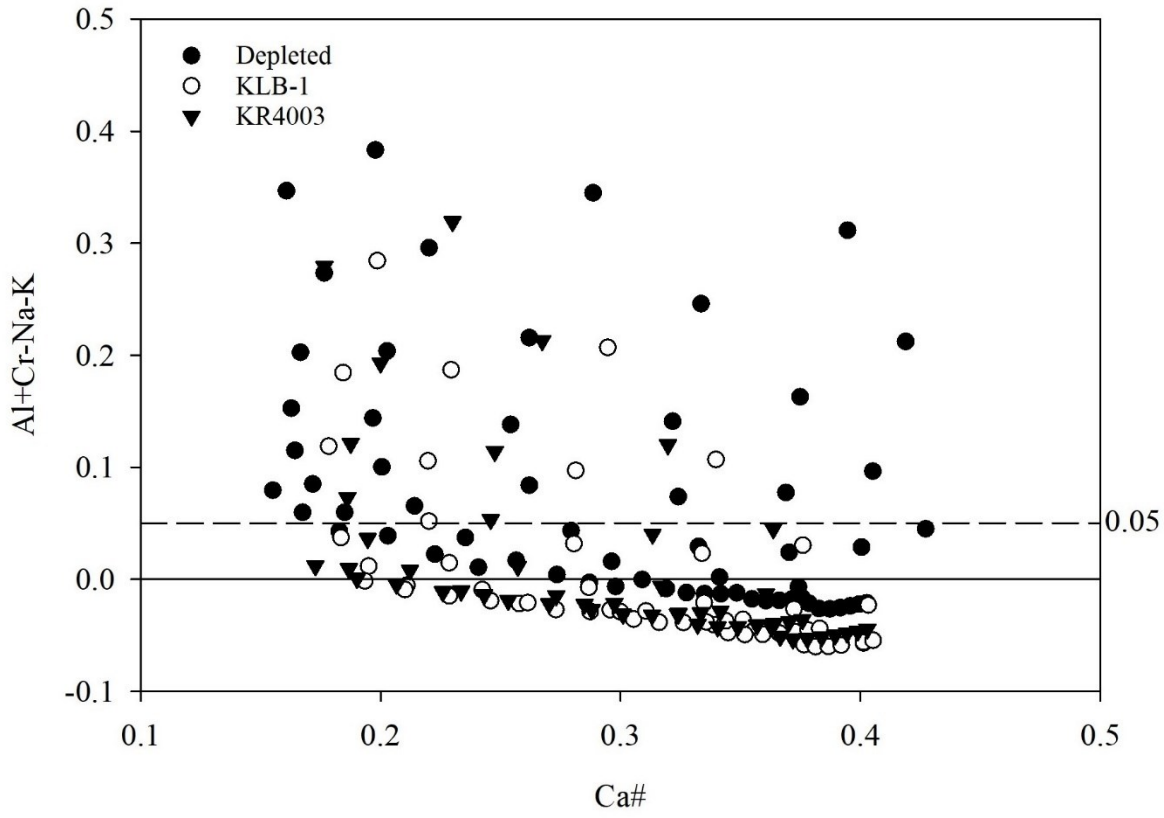

Figure 3.3 Tschermak vs Ca-number for PT modelled garnet lherzolite clinopyroxenes. Modified after Grütter (2009)

The Mg# of modelled clinopyroxene range from 0.893 to 0.940 with an average value of 0.919. Mg# increases with increasing P in modelled clinopyroxene (Figure 3.4), in contrast to the trend for natural samples, where Mg# decreases with increasing PT (Figure 2.16). Al_2O_3 contents in modelled clinopyroxenes vary from 1.005 wt% to 9.234 wt% with corresponding Al cations ranging from 0.0427 apfu to 0.3864 apfu. As outlined above, the Al content in the modelled clinopyroxenes is noticeable higher than in natural samples discussed earlier and appears more like experimental clinopyroxenes with higher Al. Al cations decrease with increasing pressure in the modelled samples (Figure 3.5). Temperature and clinopyroxene mode do not appear to affect the Al concentration as strongly as pressure.

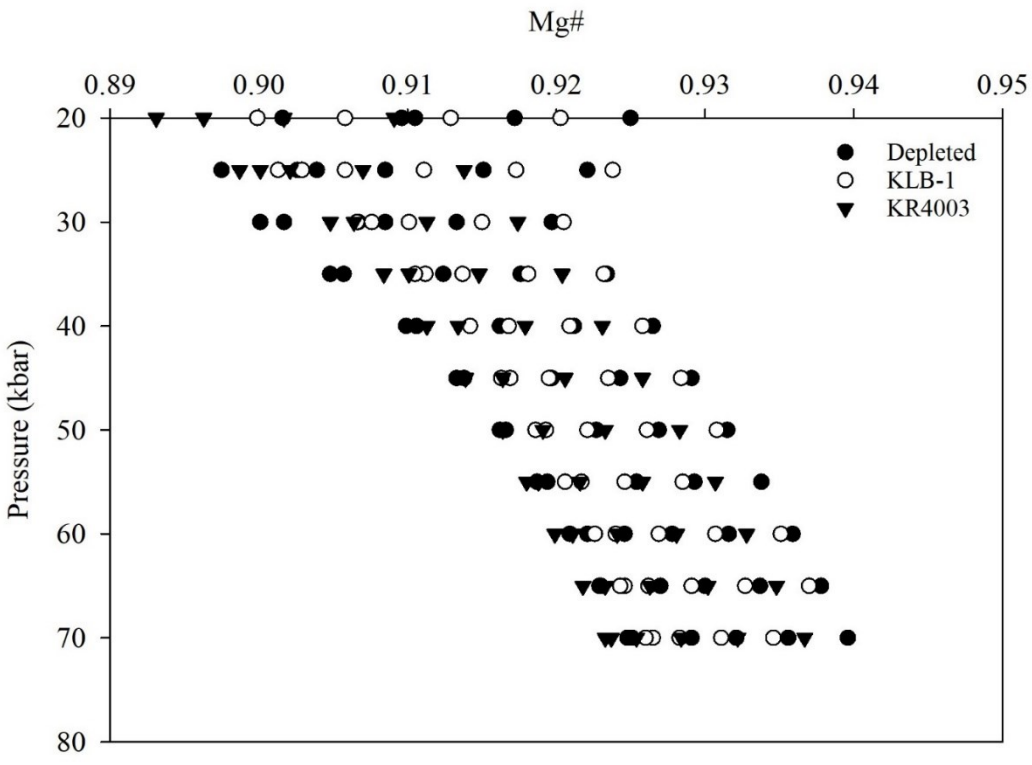

Figure 3.4 Mg# in clinopyroxene vs pressure for PT modelled garnet lherzolite clinopyroxenes. The variation in Mg# at constant pressure is due to different temperatures

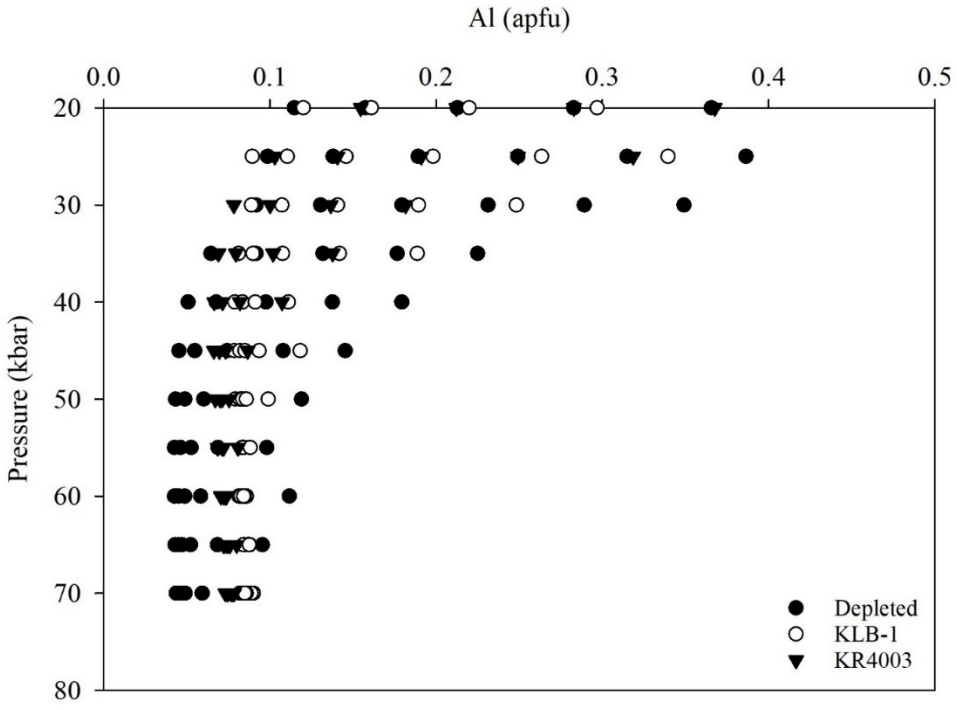

Figure 3.5 Al cations vs pressure for PT modelled garnet lherzolite clinopyroxenes. The variation in Al at constant pressure is due to different temperatures

Cr_2O_3 content in modelled clinopyroxenes varies from 0.077 wt% to 0.959 wt% with the majority of the samples being below 0.5 wt% (Figure 3.1). Corresponding Cr cations range from 0.0021 apfu to 0.0269 apfu. Cr cations decrease with increasing pressure in the modelled samples (Figure 3.6). Temperature and clinopyroxene mode do not appear to affect the Cr concentration as strongly as pressure. Na_2O content varies from 0.37 wt% to 2.15 wt% with corresponding Na cations ranging from 0.025 apfu to 0.151 apfu. Na cations decrease with increasing temperature and mode (Figure 3.7). Pressure does not seem to have a large effect on Na cations in modelled clinopyroxenes. Na and Al+Cr do not appear to be positively correlated in modelled clinopyroxenes, unlike the strong correlation between Na and Al+Cr seen for natural samples (Figure 2.6).

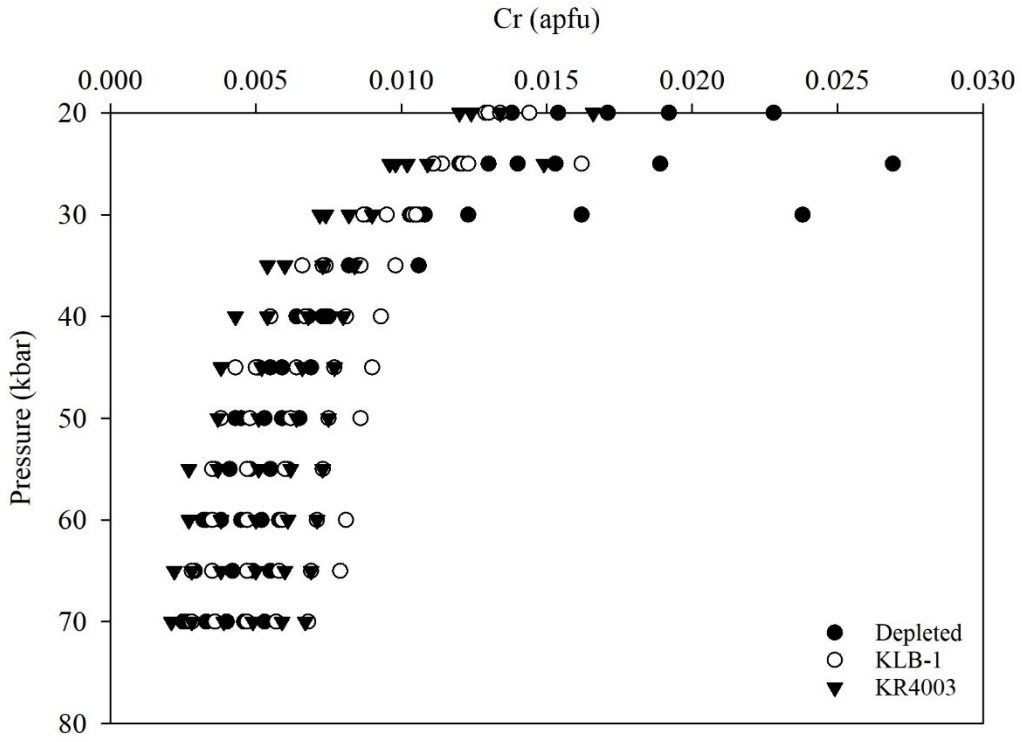

Figure 3.6 Cr cations vs pressure for PT modelled garnet lherzolite clinopyroxenes. The variation in Cr at constant pressure is due to different temperatures

When Al is separated into Al_{M1} and Al_T (using the formula $Al_T = 2 - Si$ and $Al_{M1} = Al - Al_T$) there is a strong correlation between Al_{M1} and Al_T at high Al values. This suggests that THERMOCALC favours Al as a tschermak component in clinopyroxene. This differs from natural samples as clinopyroxene from natural garnet lherzolites has a higher jadeite and kosmochlor component as seen from the Na:Al+Cr ratio of ~1 (Figure 2.6).

MgO content varies from 17.06 wt% to 28.17 wt% (0.924 to 1.470 Mg apfu), with Mg increasing with increasing temperature in modelled clinopyroxene (Figure 3.8).

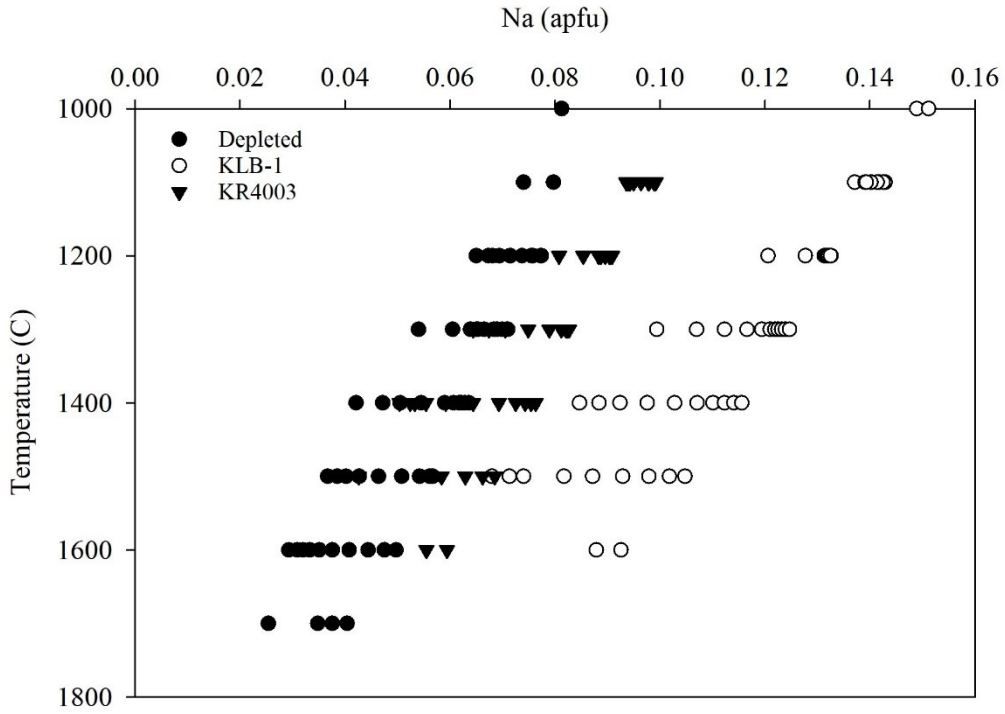

Figure 3.7 Na cations vs temperature for PT modelled garnet lherzolite clinopyroxenes. The variation in Na at constant temperature is due to different pressures

CaO content varies from 7.46 wt% to 19.68 wt% (0.284 to 0.768 Ca apfu), with Ca decreasing with increasing temperature (Figure 3.9). FeO ranges from 2.69 wt% to 5.33 wt% (0.064 to 0.141 Fe apfu), with Fe^{2+} increasing with increasing temperature (Figure 3.10). The trend in Mg, Ca and Fe^{2+} for the modelled clinopyroxenes agree with natural samples with temperature (Figures 2.13, 14, 15).

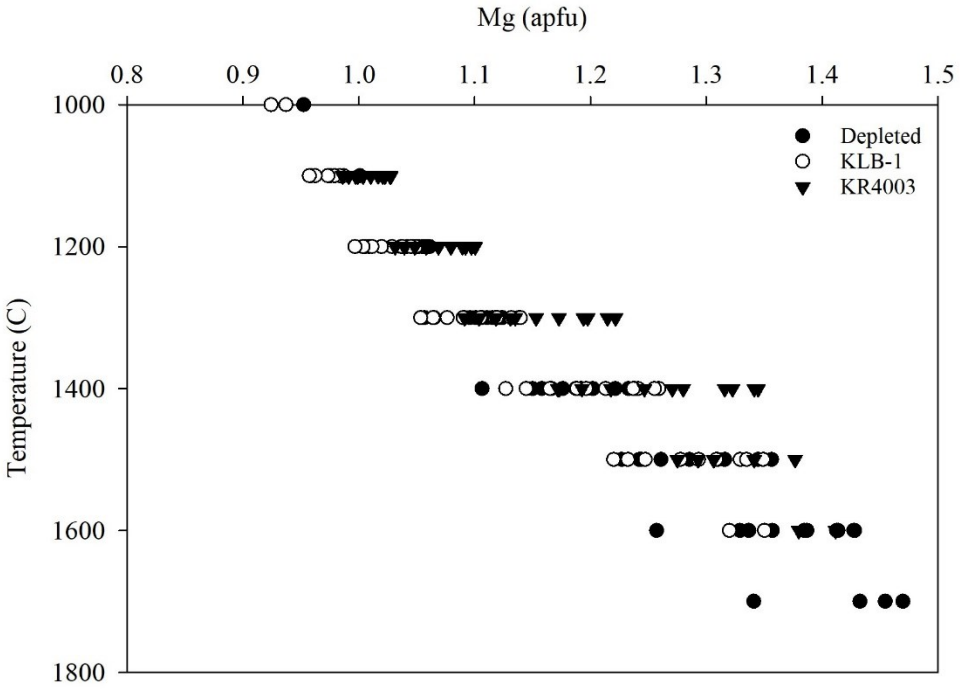

Figure 3.8 Mg cations vs temperature for PT modelled garnet lherzolite clinopyroxenes. The variation in Mg at constant temperature is due to different pressures

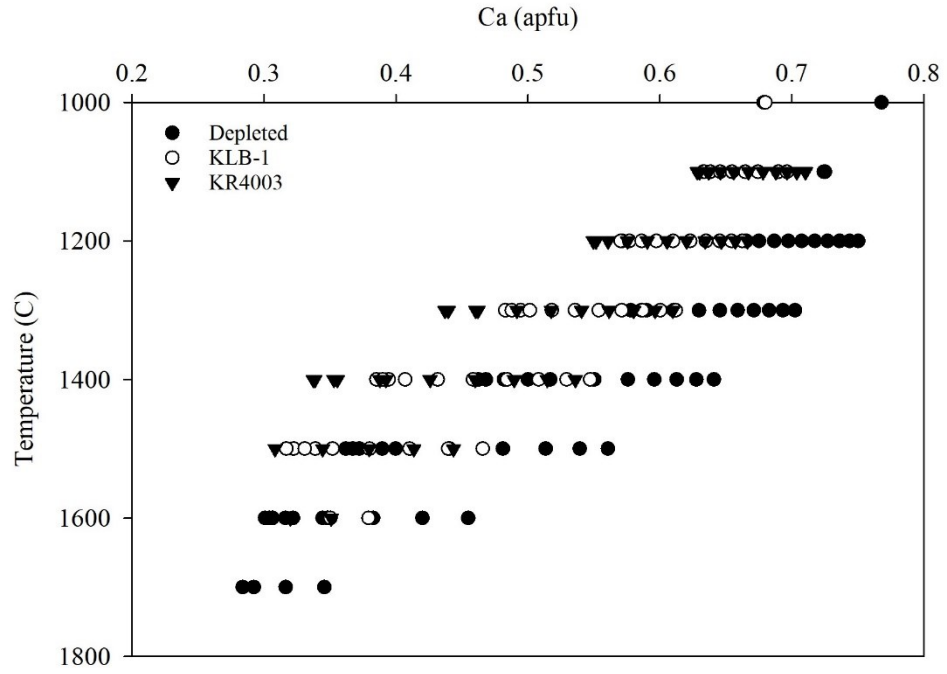

Figure 3.9 Ca cations vs temperature for PT modelled garnet lherzolite clinopyroxenes. The variation in Ca at constant temperature is due to different pressures

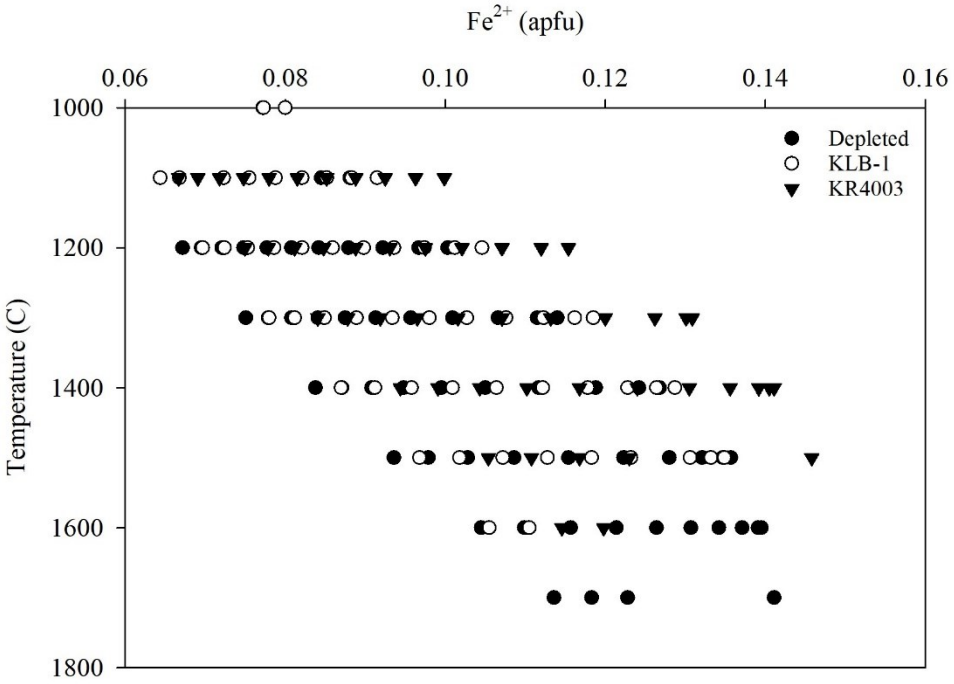

Figure 3.10 Fe^{2+} cations vs temperature for PT modelled garnet lherzolite clinopyroxenes. The variation in Fe^{2+} at constant temperature is due to different pressures

3.3.4 Modelled Clinopyroxene on a 40 mW/m^2 and 45 mW/m^2 Geotherm

Next, phase compositions were calculated for these bulk compositions along representative geotherms to allow for more realistic comparisons to natural samples. 40 mW/m^2 and 45 mW/m^2 geotherms of Hasterok and Chapman (2011) were used to see how clinopyroxene changes with depth along an "average" geotherm and a "hotter" geotherm. The depths were calculated from surface heat flows of Hasterok and Chapman (2011) based on the temperature and pressure output by THERMOCALC.

For this exercise, KLB-1, KR4003 and the depleted bulk composition modified after Workman and Hart (2005) were again used as model garnet lherzolites. Clinopyroxene Cr and Na decrease with increasing depth along both geotherms (Figure 3.11 and 3.12). This is consistent with the decrease in Cr in modelled PT clinopyroxenes due to increasing pressure (Figure 3.6) and Na decreasing in modelled PT clinopyroxenes due to increasing temperature (Figure 3.7). The decrease in Cr and Na is also seen in natural samples with increasing pressure and temperature (Figure 2.9 and 2.10).

Total Al cations in clinopyroxenes increase with increasing depth along these geotherms (Figure 3.13). Al_T matches the trend seen with total Al as Al_T increases with depth (Figure 3.14). Al_{M1} initially increases and then decreases showing a curved trend with depth (Figure 3.15). This differs from the total Al as that only increases with depth. This differs from Al in modelled PT clinopyroxenes when compared as Al cations decrease with increasing pressure (Figure 3.5) and do not have a clear correlation with temperature. The geotherm modelled clinopyroxenes differ from natural clinopyroxenes as natural clinopyroxenes have decreasing Al with increasing temperature and pressure. This difference again suggests the solution model for clinopyroxene in THERMOCALC is not able to reproduce the behaviour of clinopyroxene in the natural system.

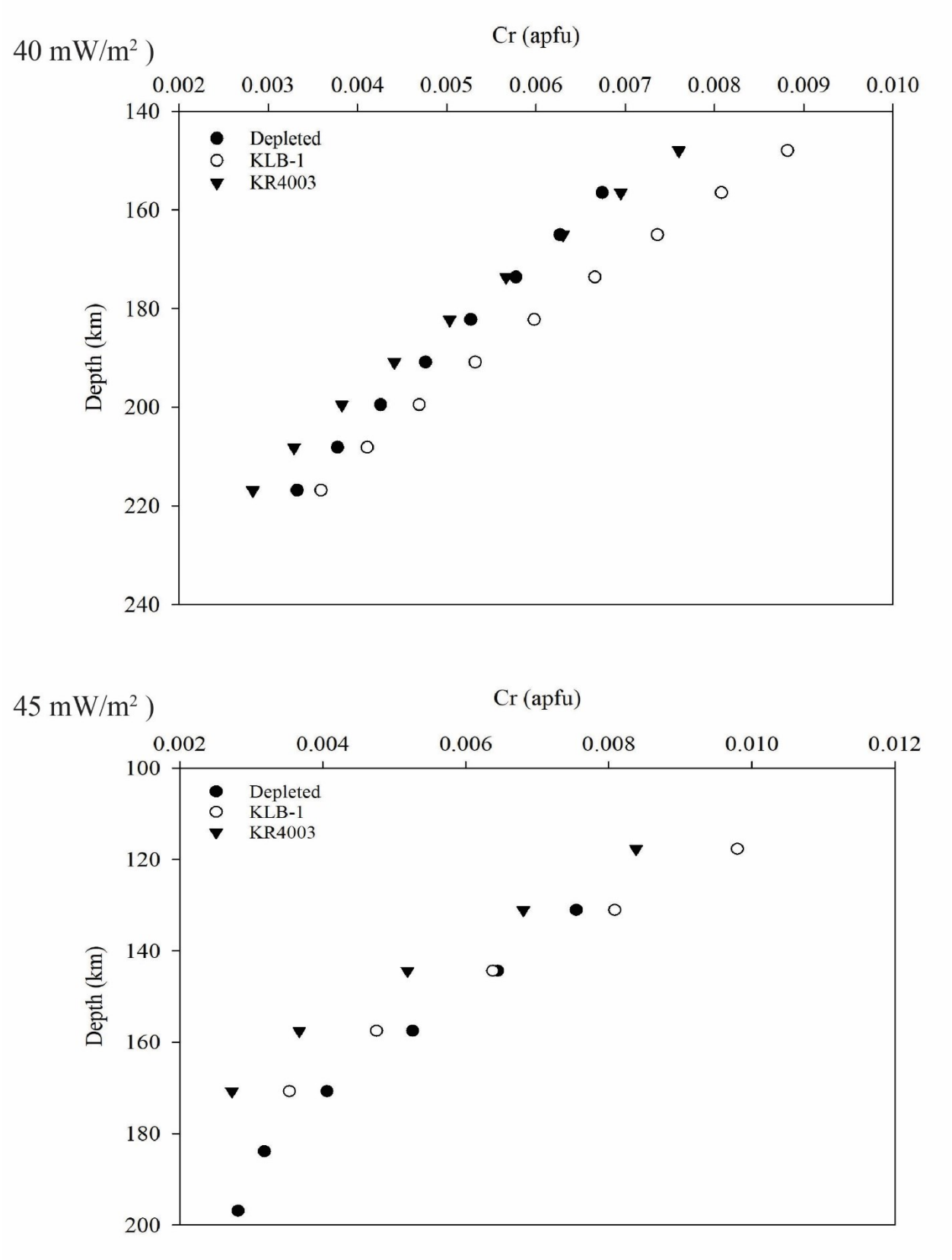

Figure 3.11 Cr vs depth of geotherm modelled garnet lherzolite clinopyroxenes on a 40 mW/m^2 geotherm and 45 mW/m^2 geotherm

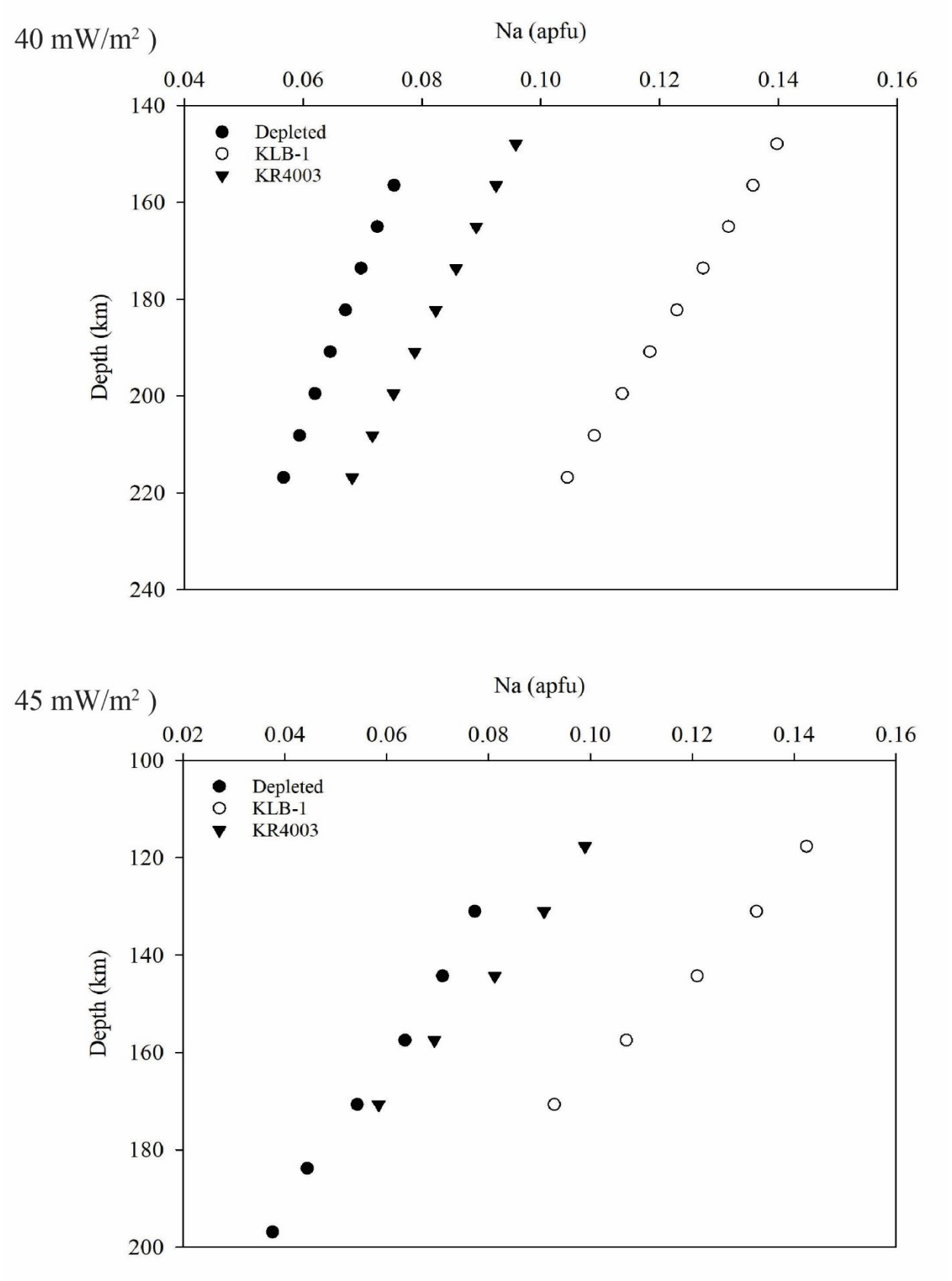

Figure 3.12 Na vs depth of geotherm modelled garnet lherzolite clinopyroxenes on a 40 mW/m^2 geotherm and 45 mW/m^2 geotherm

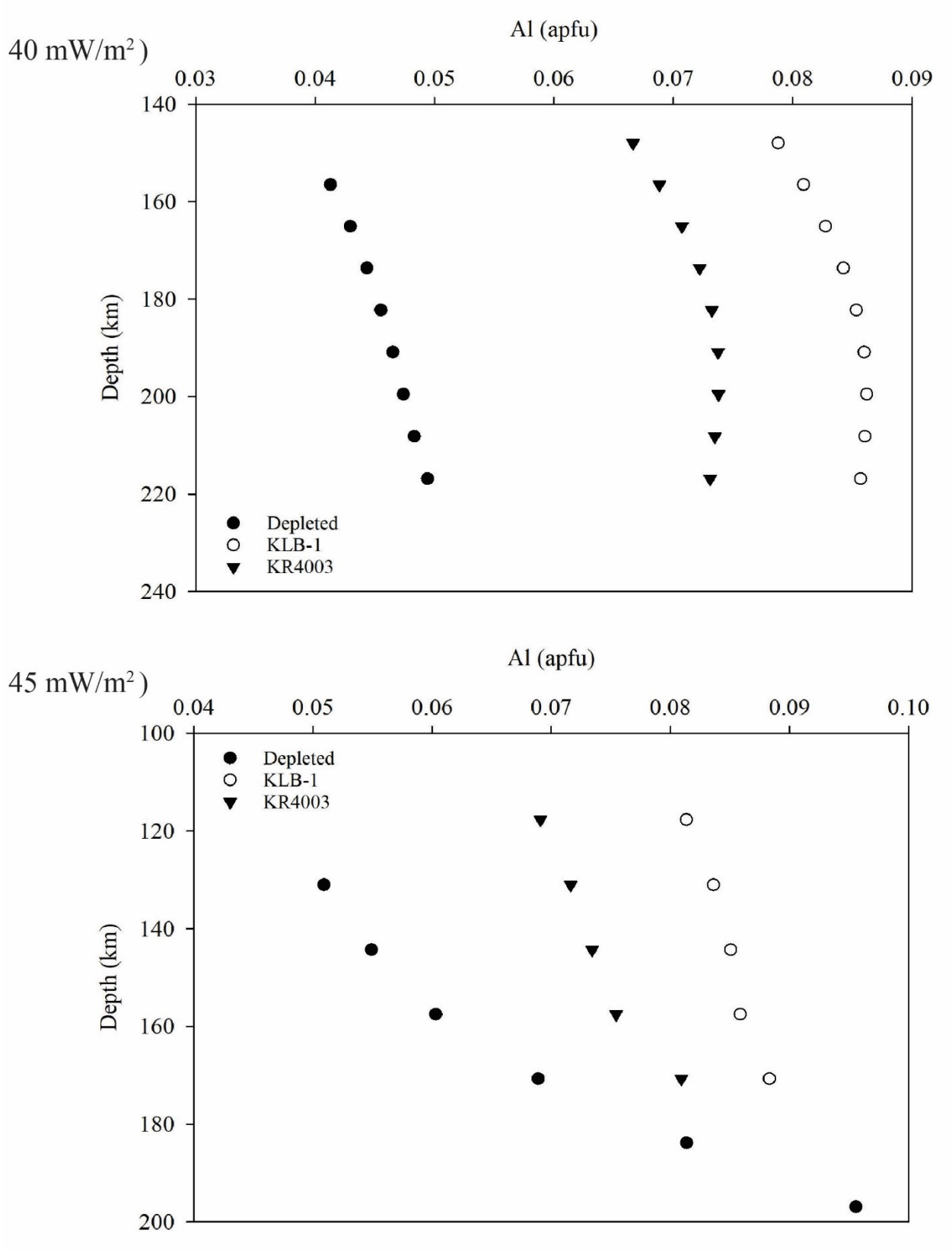

Figure 3.13 Al vs depth of geotherm modelled garnet lherzolite clinopyroxenes on a 40 mW/m^2 geotherm and 45 mW/m^2 geotherm

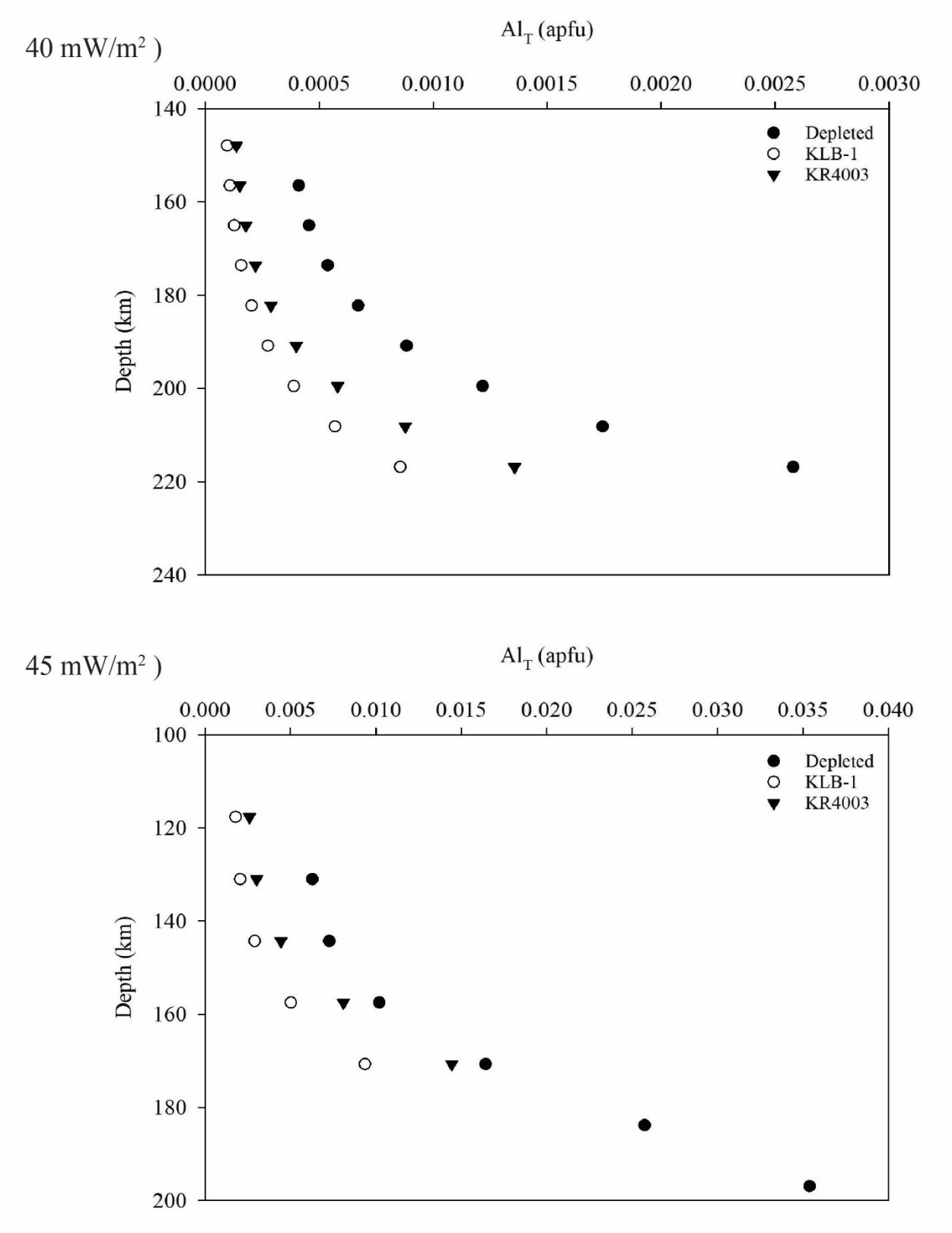

Figure 3.14 Al_T vs depth of geotherm modelled garnet lherzolite clinopyroxenes on a 40 mW/m^2 geotherm and 45 mW/m^2 geotherm

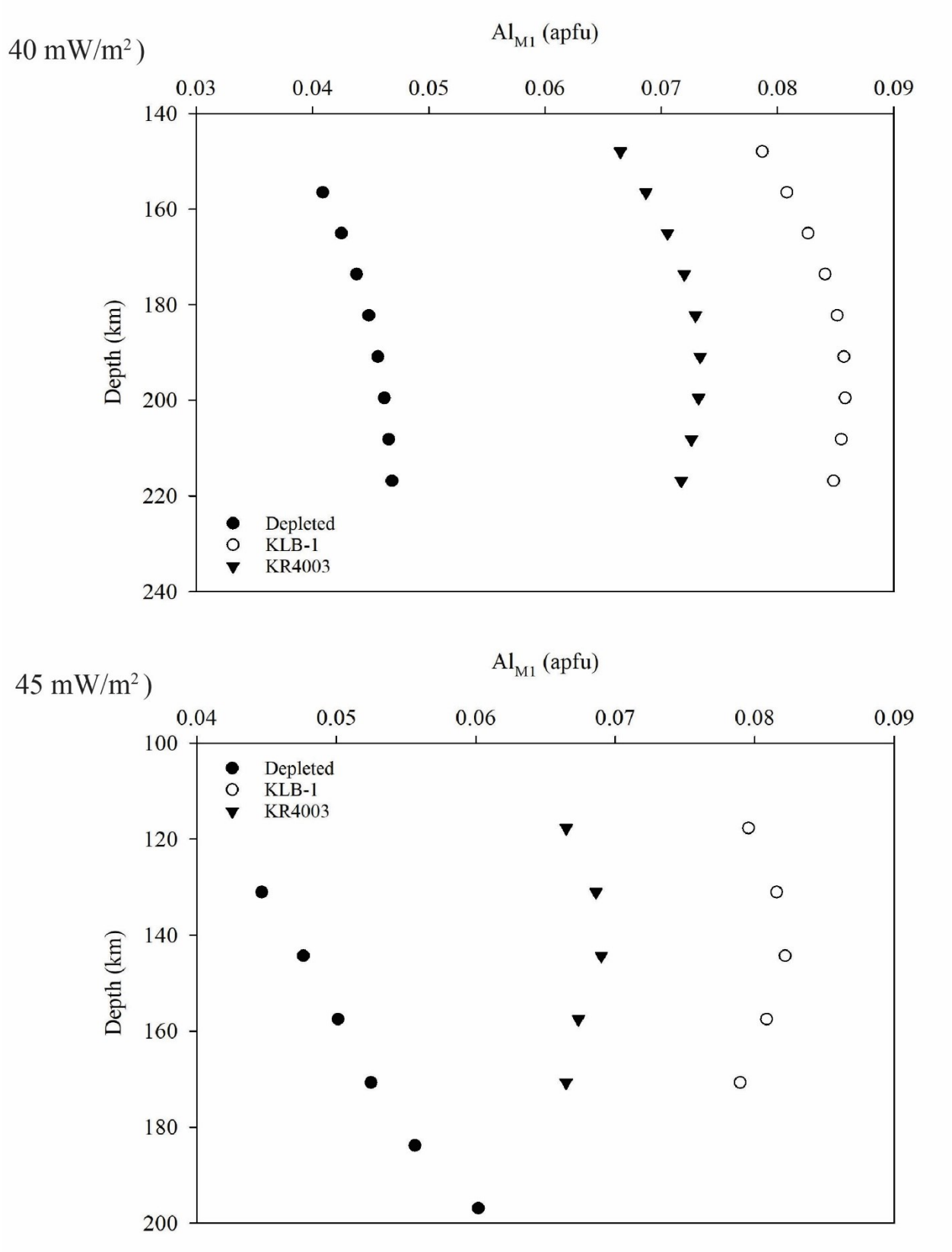

Figure 3.15 Al_{M1} vs depth of geotherm modelled garnet lherzolite clinopyroxenes on a 40 mW/m^2 geotherm and 45 mW/m^2 geotherm

Mg cations increase with depth in geotherm modelled clinopyroxene (Figure 3.16). Geotherm modelled Mg agrees with PT modelled Mg and natural Mg cations where both have decreasing Mg with increasing temperature (Figures 3.8 and 2.13, respectively). Ca cations decrease with depth in geotherm modelled clinopyroxene (Figure 3.17). This agrees with PT modelled and natural Ca in clinopyroxene as both have decreasing Ca with increasing temperature (Figures 3.9 and 2.15, respectively). Geotherm modelled Fe^{2+} cations increase with depth (Figure 3.18). This agrees with PT modelled and natural clinopyroxene Fe^{2+} as both have increasing Fe^{2+} with increasing temperature (Figures 3.10 and 2.14, respectively).

Ca# in geotherm modelled clinopyroxenes decrease with increasing depth (Figure 3.19). This agrees with PT modelled and natural clinopyroxene as both have decreasing Ca# with increasing temperature (Figure 3.2). Al+Cr-Na-K of geotherm modelled clinopyroxenes for the 40 mW/m^2 geotherm range from -0.0600 apfu to -0.0053 apfu. Al+Cr-Na-K range from -0.0606 apfu to 0.0594 apfu for the 45 mW/m^2 geotherm (Figure 3.20). All but one of these values <0.05, consistent with the Read et al. (2004) cut off for clinopyroxenes derived from garnet lherzolites. The Mg# of geotherm modelled clinopyroxene initially decreases and then increases with increasing depth (Figure 3.21). This differs from natural samples as natural clinopyroxene Mg# decreases with increasing PT (Figure 2.16). This also differs from the PT modelled clinopyroxenes as Mg# increases with increasing pressure (Figure 3.4). Na and Al+Cr are not positively correlated in geotherm modelled clinopyroxenes (Figure 3.22). This differs from natural samples where there is a strong correlation between Na and Al+Cr (Figure 2.6). Na is greater than Al+Cr in the majority of geotherm modelled clinopyroxenes as seen from Al+Cr-Na-K (Figure 3.20).

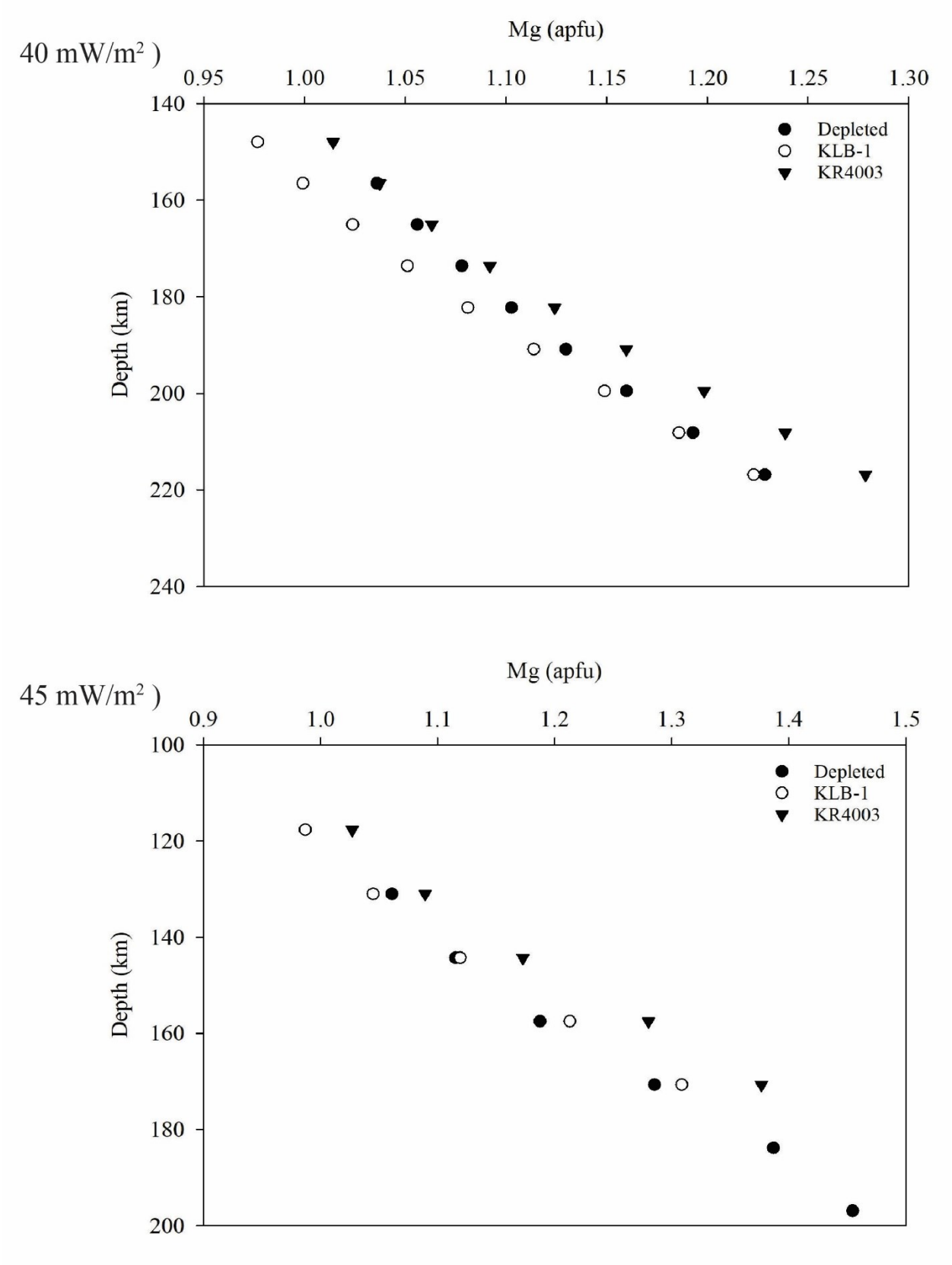

Figure 3.16 Mg vs depth of geotherm modelled garnet lherzolite clinopyroxenes on a 40 mW/m^2 geotherm and 45 mW/m^2 geotherm

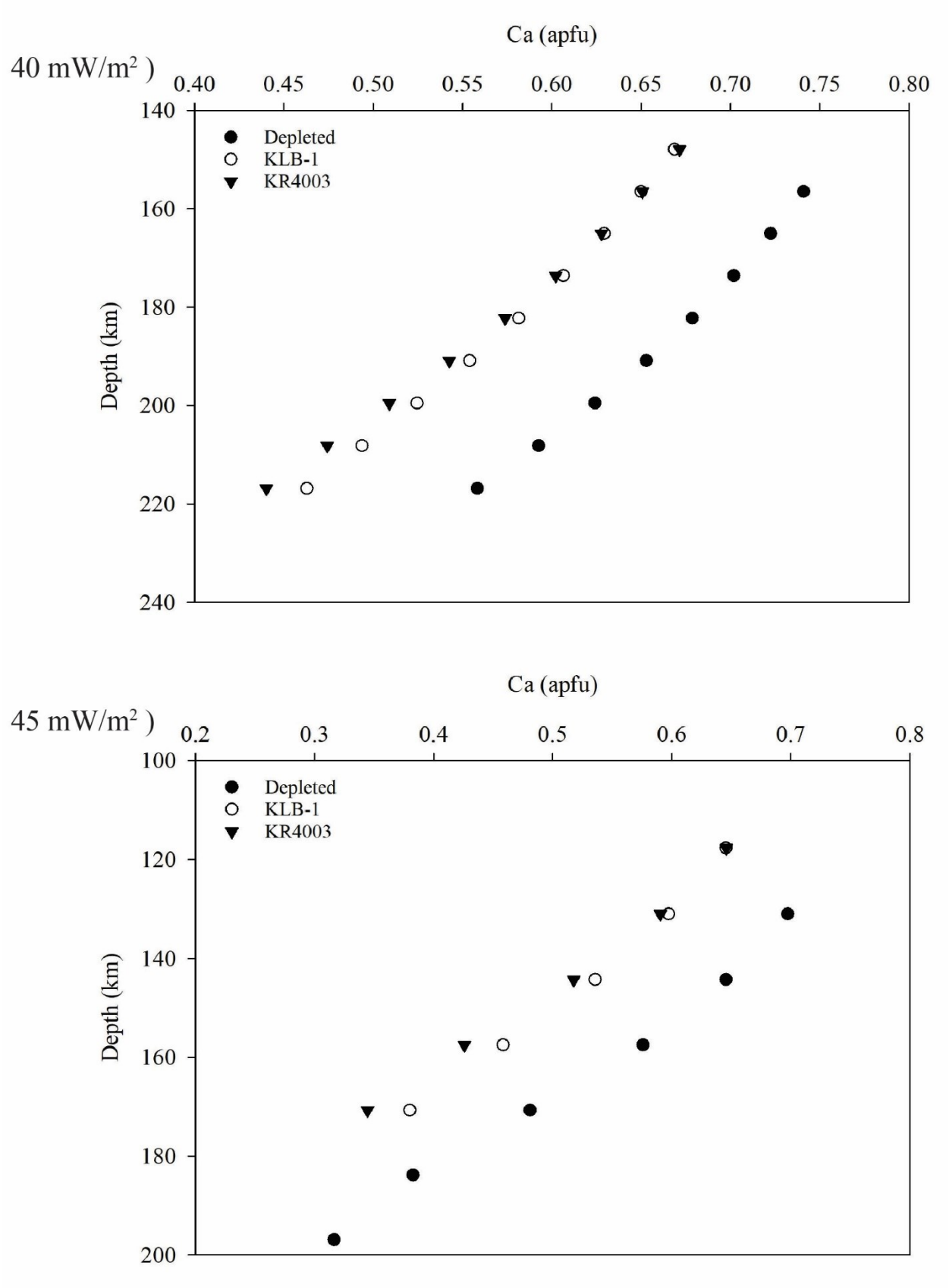

Figure 3.17 Ca vs depth of geotherm modelled garnet lherzolite clinopyroxenes on a 40 mW/m^2 geotherm and 45 mW/m^2 geotherm

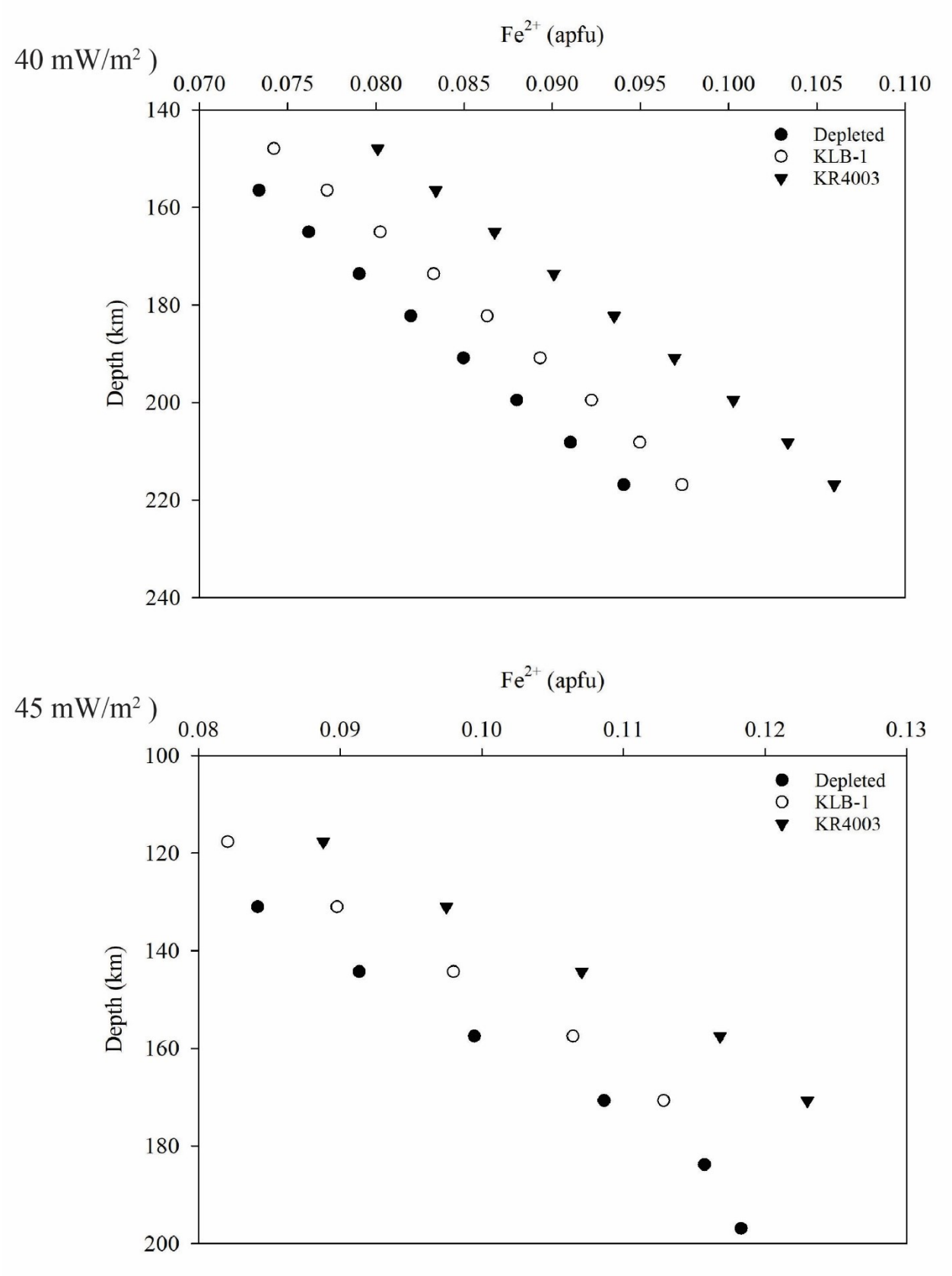

Figure 3.18 Fe^{2+} vs depth of geotherm modelled garnet lherzolite clinopyroxenes on a 40 mW/m^2 geotherm and 45 mW/m^2 geotherm

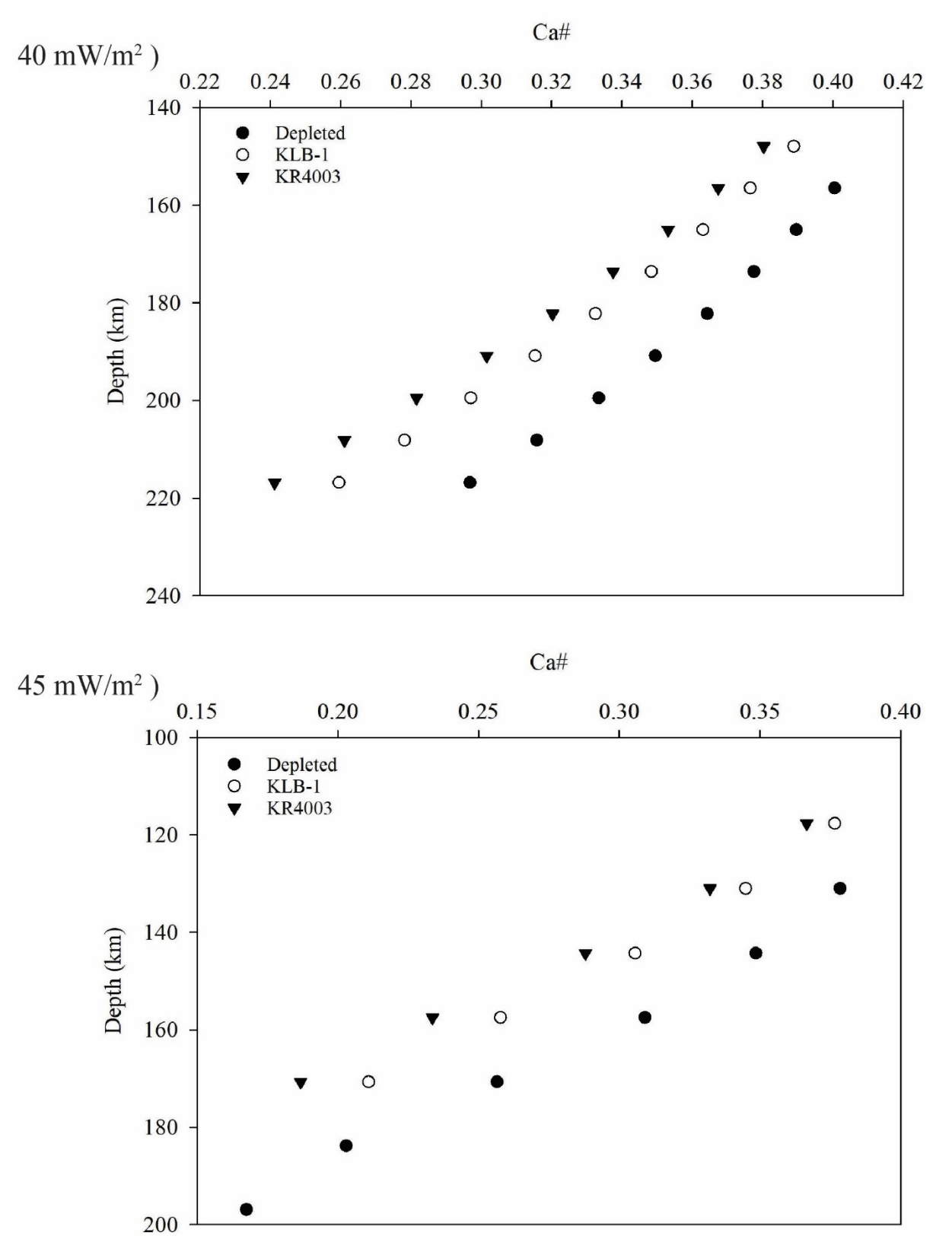

Figure 3.19 Ca# vs depth of geotherm modelled garnet lherzolite clinopyroxenes on a 40 mW/m^2 geotherm and 45 mW/m^2 geotherm

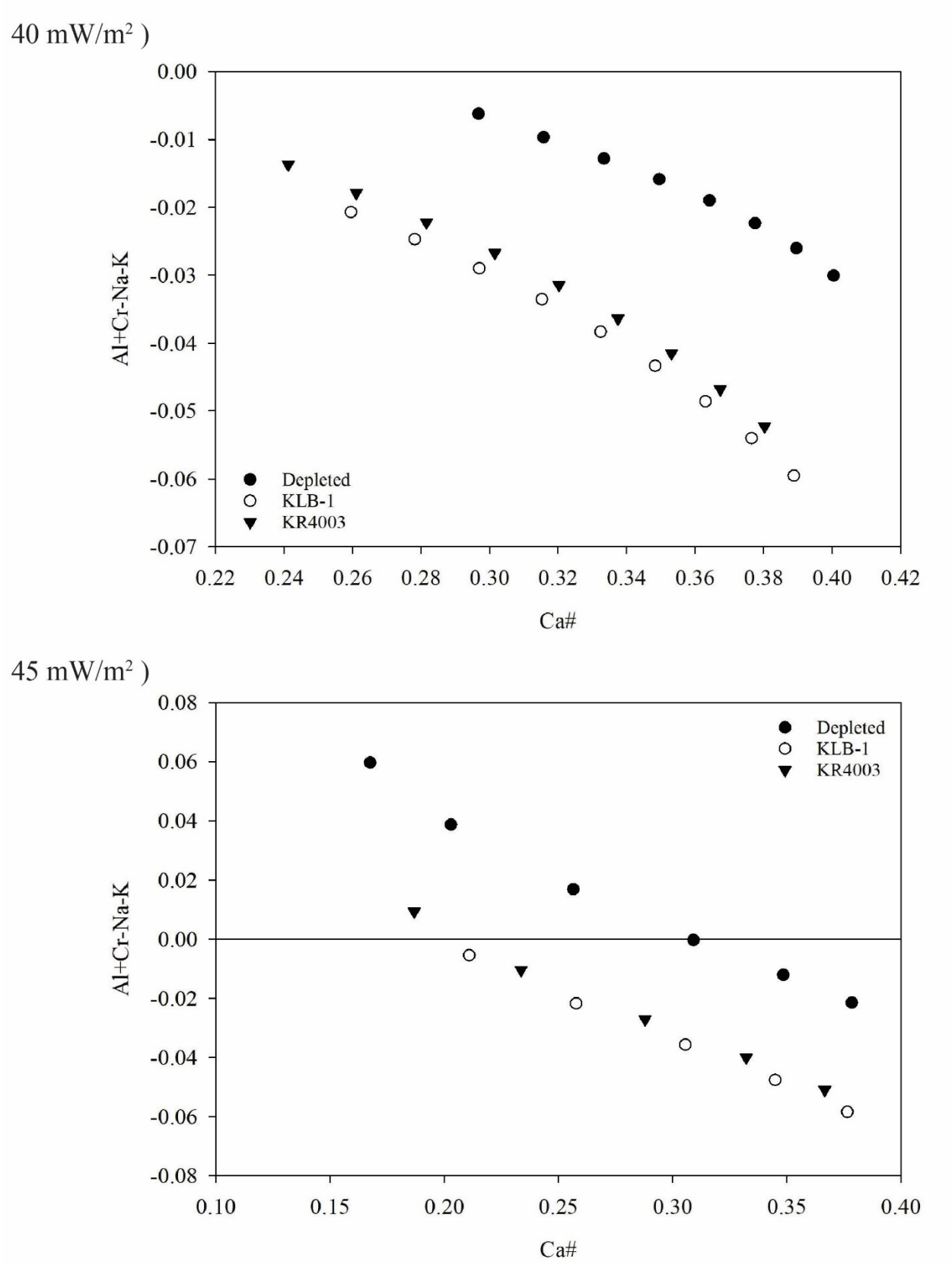

Figure 3.20 Ca# vs Tschermak component of geotherm modelled garnet lherzolite clinopyroxenes on a 40 mW/m^2 geotherm and 45 mW/m^2 geotherm

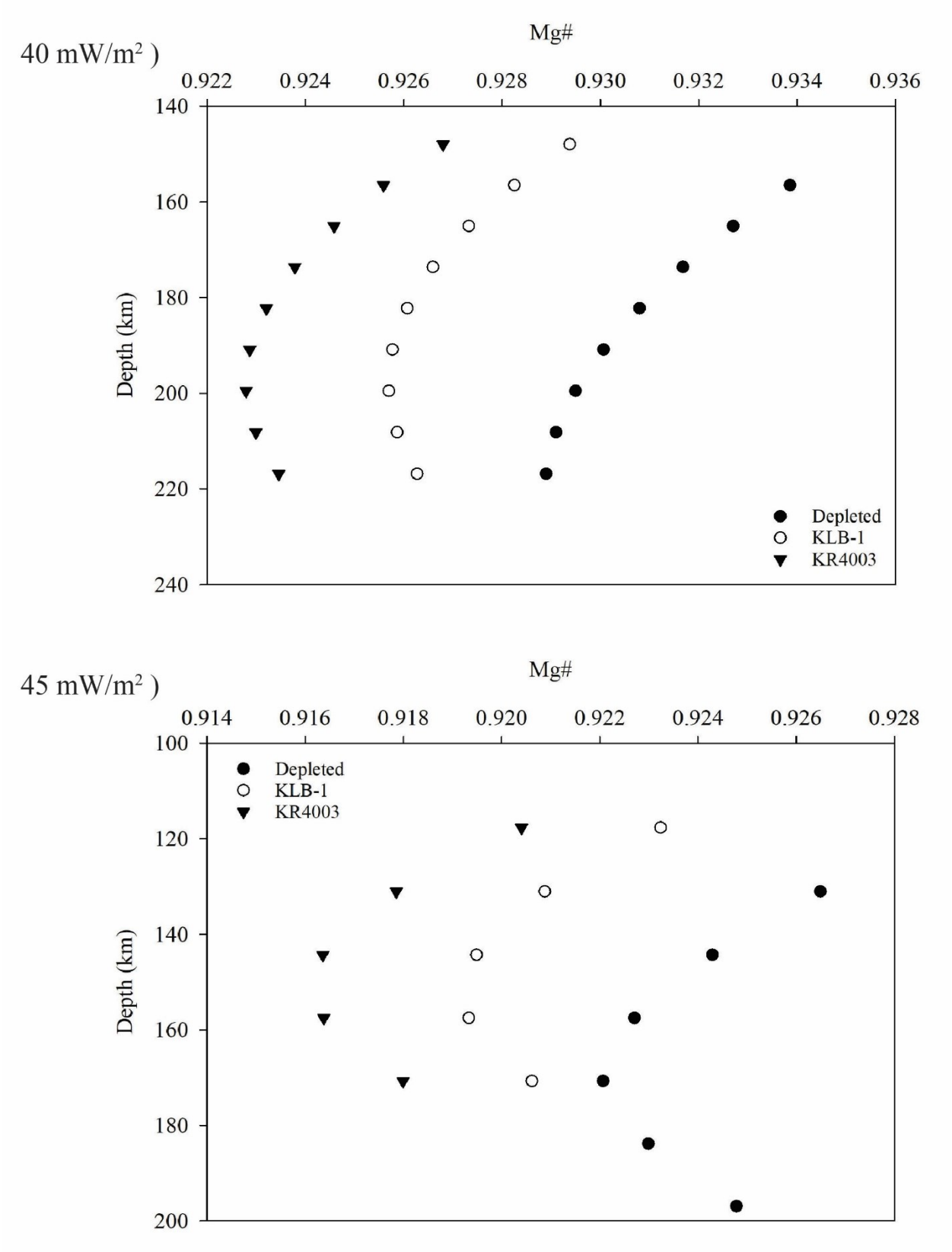

Figure 3.21 Mg# vs depth of geotherm modelled garnet lherzolite clinopyroxenes on a 40 mW/m^2 geotherm and 45 mW/m^2 geotherm

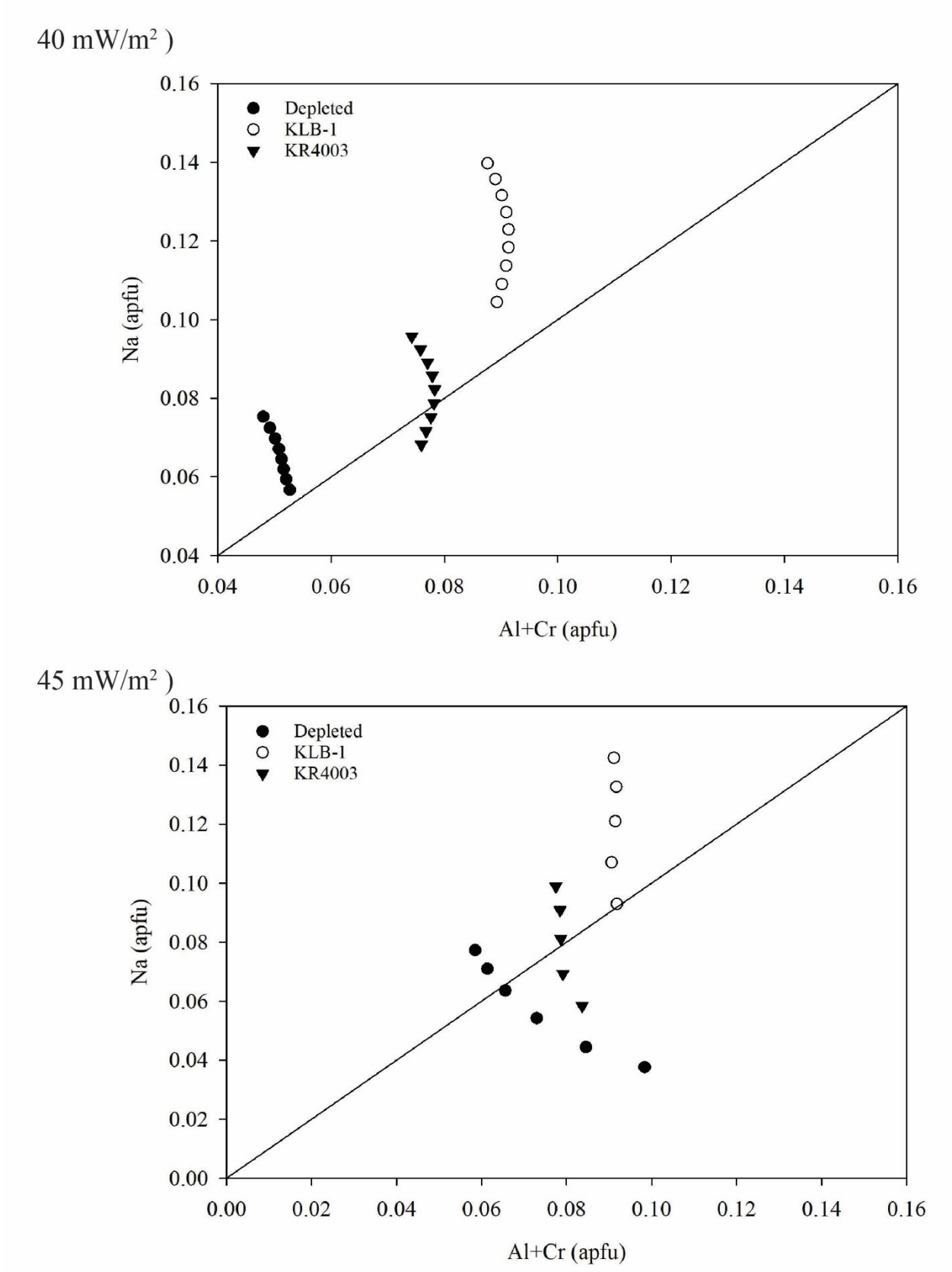

Figure 3.22 Na vs Al+Cr of geotherm modelled garnet lherzolite clinopyroxenes on a 40 mW/m^2 geotherm and 45 mW/m^2 geotherm

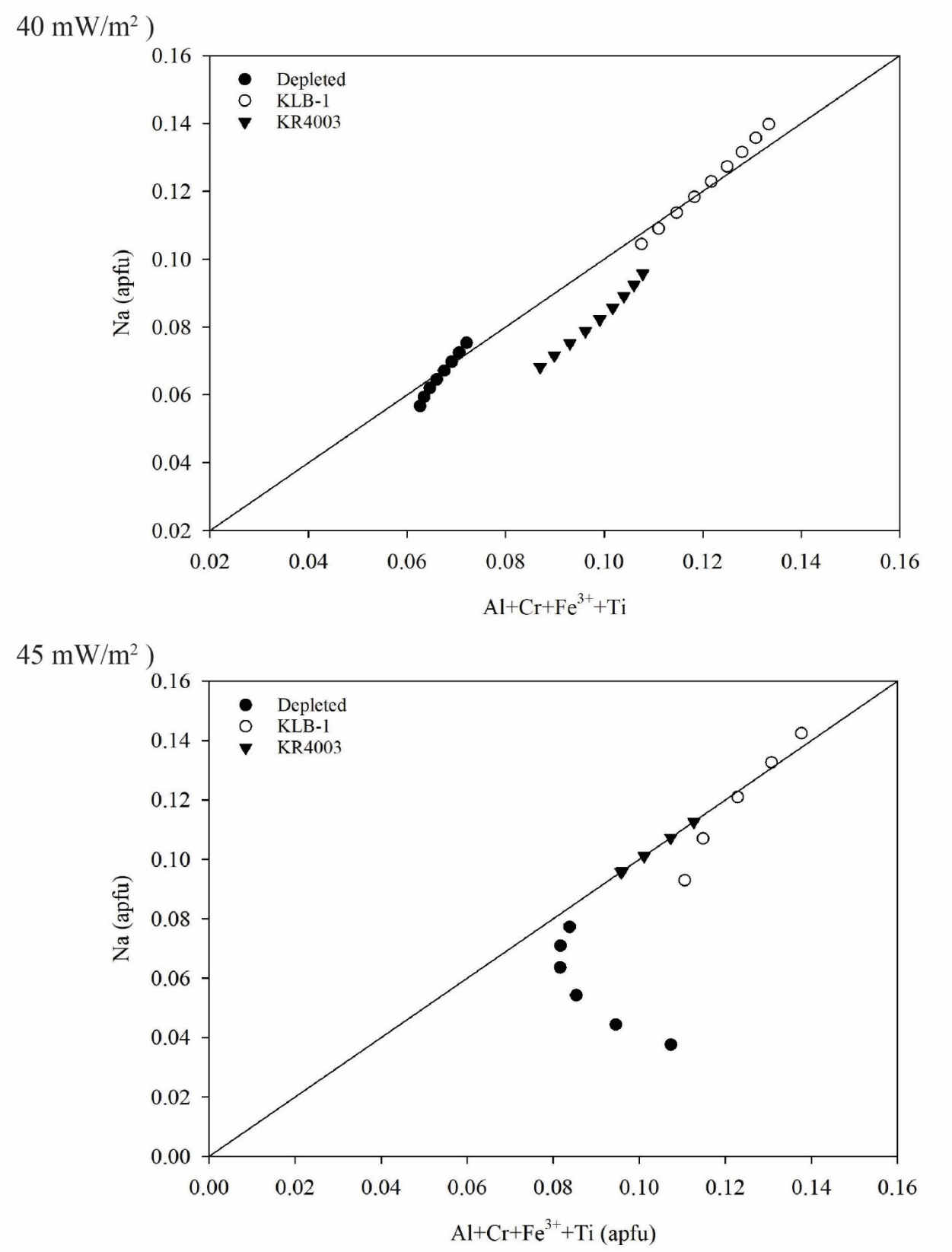

Figure 3.23 Na vs Al+Cr+Fe^{3+}+Ti of geotherm modelled garnet lherzolite clinopyroxenes on a 40 mW/m^2 geotherm and 45 mW/m^2 geotherm

Na has an approximate 1:1 ratio in the geotherm modelled clinopyroxenes when compared with Al+Cr+Fe^{3+}+Ti (Figure 3.23). This suggests THERMOCALC is charge balancing Ti, as well as Al, Cr and Fe^{3+} with Na in geotherm modelled garnet lherzolite clinopyroxenes.

3.3.5 Clinopyroxene Activities in THERMOCALC

The THERMOCALC output includes the activities for all the mineral endmembers of garnet, olivine, orthopyroxene and clinopyroxene. The olivine endmembers are forsterite (fo), fayalite (fa), ordered cfm (ocfm) and monticellite (mo). The garnet endmembers are pyrope (py), almandine (alm), grossular (gr), andradite (andr), knorringite (knr) and Ti endmember garnet (tig). The orthopyroxene endmembers are enstatite (en), ferrosilite (fs), fm, ortho-diopside (odi), Mg-tschermak (mgts), Cr-enstatite (cren), Mg-buffonite (obuf), Mg-esseneite (mess) and ortho-jadeite (ojd). The clinopyroxene endmembers THERMOCALC provides are diopside (di), clinoferrosilite (cfs), Ca-tschermaks (cats), Cr-diopside (crdi), Ca-buffonite (cbuf), Ca-esseneite (cess), jadeite (jd), clinoenstatite (cen), cfm and k-jadeite (kjd). In this discussion, I focus on the Al and Cr-bearing endmembers Ca-tschermak, Cr-diopside, jadeite and diopside, because these endmembers are used in Nimis and Taylor's exchange reaction (equation 1 of Nimis and Taylor 2000) and Nimis and Taylor's (2000) Cr-diopside activity formula (equation 7 of Nimis and Taylor 2000).

THERMOCALC tabulates both ideal activities and non-ideal activities. The formulas for ideal activities are from a mixing-on-sites model. The non-ideal activity results are based on a thermodynamic solution model. Unfortunately, the precise algorithms to calculate the non-ideal activities are not provided in the output files of THERMOCALC, so it is a bit of a black box. With that caveat in mind, we will explore how these activities vary with P and T.

The activity of Ca-tschermak and Cr-diopside decreases with increasing pressure in THERMOCALC modelled clinopyroxenes (Figures 3.24 and 3.25). The activity of jadeite and diopside decrease with increasing temperature (Figures 3.26 and 3.27). The activity of diopside decreasing with increasing temperature agrees with natural and experimental lherzolitic clinopyroxenes because of the solid solution between clinopyroxene and orthopyroxene increasing the enstatite component in clinopyroxene (as seen with Brey and Köhler 1990, Taylor 1998 and Nimis and Taylor 2000 thermometer exchange reactions). Ca-tschermak is the basis for Nimis' (1998) clinopyroxene geobarometer and the decrease of Ca-tschermak activity agrees with the decreasing Al in natural and experimental clinopyroxenes as the decrease in total Al would result in a decrease of Ca-tschermak activity (Figures 2.8 and 2.20, respectively). Cr-diopside is the basis for Nimis and Taylor's (2000) clinopyroxene geobarometer and the decrease of Cr-diopside activity agrees with decreasing Cr in natural and experimental clinopyroxenes as the decrease in total Cr would result in a decrease of Cr-diopside activity (Figures 2.9 and 2.21, respectively). Jadeite activity decreasing is consistent with Na decreasing in natural samples as pressure and temperature increases (Figure 2.10). Jadeite activity decreasing with increasing temperature and not pressure in PT modelled clinopyroxenes suggests Na decreasing in natural samples is a result of increasing temperature. Diopside activity decreasing with increasing temperature in modelled PT agrees with Ca decreasing and Mg increasing in natural samples as temperature increases (Figure 2.15 and 2.13, respectively).

Geotherm calculated activities were also modelled to see how activities evolve with depth along a geotherm. The activity of Ca-tschermak initially decreases and then increases as depth increases on the 40 mW/m^2 geotherm (Figure 3.28). This differs from PT modelled clinopyroxene as Ca-tschermak activity decreases as pressure increases (Figure 3.24).

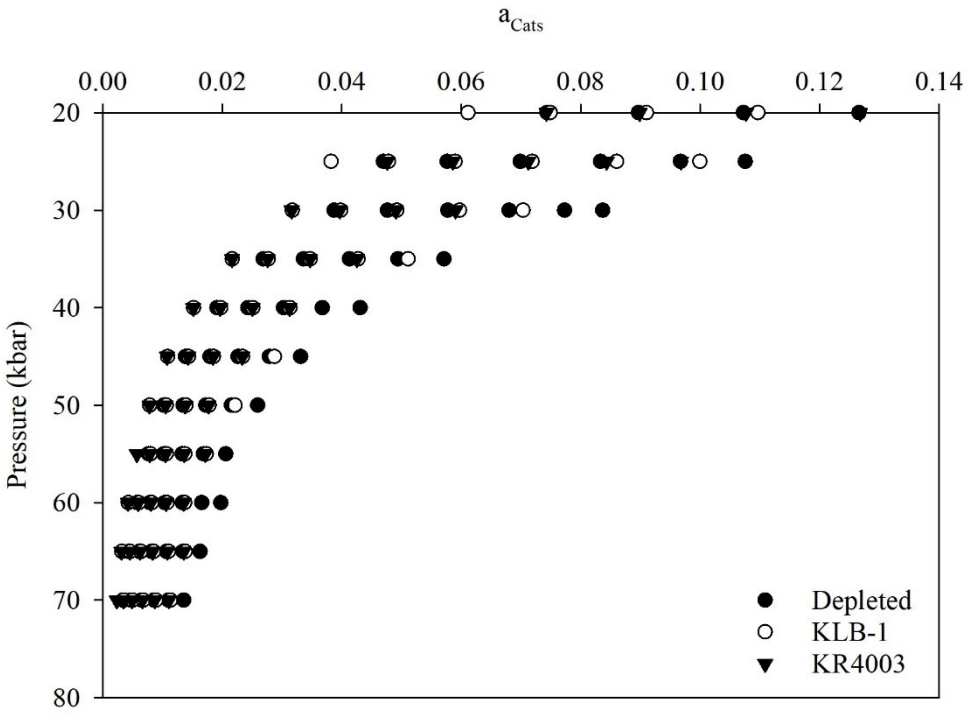

Figure 3.24 Ca-tschermak activity of PT modelled clinopyroxenes vs pressure

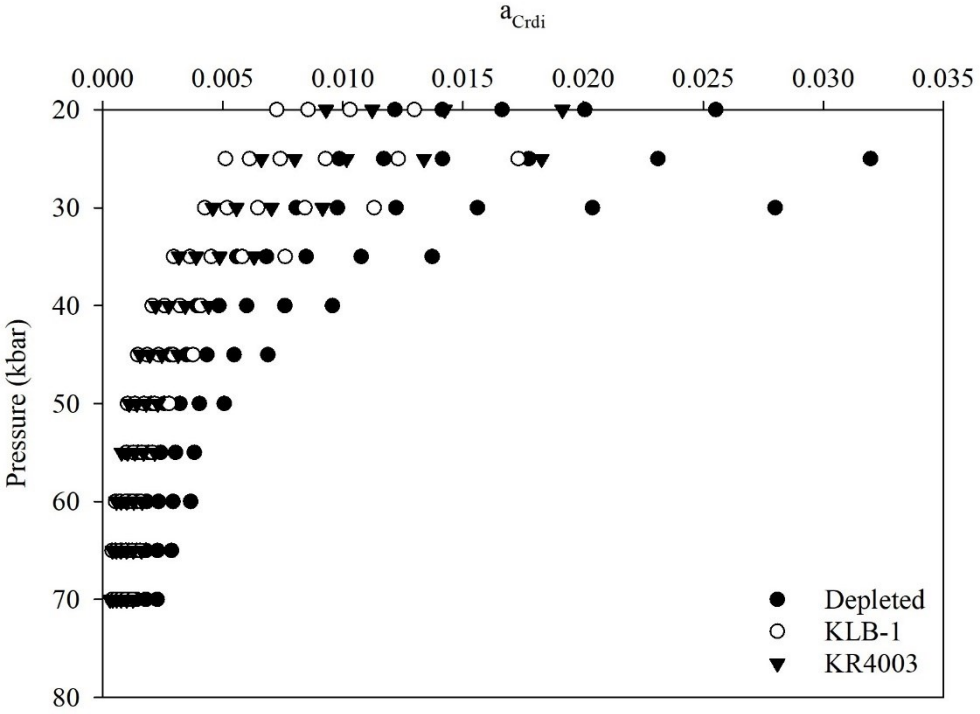

Figure 3.25 Cr-diopside activity of PT modelled clinopyroxenes vs pressure

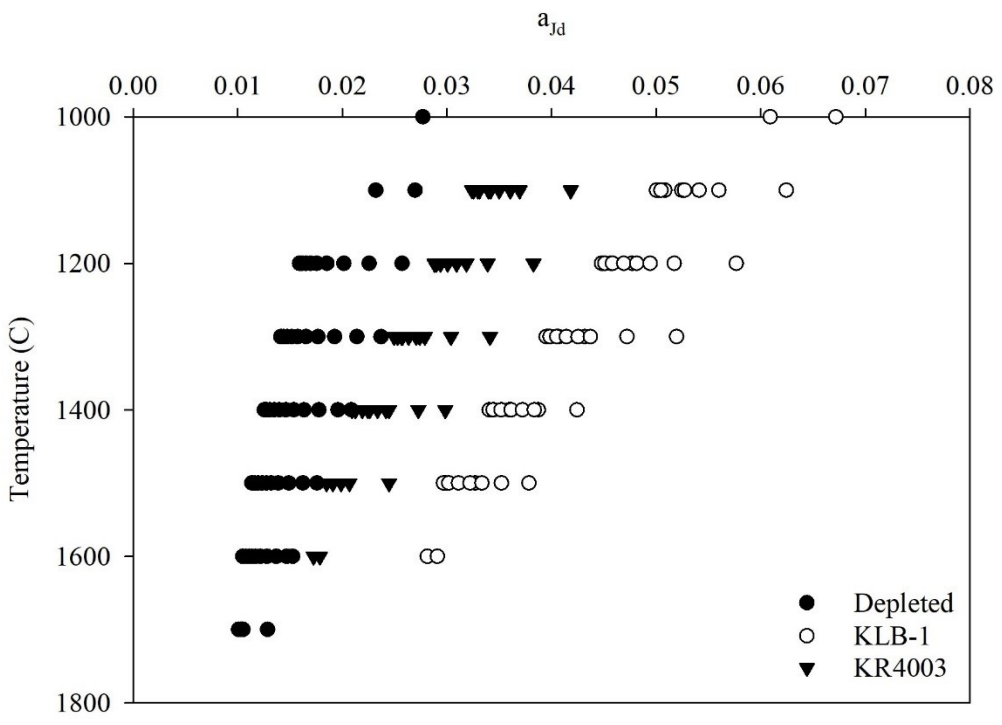

Figure 3.26 Jadeite activity of PT modelled clinopyroxenes vs temperature

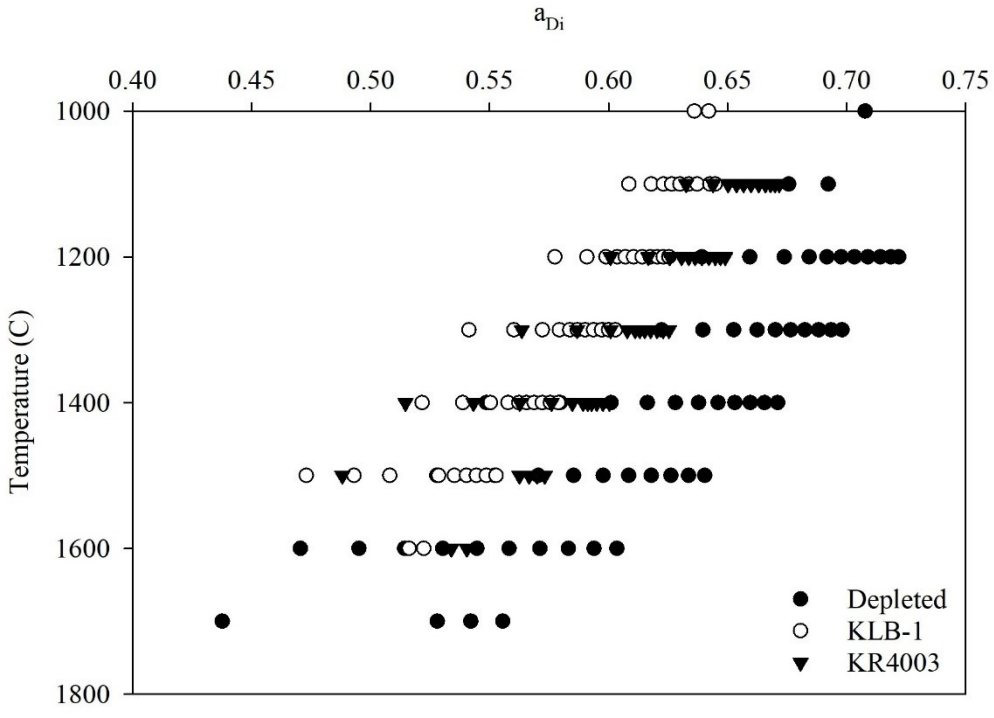

Figure 3.27 Diopside activity of PT modelled clinopyroxenes vs temperature

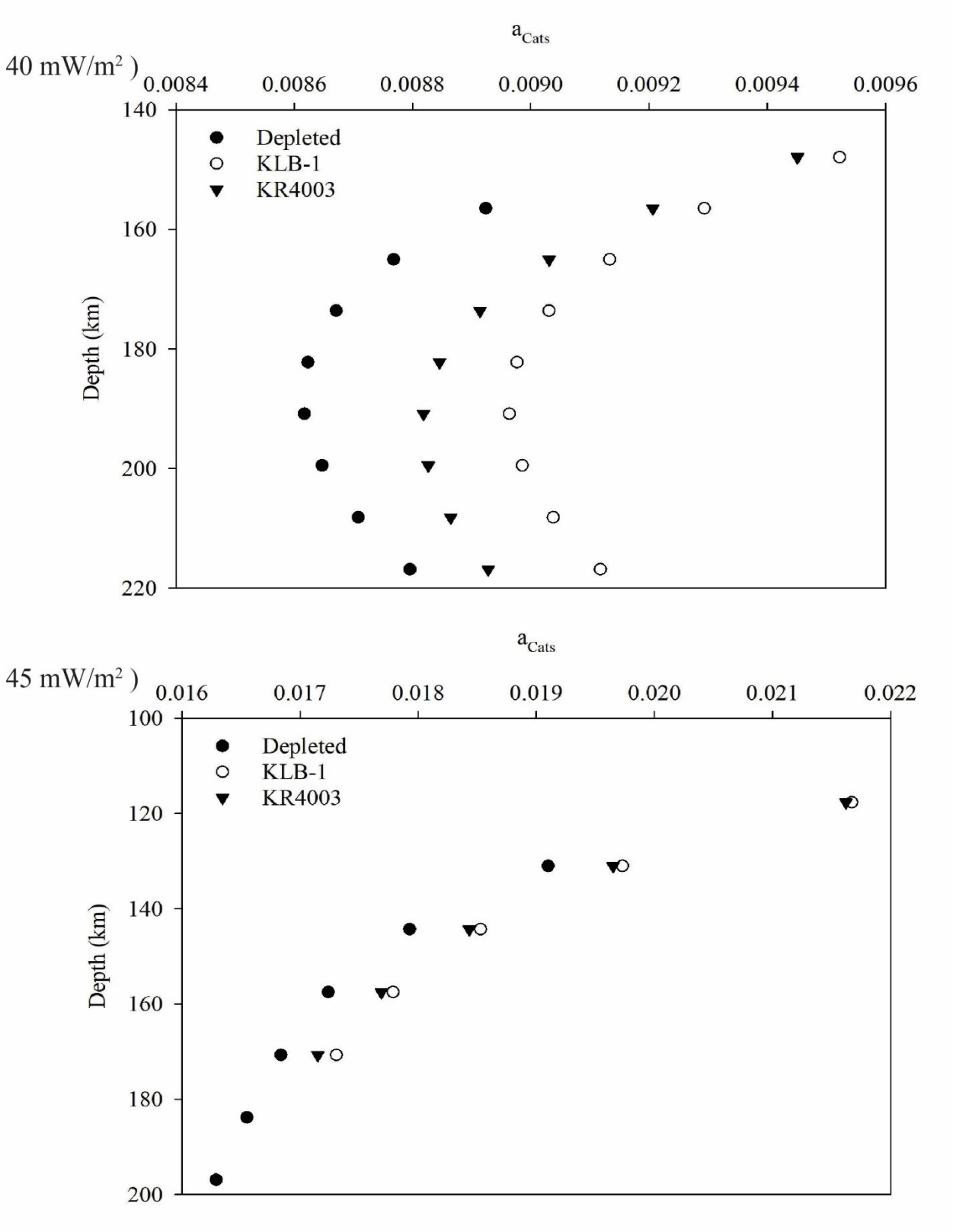

Figure 3.28 Ca-Tschermak activity vs depth of geotherm modelled garnet lherzolite clinopyroxenes on a 40 mW/m^2 and 45 mW/m^2 geotherms

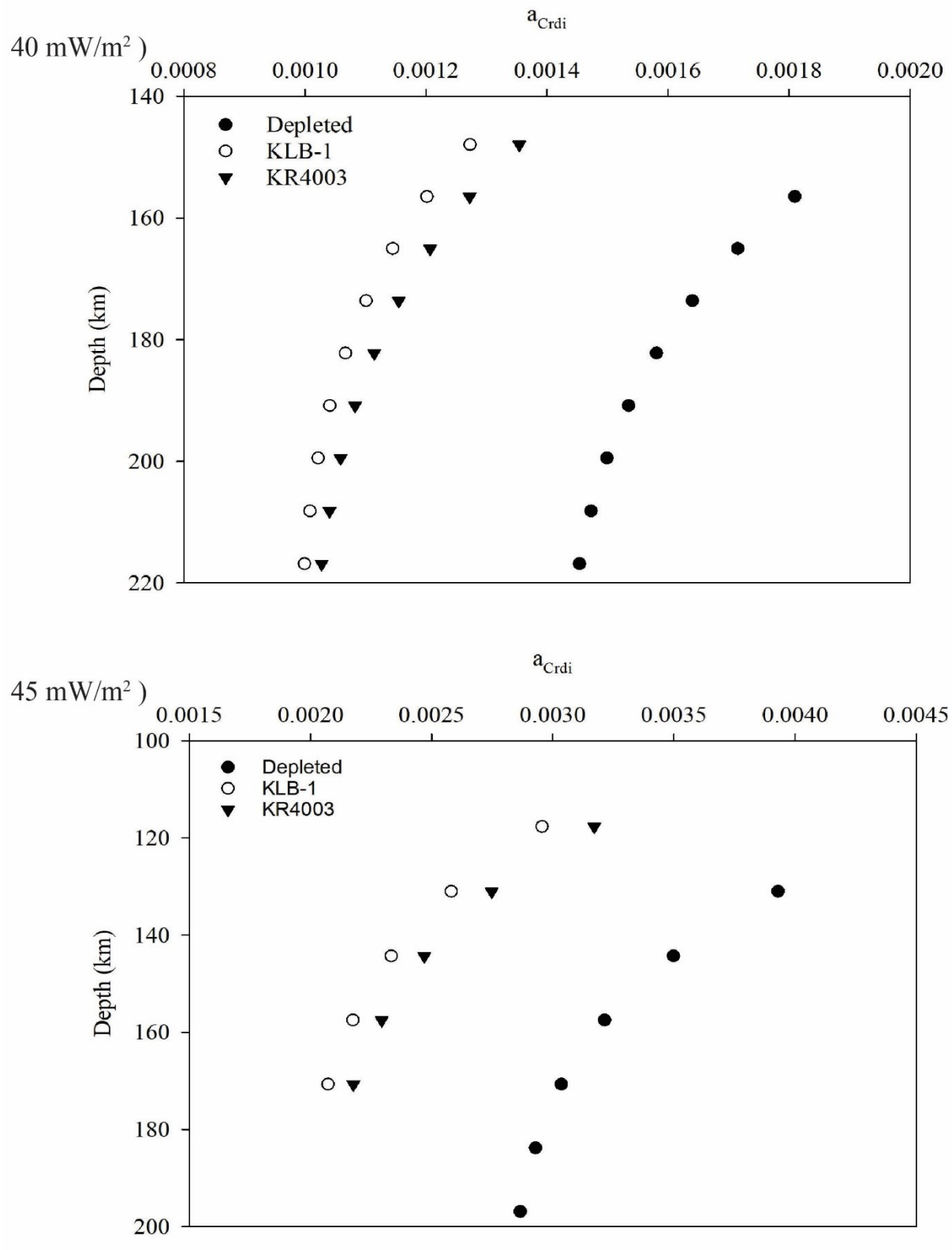

Figure 3.29 Cr-diopside activity vs depth of geotherm modelled garnet lherzolite clinopyroxenes on a 40 mW/m^2 and 45 mW/m^2 geotherms

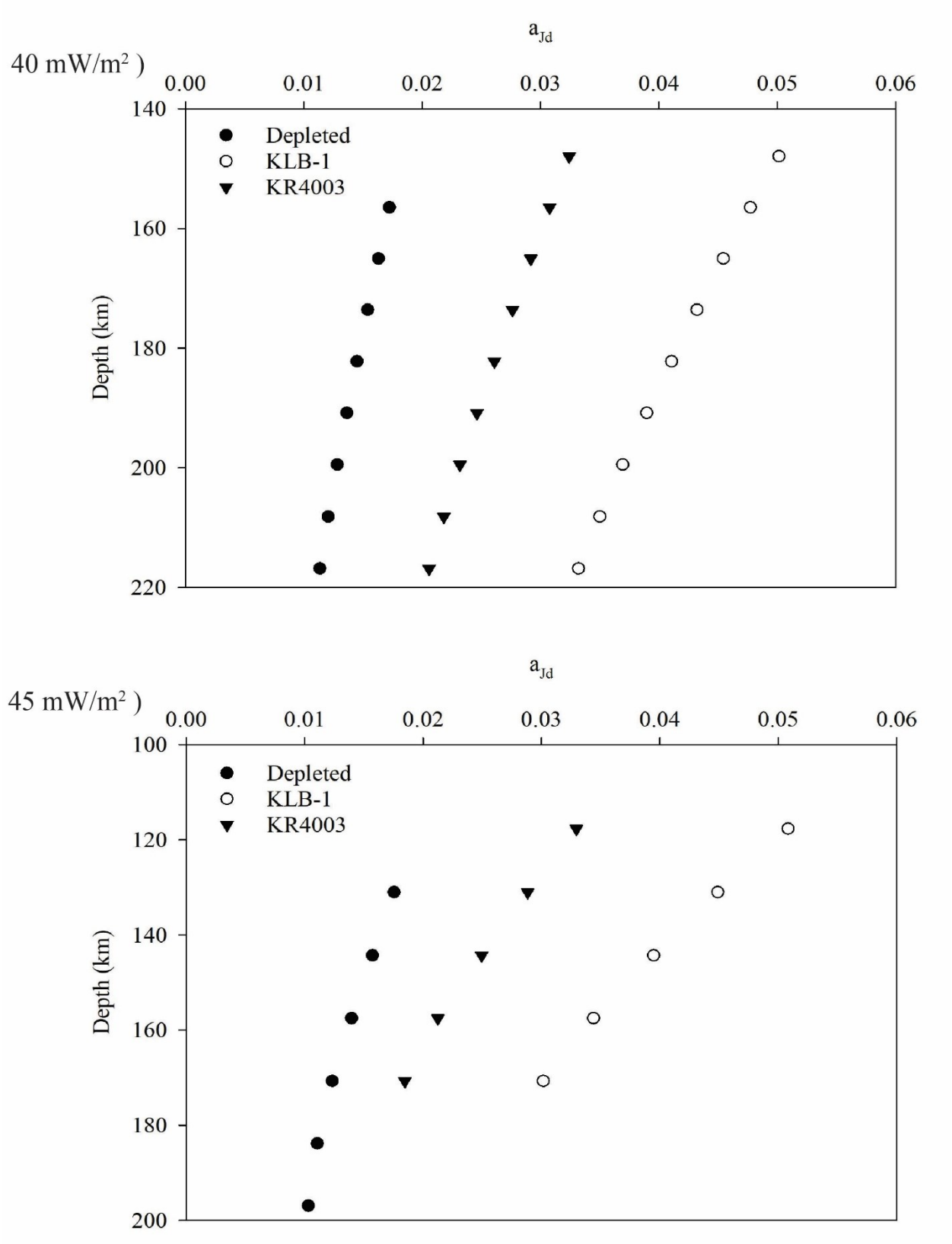

Figure 3.30 Jadeite activity vs depth of geotherm modelled garnet lherzolite clinopyroxenes on a 40 mW/m^2 and 45 mW/m^2 geotherms

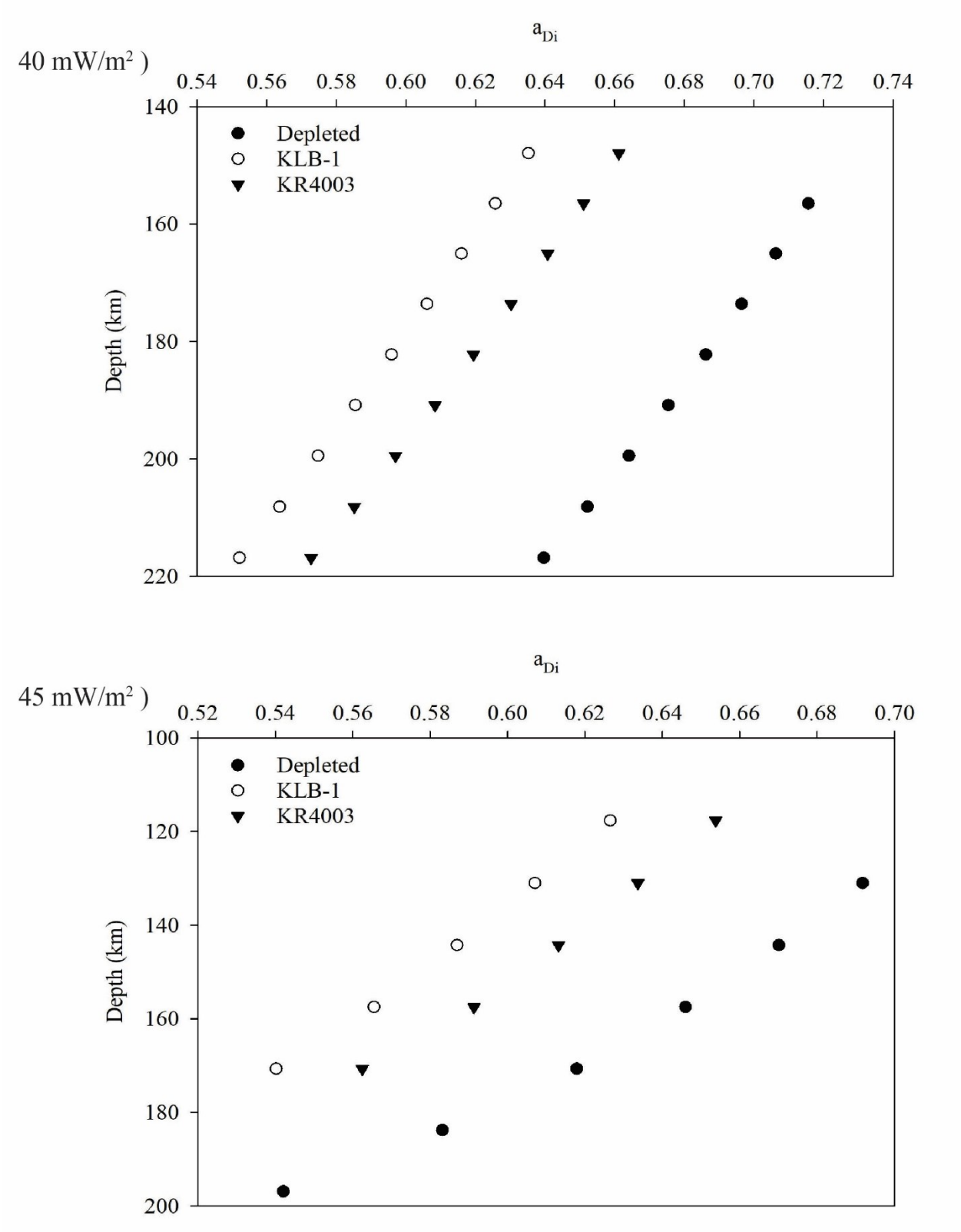

Figure 3.31 Diopside activity vs depth of geotherm modelled garnet lherzolite clinopyroxenes on a 40 mW/m^2 and 45 mW/m^2 geotherms

For Ca-tschermak activity in 45 mW/m^2 modelled samples the activity only decreases with increasing depth (Figure 3.28). The 45 mW/m^2 modelled samples Ca-tschermak activity agrees with PT modelled clinopyroxene Ca-tschermak activity as PT modelled activity decreases with increasing pressure (Figure 3.24). Cr-diopside activity of geotherm modelled clinopyroxene decreases with increasing depth for both geotherms (Figure 3.29). This agrees with PT modelled clinopyroxene as Cr-diopside activity decreases with increasing pressure (Figure 3.25). Jadeite activity of geotherm modelled clinopyroxene decreases with increasing depth for both geotherms (Figure 3.30). This agrees with the PT modelled clinopyroxenes as jadeite activity decreases with increasing temperature (Figure 3.26). Diopside activity of geotherm modelled clinopyroxene decreases with increasing depth for both geotherms (Figure 3.31). This agrees with PT modelled clinopyroxenes as diopside activity decreases with increasing temperature (Figure 3.27).

3.4 Discussions and Conclusions

Thermodynamic modelling is a useful tool to predict mineral chemistry, modal percentages and activities at specific temperatures and pressures in the program THERMOCALC. Three bulk compositions were modelled and the clinopyroxene output by these models were compared with natural clinopyroxene chemistry. Two different outputs were used for modelling clinopyroxenes. One output was comparing the modelled clinopyroxene chemistry and activities to temperature and pressure. The other output was modelled clinopyroxene chemistry and activities projected onto a 40 mW/m^2 and 45 mW/m^2 geotherms. The P-T modelled clinopyroxenes did not match well with natural garnet lherzolite clinopyroxenes as the samples failed garnet lherzolite clinopyroxene discrimination plots. However, the cation trends against pressure and temperature appeared to follow the trends seen in natural samples. The geotherm modelled garnet lherzolite clinopyroxene chemistry better matched natural samples based on garnet lherzolite

clinopyroxene discrimination methods. The cations output by THERMOCALC on geotherm projected models agree with natural samples except for Al.

The endmember activities output by THERMOCALC agree with the cation trends seen in the modelled clinopyroxenes. This may provide insight into how activities of clinopyroxene endmembers evolve in natural samples. These modelled activities could be useful as Nimis and Taylor (2000) use their formulated activity for Cr-tschermak for their barometer. Since THERMOCALC uses the most up to date thermodynamic data, THERMOCALC's calculation for the Cr-tschermak endmember is likely more correct than Nimis and Taylor's (2000) activity formulation. The only issue with these activities is THERMOCALC does not provide the formulas for how these activities are calculated, so incorporating them into an independent geobarometer is not possible at present.

THERMOCALC appears to be a useful tool to understand mantle garnet lherzolites, but it does not match natural garnet lherzolites perfectly. Further development is needed for THERMOCALC to better match natural samples.

Chapter 4 Towards Improving the Clinopyroxene Geobarometer

4.1 Attempting to Calibrate a Clinopyroxene Geobarometer using Thermodynamic Data

Using THERMOCALC data, a single grain clinopyroxene geobarometer calibration was attempted using compositions of clinopyroxene and garnet from natural garnet lherzolites and thermodynamic data from THERMOCALC. Using the thermodynamic data from THERMOCALC, a Cr-Al exchange reaction using kosmochlor ($NaCrSi_2O_6$) and jadeite ($NaAlSi_2O_6$) endmembers were attempted due to the Na:(Al+Cr) ratio of ~1:1 seen in the natural samples. The reaction is:

$Mg_3Al_2Si_3O_{12}$ (pyrope) + 2 $NaCrSi_2O_6$ (kosmochlor) = $Mg_3Cr_2Si_3O_{12}$ (knorringite) + 2 $NaAlSi_2O_6$ (jadeite)

Using THERMOCALC the $\Delta G°$ of the reaction can be calculated as a function of P and T using the parameterization of Miller et al. (2016):

$$\Delta G = a + bT + cP + dT^2 + eP^2 + fPT$$

With a, b, c, d, e and f being constants.

Using the equilibrium expression of $\Delta G° = -RTlnK$ this can be used to calculate for the effects of composition on the barometer. This includes a formula for a correlation between $ln(Cr/Al)^{garnet}$ and $ln(Cr/Al_{M1})^{clinopyroxene}$ to enable use for a clinopyroxene-only barometer, activities of the non-ideal clinopyroxene endmembers and the endmember proportions calculated consistent with THERMOCALC (calculations are given in Appendix D).

However, the method of using thermodynamic data did not work as the barometer calculated through the equation derived to solve for pressure gave results that were not comparable with other geobarometers (Figure 4.1). This failure meant abandoning this approach and turning back to the Nimis and Taylor (2000) formulation of the geobarometer and exploring possibilities to refine this empirical geobarometric expression.

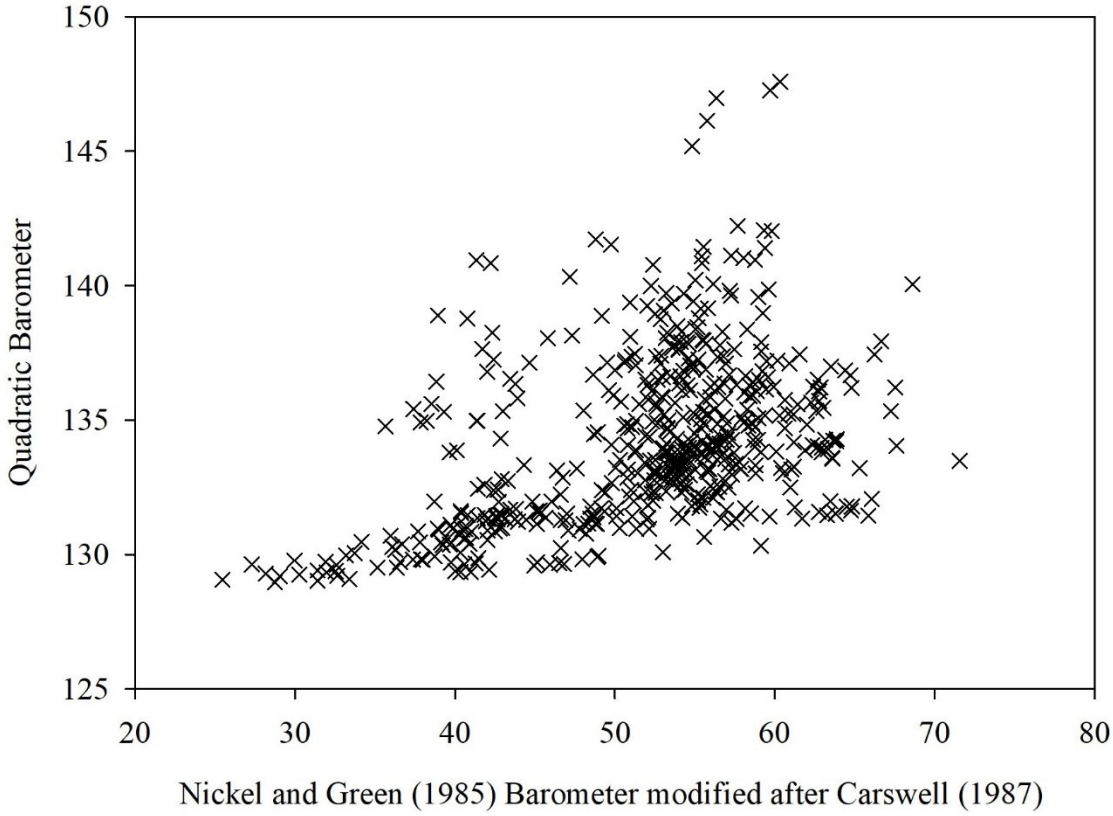

Figure 4.1 Thermodynamically calculated geobarometer ("quadratic barometer") vs the NG1985 barometer. The thermodynamically calculated geobarometer fails to calculate similar results as the NG1985 barometer (the recommended geobarometer of Nimis and Grütter 2010)

4.2 Recalibration of Cr-in-clinopyroxene geobarometer

The original Nimis and Taylor (2000) Cr-diopside activity is based on the Cr-tschermak component represented by the formula $a_{CaCrTs} = Cr - 0.81 \cdot Cr\# \cdot (Na + K)$. This approach appears to be too simplistic for calculating activity as this activity formula was developed from experimental data. As discussed previously, (Section 2.6), many of the experimental clinopyroxenes are richer in Al than natural samples, and do not show the strong correlation of Na with Al+Cr seen in natural samples. Nimis and Taylor (2000) also described cation allocation of Morimoto et al. (1988), specifically for Na, Cr and Al_{M1} as, "too simplistic for natural samples that typically show large and often uncorrelated variations in Na, Cr and Al_{M1}". This statement is

not consistent with the natural samples in the updated and expanded database used for this thesis. There is a strong correlation between Na and Al+Cr (Figures 2.6 and 2.7) and Al_{M1} follows the same trends as Al (Figure 2.11). The strong correlation between Na and Al+Cr has also been observed by others (e.g. Morris et al. 2002, Read et al. 2004, Grütter 2009). Therefore, revisiting the Nimis and Taylor (2000) geobarometer in light of both the expanded database of natural samples and the recognition of the disconnect between experimental and natural clinopyroxenes would be useful.

Using the data for natural garnet lherzolite, I explore variants of the original Nimis and Taylor (2000) geobarometer formula to create a single grain clinopyroxene geobarometer that agrees better with the results of the with Al-in-orthopyroxene geobarometer of Nickel and Green (1985) that I am using as a baseline.

4.3 Geobarometer Calibration

Using natural garnet lherzolite data, I explored different variants of a single grain clinopyroxene geobarometer developed based on the Nimis and Taylor (2000) geobarometric equation. The variants were developed through multiple linear regression of the natural garnet lherzolite clinopyroxene data. The variant that worked best incorporated as variables T(K), $Cr/(Cr+Al_{M1})$, Cr/Al, Cr+Al-0.86(Na+K) and Ca/(Ca+Mg+Fe). The barometer expression becomes:

$$P_{E23}(kbar) = 1239.28(\pm154.67) - 0.0076(\pm0.0013) \cdot T(K) \cdot \ln(Cr/(Cr+Al_{M1})) + 9.2988(\pm1.4374) \cdot \ln(Cr/Al) + 0.2056(\pm0.0204) \cdot T(K) - 0.0051(\pm0.0003) \cdot T(K) \cdot \ln(Cr+Al-0.86(Na+K)) - 201.2262(\pm24.8941) \cdot \ln(T(K)) + 56.8249(\pm4.7786) \cdot \ln(Ca/(Ca+Mg+Fe))$$

With Al_{M1} calculated as:

$$Al_{M1} = Al - 0.5(Al + Cr + 2Ti - Na - K)$$

With all mineral cations calculated with six oxygen anions per formula unit of clinopyroxene. Al_{M1} was used instead of Al_{total} in the Cr# calculation as Cr and Al on the M1 site are what charge balance with Na or tetrahedral Al. Nimis and Taylor (2000) even discuss Al_{M1} as seen with their equations 3, 4 and 5, however they decided to approximate the $Cr/(Cr+Al_{M1})$ ratio with Al_{total}. This is puzzling given that they use Al_{M1} for their geothermometer.

The barometer was calibrated using temperatures from the Taylor's (1998) two pyroxene thermometer (the recommend thermometer of Nimis and Grütter 2010) and pressures the Nickel and Green (1985) barometer, with Al calculated after Carswell and Gibb (1987). The natural database compositions span a temperature range of 980 to 1722 °C and a pressure range from 25.5 to 68.6 kbar. The R^2 value from the multiple linear regression of the natural garnet lherzolite clinopyroxene data for the updated barometer is 0.881. The associated uncertainties within the updated barometer formula are calculated from the multiple linear regression of the natural data and gives a calculated standard error of ±2.8 kbar.

4.4 Barometer Comparisons

The new clinopyroxene geobarometer requires filtration based on chemical data to obtain meaningful results. The suggested filters are Ramsay's (1992) Cr_2O_3 vs. Al_2O_3 classification diagram (following methods of Ramsay and Tompkins 1994), Cr_2O_3 content less than 5 wt% and Nimis' 1998 Al_2O_3 vs. MgO diagram. Cation totals of >3.96 and <4.04 per 6 oxygens and $Al+Cr–Na–K \leq 0.05$ are also recommended. The last filter is a limit of $Cr+Al–0.86(Na+K) \geq 0.005$ as values less than 0.005 give large pressure overestimates. The natural samples that used for barometer comparisons are xenoliths from Chidliak, Diavik-Ekati, Finsch and Jagersfontein kimberlites.

The updated geobarometer performs well and is comparable with the Sudholz et al. (2021) geobarometer and the empirical correction applied by Nimis et al. (2020) to the original Nimis and Taylor (2000) geobarometer in natural samples. The calculated pressures from the Al-in-orthopyroxene geobarometer from Nickel and Green (1985), the recommend barometer of Nimis and Grütter 2010, are compared with the new and existing clinopyroxene geobarometers in natural samples ($P_{NG1985} - P_{calc} = \Delta P$, all values summarize in Table 3.1).

$P_{NG1985} - P_{E23}$ of the updated clinopyroxene geobarometer has a mean difference of 2.6 kbar, with a range of -3.8 kbar to 17.3 kbar for xenoliths from Chidliak. $P_{NG1985} - P_{SUD2021}$ has a mean difference of -1.6 kbar, with a range of -10.5 kbar to 7.0 kbar for xenoliths from Chidliak. $P_{NG1985} - P_{NT2020\ Corrected}$ has a mean difference of 0.1 kbar, with a range of -8.6 kbar to 9.2 kbar for xenoliths from Chidliak. $P_{NG1985} - P_{NT2000}$ has a mean difference of 3.9 kbar, with a range of -4.0 kbar to 16 kbar for xenoliths from Chidliak (Figure 4.1).

$P_{NG1985} - P_{E23}$ of the updated clinopyroxene geobarometer has a mean difference of -1.8 kbar, with a range of -13.1 kbar to 5.2 kbar for xenoliths from Diavik-Ekati. $P_{NG1985} - P_{SUD2021}$ has a mean difference of -5.5 kbar, with a range of -13.0 kbar to 1.4 kbar for xenoliths from Diavik-Ekati. $P_{NG1985} - P_{NT2020\ Corrected}$ has a mean difference of 3.7 kbar, with a range of -12.7 kbar to 4.3 kbar for xenoliths from Diavik-Ekati. $P_{NG1985} - P_{NT2000}$ has a mean difference of 0.2 kbar, with a range of -10.7 kbar to 6.8 kbar for xenoliths from Diavik-Ekati (Figure 4.2).

$P_{NG1985} - P_{E23}$ of the updated clinopyroxene geobarometer has a mean difference of -0.8 kbar, with a range of -7.2 kbar to 7.7 kbar for xenoliths from Finsch. $P_{NG1985} - P_{SUD2021}$ has a mean difference of -1.0 kbar, with a range of -12.6 kbar to 9.4 kbar for xenoliths from Finsch. $P_{NG1985} - P_{NT2020\ Corrected}$ has a mean difference of 1.5 kbar, with a range of -10.1 kbar to 10.4 kbar for

xenoliths from Finsch. $P_{NG1985} - P_{NT2000}$ has a mean difference of 3.8 kbar, with a range of -4.1 kbar to 13.8 kbar for xenoliths from Finsch (Figure 4.3).

$P_{NG1985} - P_{E23}$ of the updated clinopyroxene geobarometer has a mean difference of 0.3 kbar, with a range of -9.1 kbar to 13.3 kbar for xenoliths from Jagersfontein. $P_{NG1985} - P_{SUD2021}$ has a mean difference of -2.0 kbar, with a range of -17.5 kbar to 11.3 kbar for xenoliths from Jagersfontein. $P_{NG1985} - P_{NT2020\ Corrected}$ has a mean difference of 1.8 kbar, with a range of -13.4 kbar to 16.0 kbar for xenoliths from Jagersfontein. $P_{NG1985} - P_{NT2000}$ has a mean difference of 3.2 kbar, with a range of -7.4 kbar to 18.4 kbar for xenoliths from Jagersfontein (Figure 4.4).

Table 4.1 ΔP results of NG1985 barometer – different single grain clinopyroxene geobarometers from four localities

		Chidliak	Diavik-Ekati	Finsch	Jagersfontein
$P_{NG1985} - P_{E23}$	Average	2.6	-1.8	-0.8	0.3
	Minimum	-3.8	-13.1	-7.2	-9.1
	Maximum	17.3	5.2	7.7	13.3
$P_{NG1985} - P_{SUD2021}$	Average	-1.6	-5.5	-1.0	-2.0
	Minimum	-10.5	-13.0	-12.6	-17.5
	Maximum	7.0	1.4	9.4	11.3
$P_{NG1985} - P_{NT2020\ Corrected}$	Average	0.1	-3.7	1.5	1.8
	Minimum	-8.6	-12.7	-10.1	-13.4
	Maximum	9.2	4.3	10.4	16.0
$P_{NG1985} - P_{NT2000}$	Average	3.9	0.2	3.8	3.2
	Minimum	-4.0	-10.7	-4.1	-7.4
	Maximum	16.0	6.8	13.3	18.4

The ΔP comparisons show good agreement between the updated clinopyroxene geobarometer and the Al-in-orthopyroxene geobarometer of Nickel and Green (1985), with the averages from the four localities being close to zero and the minimum and maximum ranges being similar between the different single clinopyroxene geobarometers ΔP (Table 4.1). The main differences

between the minimum and maximum values between the four clinopyroxene geobarometers come down to the locality of the samples and differences between the individual barometers. There are slight ΔP differences between each locality and this is a result of which samples passed filtration (e.g. Grütter 2009 and Ziberna et al. 2016). The Nimis et al. (2020) correction to the Nimis and Taylor (2000) barometer also shows good agreement with the Nickel and Green (1985) barometer. This should be expected as the empirical correction applied by Nimis et al. (2020) was calculated to fit the Nimis and Taylor (2000) barometer to the Nickel and Green (1985) barometer pressure estimates to a database of natural samples. The Sudholz et al. (2021) barometer tends to overestimate pressure relative to the Nickel and Green (1985) barometer as it consistently has the most minimum ΔP ($P_{NG1985} - P_{SUD2021}$) values for the four localities and the average ΔP ($P_{NG1985} - P_{SUD2021}$) values for all four localities were negative (Table 4.1). The Nimis and Taylor (2000) barometer tends to underestimate compared to the Nickel and Green (1985) barometer and this underestimation is well known (e.g. Nimis 2002).

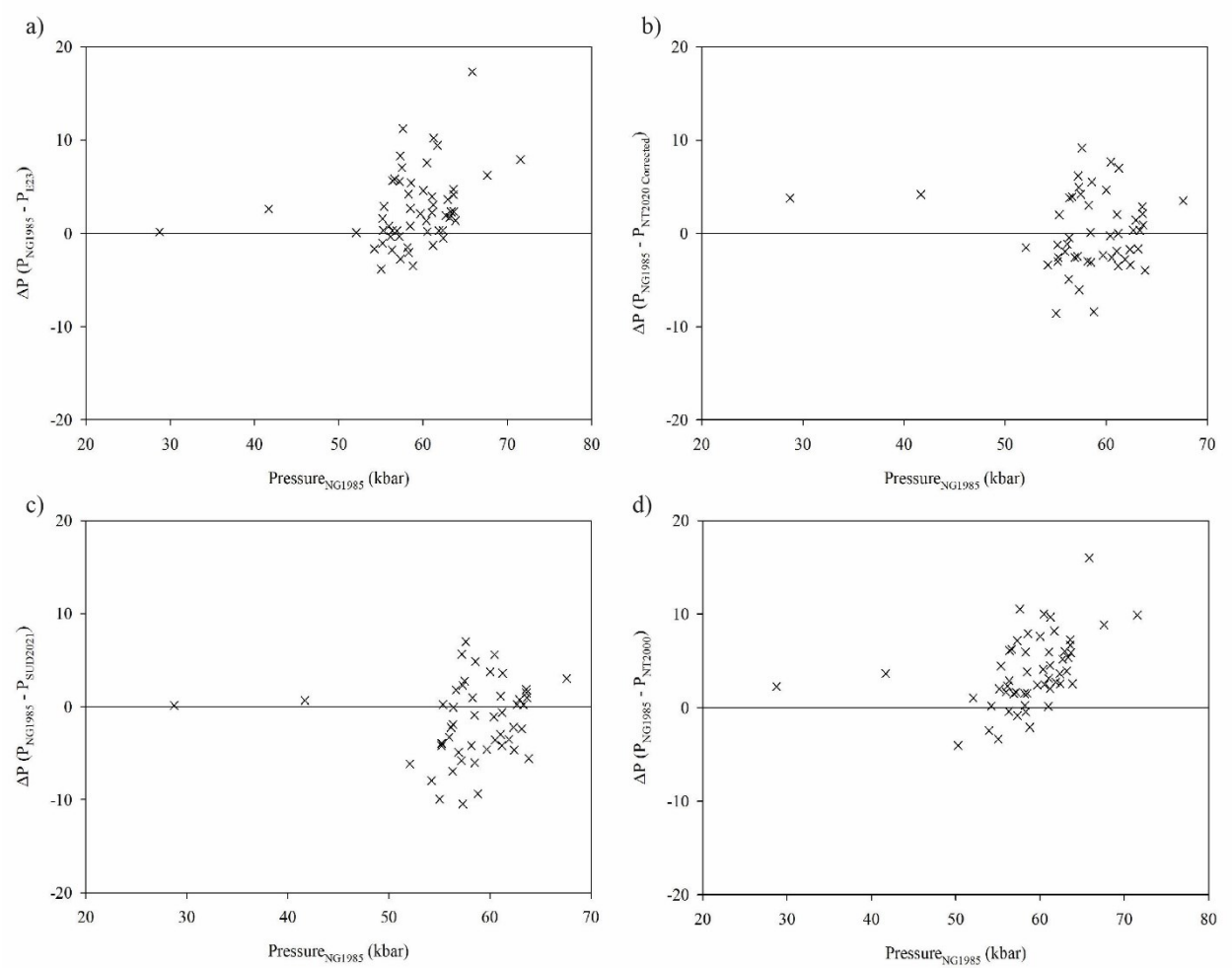

Figure 4.2 Comparison between P_{NG1985} – P of clinopyroxene barometers of xenolith samples from Chidliak kimberlite field

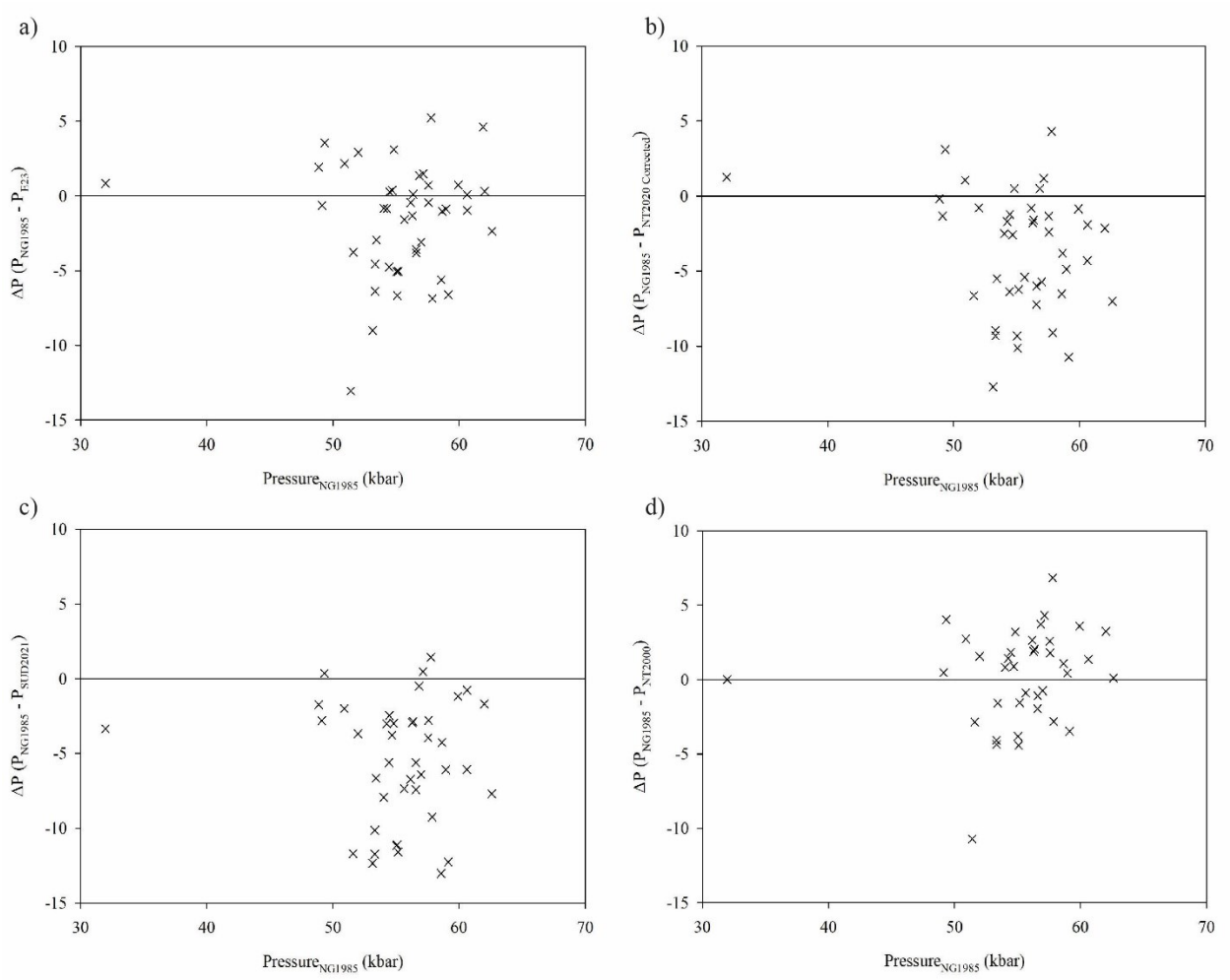

Figure 4.3 Comparison between P_{NG1985} – P of clinopyroxene barometers of xenolith samples from Diavik and Ekati kimberlites

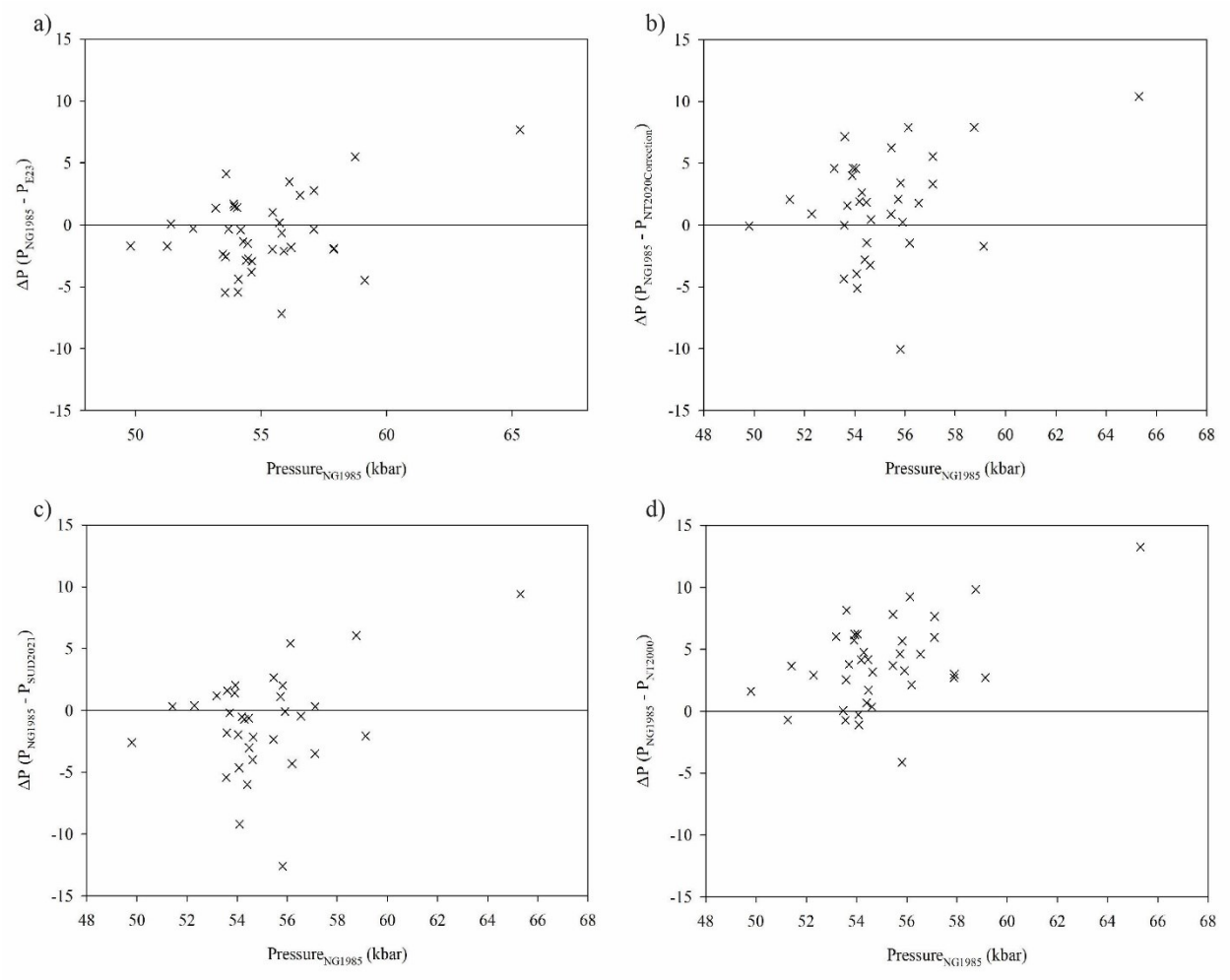

Figure 4.4 Comparison between P_{NG1985} – P of clinopyroxene barometers of xenolith samples from Finsch Diamond Mine

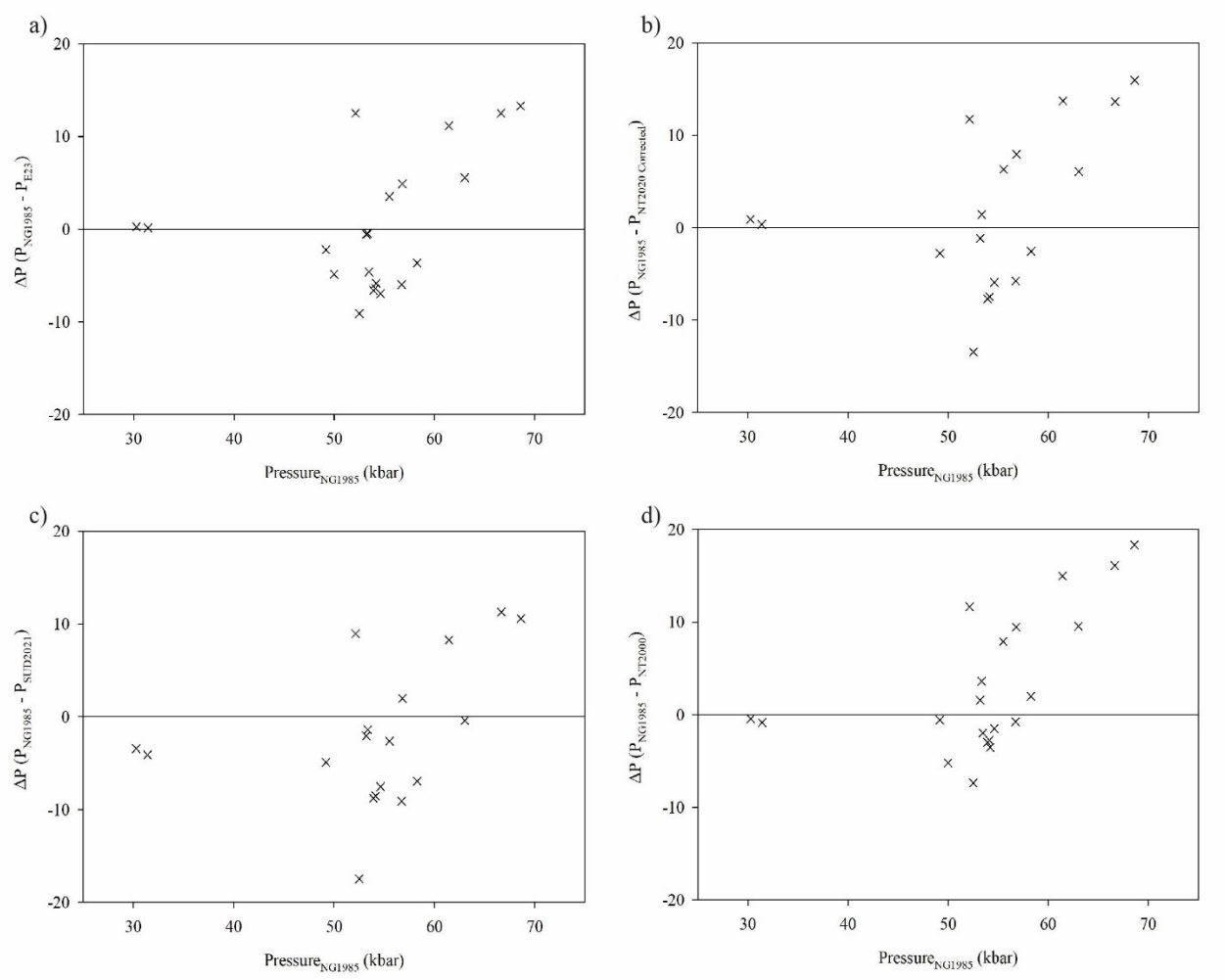

Figure 4.5 Comparison between P_{NG1985} – P of clinopyroxene barometers of xenolith samples from Jagersfontein Diamond Mine

Are the differences in pressures calculated related to mineral chemistry? To explore this question, plotting ΔP against mineral chemistry might be useful. The data from Chidliak, Diavik-Ekati, and Jagersfontein do not appear to have any clear dependence on cations such as Al or Ti. On the other hand, there is a correlation in natural Finsch samples between Al and ΔP, with increasing ΔP with increasing Al (Figure 4.5). This agrees with Sudholz et al. (2021), who also observed this same trend with their barometer when compared with Brey and Köhler (1990) barometer (Figure 6a in Sudholz et al. 2021). Ti cations in natural samples from Finsch have a correlation with ΔP and this correlation has increasing ΔP with increasing Ti (Figure 4.6). This is

the same trend seen with the Al cations and ΔP (Figure 4.5). Na and Cr cations in natural samples do not show any correlation with ΔP for any of the localities.

The updated clinopyroxene geobarometer and the existing clinopyroxene geobarometers (Nimis and Taylor 2000, Nimis et al. 2020, Sudholz et al. 2021) display the same Al and Ti cation trends with Finsch being the only locality that displays these trends. (Figure 4.5 and 4.6, respectively). This shows the clinopyroxene barometers behave similarly in comparison to the Nickel and Green (1985) barometer and cations used to calculate pressure estimates.

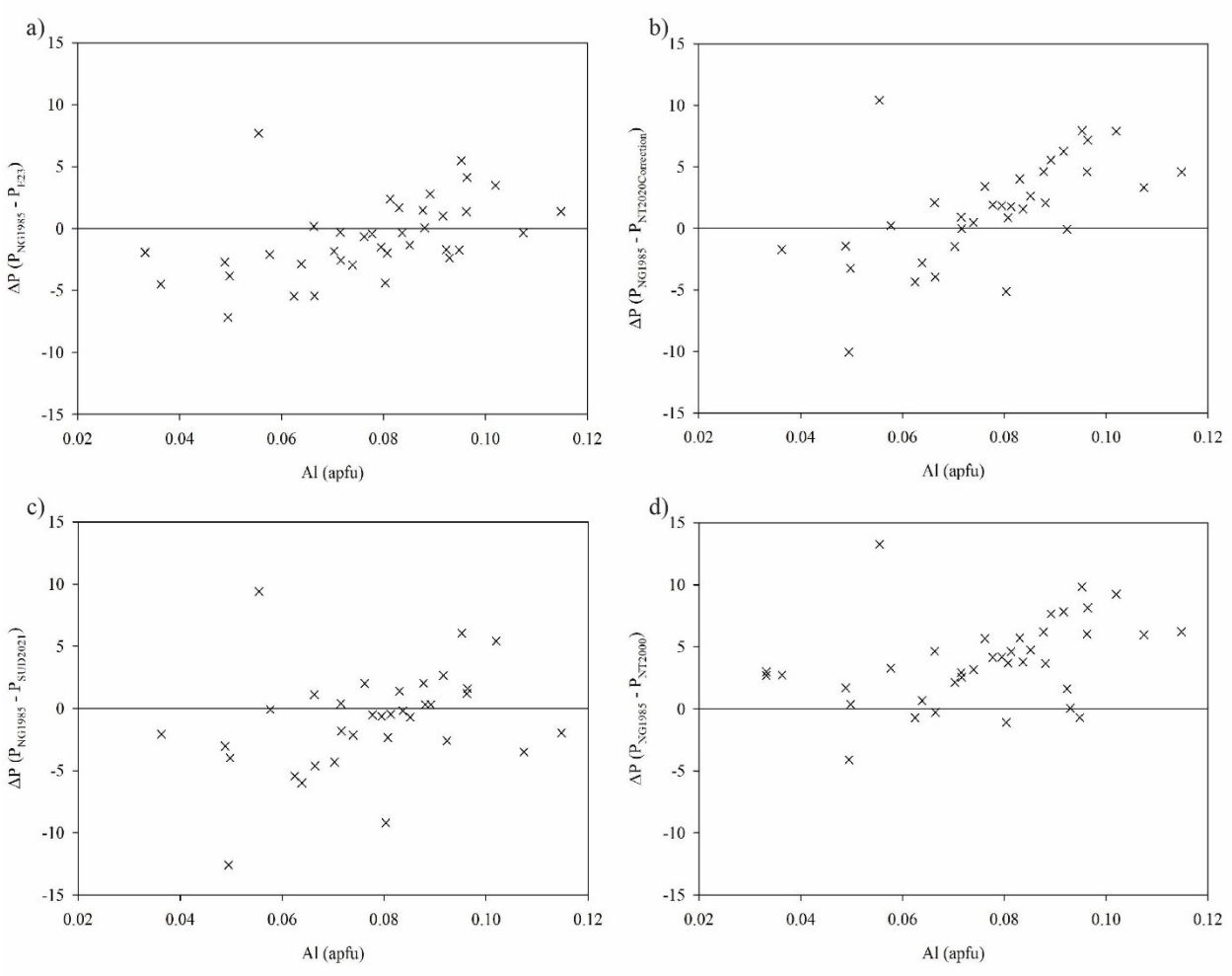

Figure 4.6 Comparison between P_{NG1985} – P of clinopyroxene barometers and the Al cations of clinopyroxene of xenolith samples from Finsch Diamond Mine

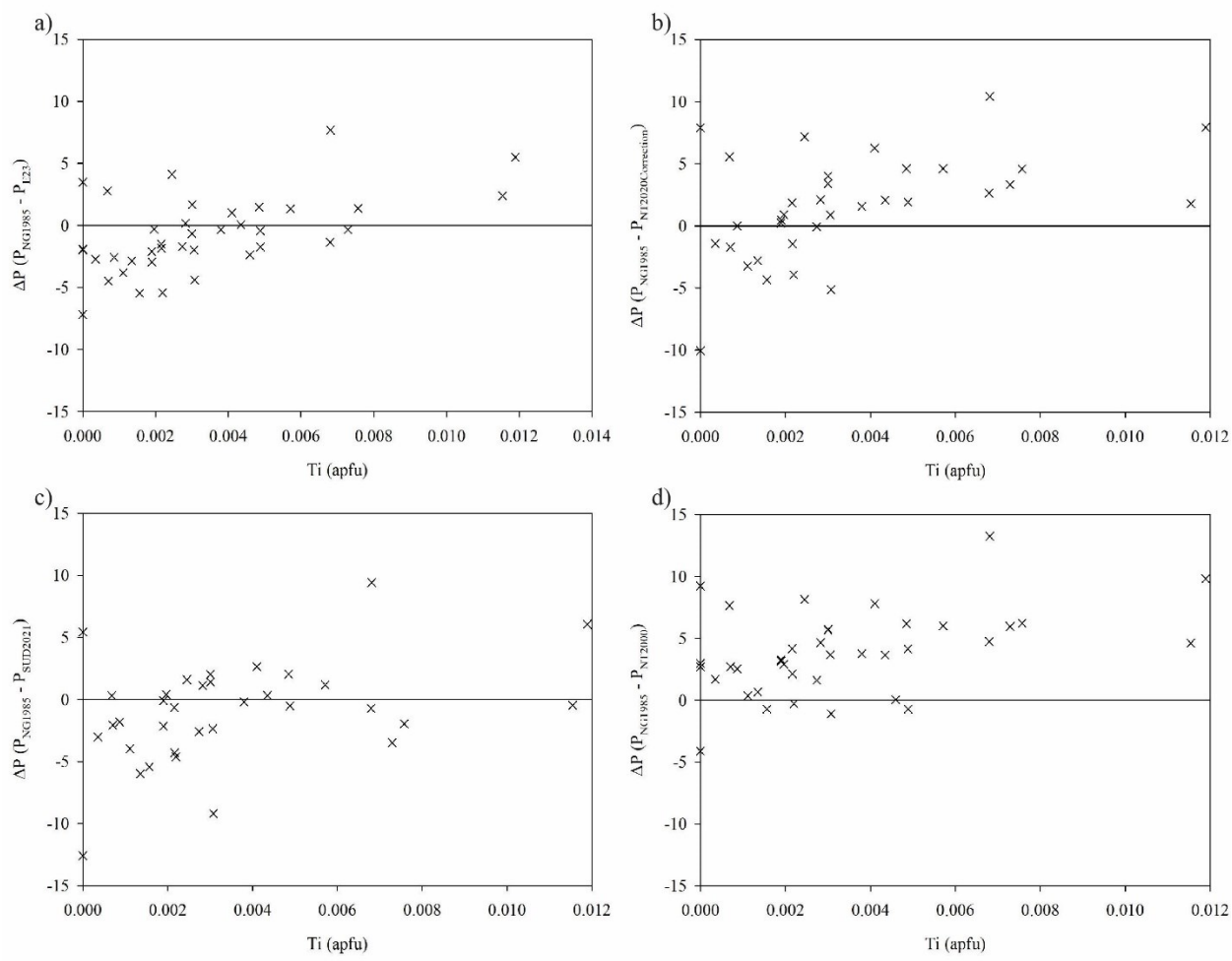

Figure 4.7 Comparison between P_{NG1985} – P of clinopyroxene barometers and the Ti cations of clinopyroxene of xenolith samples from Finsch Diamond Mine

4.5 Compositional Changes with Updated Geobarometer Calculated Pressure

The Al, Cr and Na contents of clinopyroxenes from Chidliak, Diavik-Ekati, Finsch and Jagersfontein garnet lherzolites decrease with increasing pressure with the updated geobarometer (Figure 4.7, 4.8, 4.9). This matches the relation between Al, Cr and Na cations with the previously discussed barometers where Al, Cr and Na decrease with increasing pressure with the previous clinopyroxene and Al-in-orthopyroxene barometers (Figures 2.8, 2.9, 2.10). This agrees with the previously discussed correlation of (Al+Cr):Na ratio of ~1, as Na and Al+Cr decrease sympathetically with increasing pressure and temperature (Figures 2.5, 2.6, 2.7).

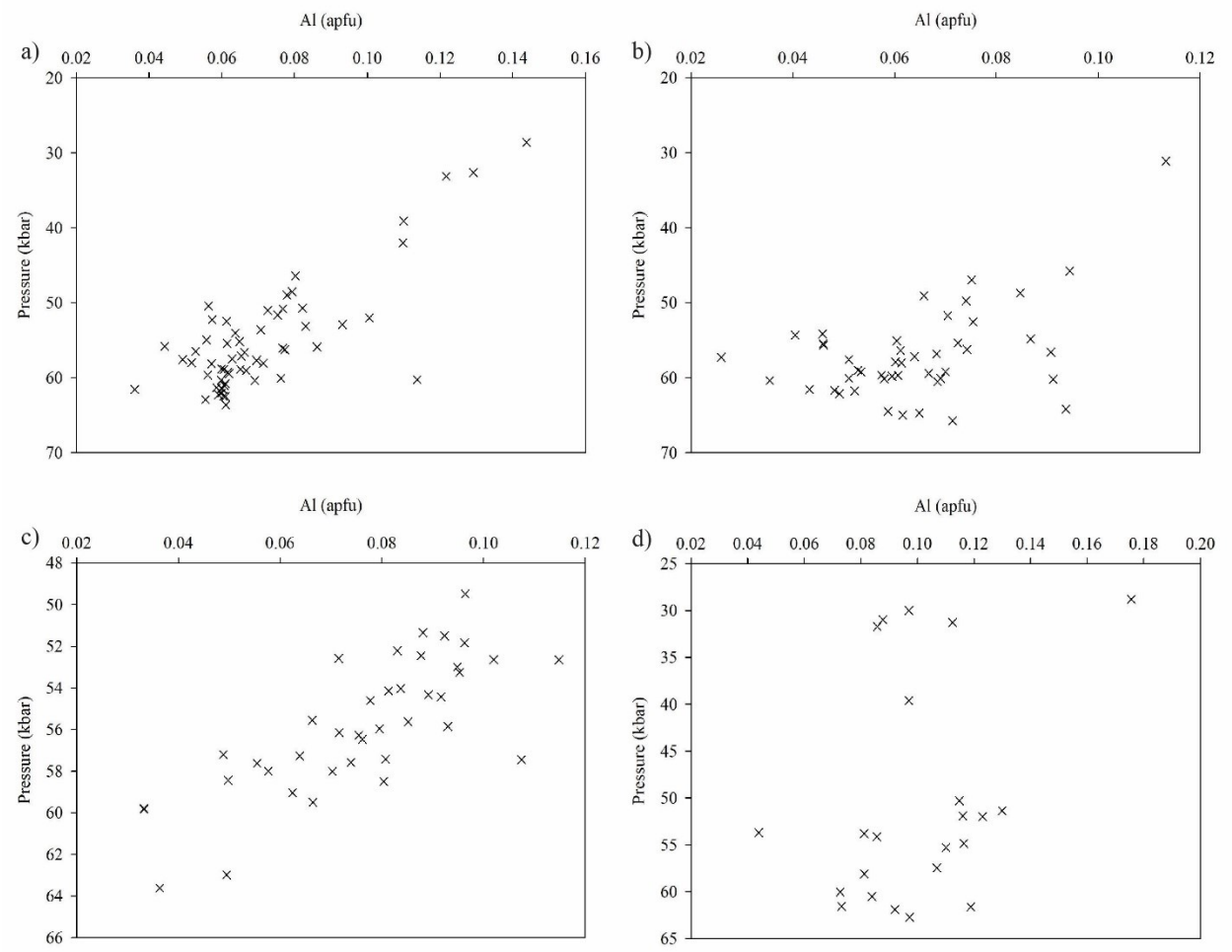

Figure 4.8 Al cations compared with pressure calculations from updated barometer from a) Chidliak kimberlite field, b) Diavik and Ekati kimberlites, c) Finsch Diamond Mine and d) Jagersfontein Diamond Mine

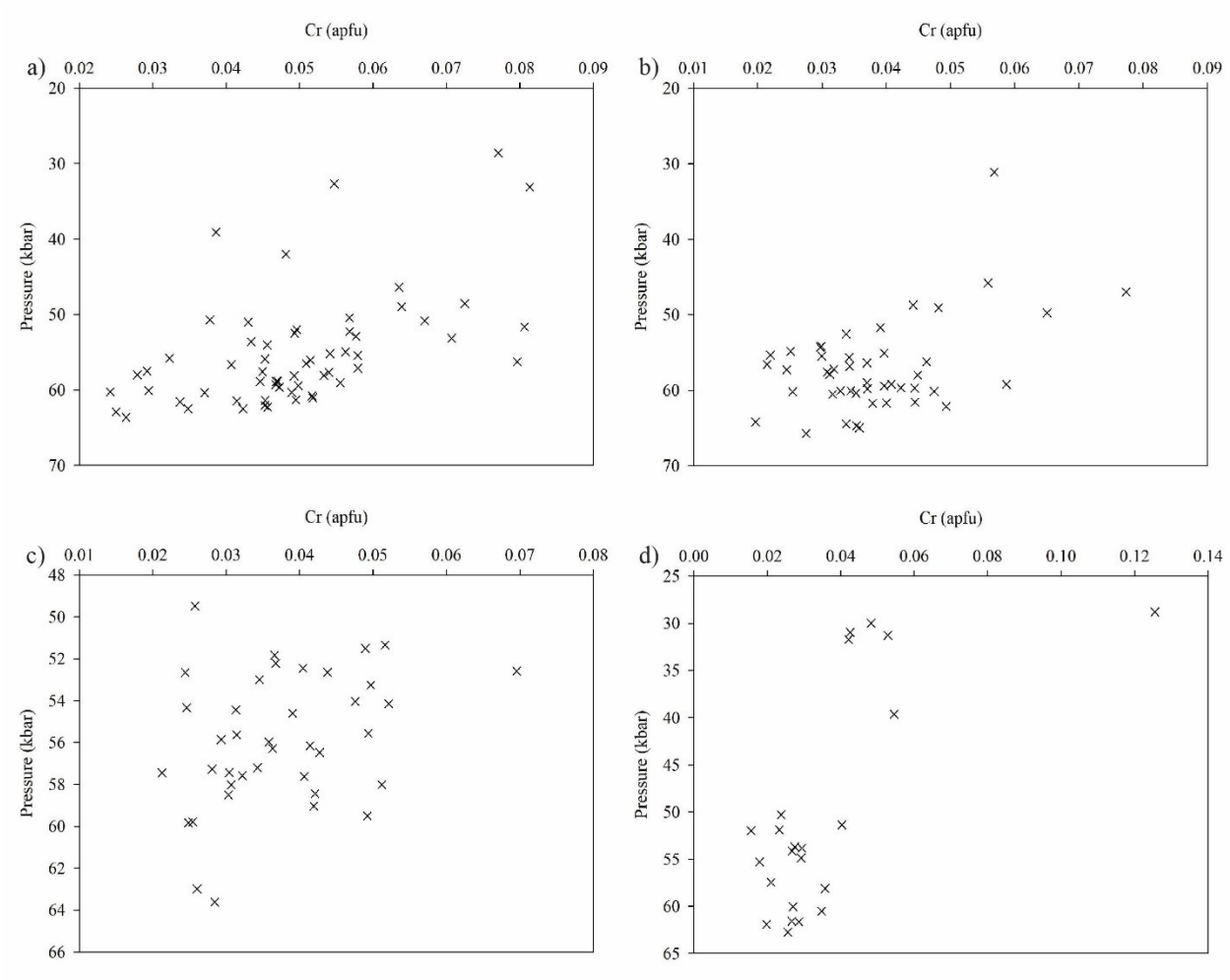

Figure 4.9 Cr cations compared with pressure calculations from updated barometer from a) Chidliak kimberlite field, b) Diavik and Ekati kimberlites, c) Finsch Diamond Mine and d) Jagersfontein Diamond Mine

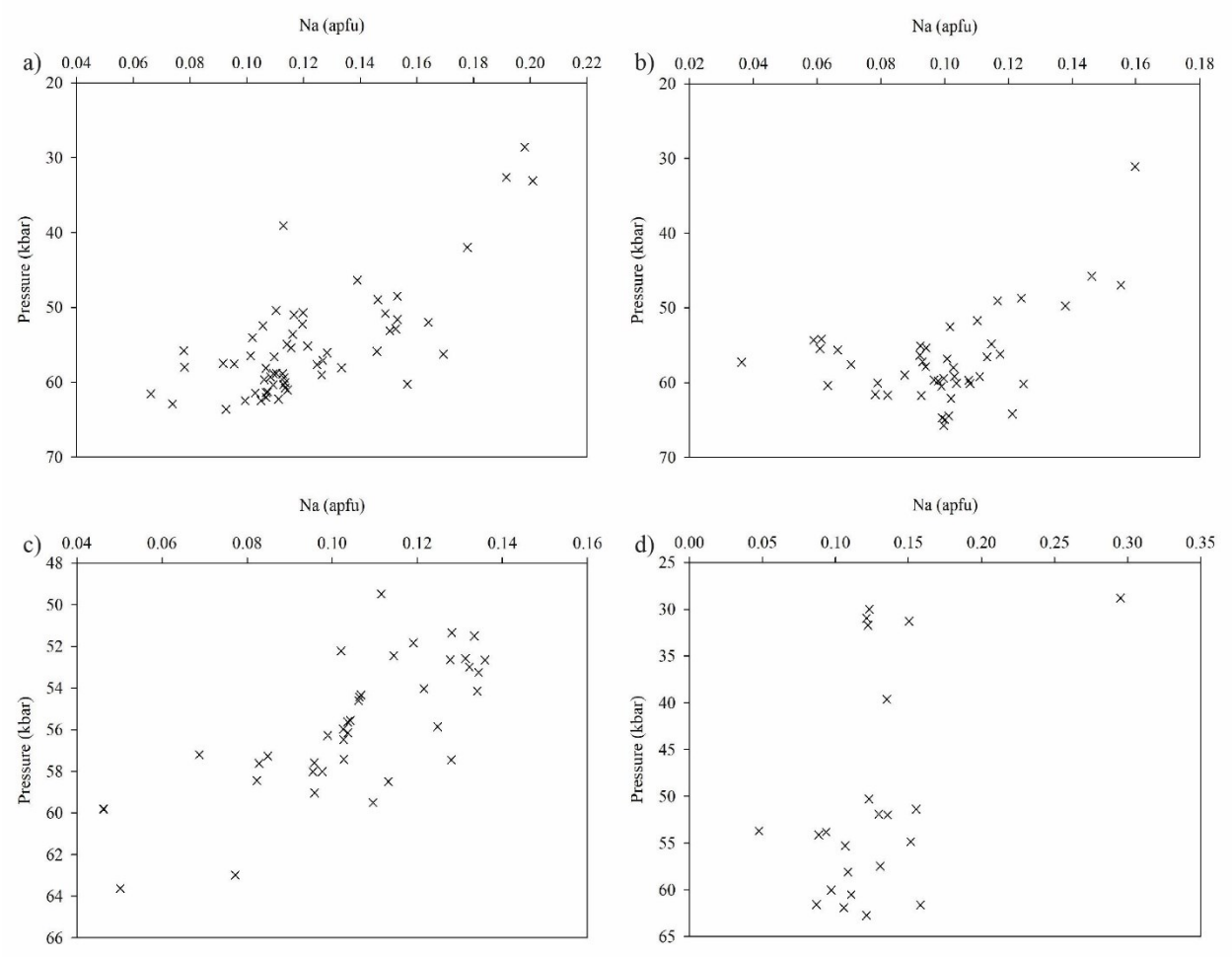

Figure 4.10 Na cations compared with pressure calculations from updated barometer from a) Chidliak kimberlite field, b) Diavik and Ekati kimberlites, c) Finsch Diamond Mine and d) Jagersfontein Diamond Mine

Ti is included in the Al_{M1} calculations used for the barometer ($Al_{M1} = Al - 0.5(Al + Cr + 2Ti - Na - K)$). Ti cations do not appear to be correlated with changes in pressure, contrasting with the behaviour of Al, Cr and Na (Figure 4.10). This may reflect the low abundance of Ti.

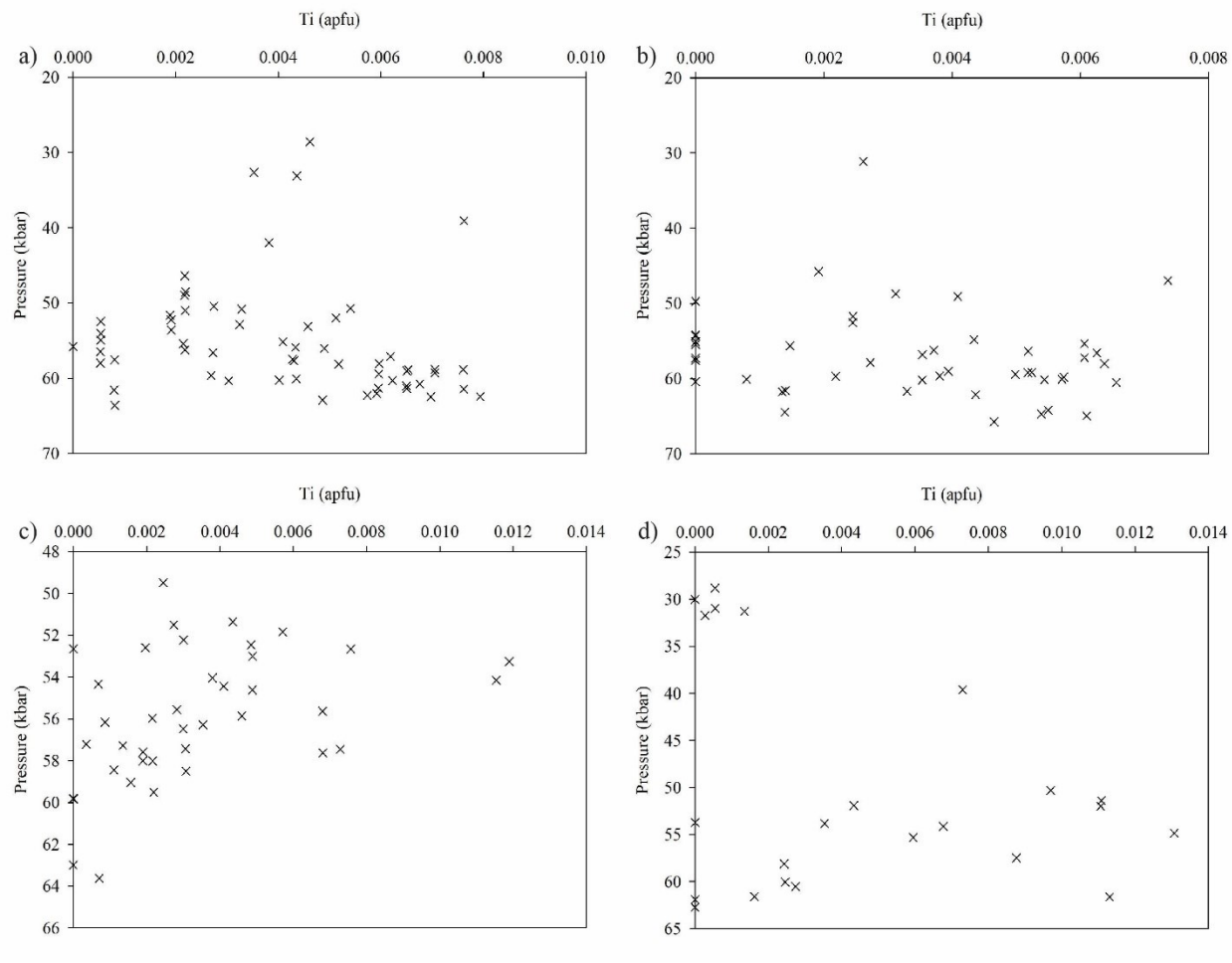

Figure 4.11 Ti cations compared with pressure calculations from updated barometer from a) Chidliak kimberlite field, b) Diavik and Ekati kimberlites, c) Finsch Diamond Mine and d) Jagersfontein Diamond Mine

4.6 Discussions and Conclusions

Our attempt to ground a barometer with thermodynamic data of THERMOCALC and simple nonideal activity models failed to produce a useable geobarometer. This is a result of either

endmember free energies or clinopyroxene solution models, or both, not being adequate to enable this approach to derive a geobarometer for natural garnet lherzolite data. As THERMOCALC evolves, we hope that this approach will be possible in the future.

A new geobarometer was produced by varying terms of the Nimis and Taylor (2000) geobarometric expression and calibrating this new geobarometer to temperatures and pressures calculated by the Taylor (1998) thermometer and pressure calculated from Nickel and Green's (1985), modified after Carswell and Gibb (1987), barometer, respectively. The update to the Nimis and Taylor (2000) barometer improved performance marginally and was in better agreement with the Al-in-orthopyroxene barometer of Nickel and Green (1985), modified after Carswell and Gibb (1987), barometer. The Nimis et al. (2020) correction to the Nimis and Taylor (2000) geobarometer was also found to be in good agreement with the Nickel and Green (1985) modified after Carswell and Gibb (1987), barometer. The Sudholz et al. (2021) barometer was found to overestimate when compared to the Nickel and Green (1985) modified after Carswell and Gibb (1987), barometer and the Nimis and Taylor (2000) barometer was found to underestimate when compared to the Nickel and Green (1985) modified after Carswell and Gibb (1987), barometer.

The different single grain clinopyroxene barometers were compared to the Nickel and Green (1985), modified after Carswell and Gibb (1987), barometer at four localities using P_{NG1985} – the pressure calculations of the single grain clinopyroxene barometers. The updated barometer performs the best for xenoliths from Finsch diamond mine, for the other three localities the barometer also performs well but is more comparable with the other single grain clinopyroxene barometers. This is mostly due to filtering of the single grain clinopyroxene and Al-in-orthopyroxene geobarometers and the basis of the single grain clinopyroxene barometers being

similar. This is noticeable with the biggest differences between the Nickel and Green (1985) and the single grain clinopyroxenes geobarometers because the maximum or minimum differences, with all the clinopyroxene geobarometers (ΔP) are consistently located in the same xenolith sample. Since the updated Sudholz et al. (2021) and Nimis et al. (2020) correction geobarometers are built upon the original Nimis and Taylor (2000) geobarometer, similar behaviours would be expected.

Chapter 5 Conclusions

The overarching goal of this thesis was to explore improving the single-mineral clinopyroxene geobarometer. This led to three objectives for this thesis; The first objective was to validate currently used classification schemes for identifying clinopyroxene from garnet lherzolites by applying these schemes to a database of clinopyroxene from natural garnet lherzolites. The chemistry of clinopyroxenes from natural garnet lherzolites was also compared to calculated experimental garnet lherzolite clinopyroxenes. The second objective was evaluating thermodynamically modelled clinopyroxene and comparing the modelled clinopyroxene to clinopyroxene from natural garnet lherzolites. Thirdly, a revised single grain clinopyroxene geobarometer was developed based on natural garnet lherzolite data. This barometer was developed with the goal of having better consistency between the single grain clinopyroxene barometer and the Al-in-orthopyroxene geobarometers.

5.1 Major-element chemistry of mantle garnet lherzolite clinopyroxenes

Exploration methods for diamonds often employ the geochemistry of single minerals to identify deposits. Clinopyroxene from garnet lherzolites are specifically sought after due to the association of garnet lherzolite with diamond-stable, higher pressure settings. The discrimination methods to identify clinopyroxenes from garnet lherzolites evaluated were Ramsay's (1992)

Cr_2O_3 vs. Al_2O_3 classification diagram, Nimis' (1998) MgO vs Al_2O_3 plot, the Al-Na-Cr ternary of Morris et al. (2002) and the Ca/(Ca+Mg+Fe) vs Al+Cr-Na-K plot of Grütter (2009). For the clinopyroxenes from garnet lherzolites in the database, the vast majority of the data falls within the garnet lherzolite fields of these classification plots. Therefore, these discrimination plots are robust and remain useful for identifying clinopyroxenes from garnet lherzolites.

When comparing natural garnet lherzolite clinopyroxenes with experimental garnet lherzolite clinopyroxenes, there is a clear disconnect between the two, in particular their contents of Al, Cr and Na. Experimental clinopyroxenes are a lot richer in Al and poorer in Cr and Na in comparison with natural clinopyroxenes. Essentially, the experimental clinopyroxenes are unrealistically biased towards high Al, and higher Al_T in particular, relative to natural clinopyroxenes. This shows there is considerable scope to be done experimentally on more representative clinopyroxene compositions.

5.2 Thermodynamic modelling of garnet lherzolites

Recent updates in the program THERMOCALC allows for the thermodynamic modelling of garnet lherzolites for a given bulk composition. Mineral chemistry, modal amounts, activities, and Gibbs free energies at specific temperatures and pressures are among the outputs of the THERMOCALC calculations. Of these outputs, the chemistry of the clinopyroxenes as functions of bulk compositions, pressure, and temperature are primary interest for this work. In summary, the chemistry of modelled clinopyroxenes did not appear to match well with natural garnet lherzolites. For example, many of the clinopyroxenes failed garnet lherzolite clinopyroxene discrimination plots used for natural samples. On the other hand, the cation trends with pressure and temperature follow the trends seen in natural samples. Modelled garnet lherzolites were also modelled along geotherms. The clinopyroxene from these geotherm modelled samples appeared

more like natural samples based on garnet lherzolite clinopyroxene discrimination methods. Most of the cations output by THERMOCALC on geotherm models agree with natural samples except for Al, which is a critical variable for geobarometry. THERMOCALC appears to be a useful tool to understand mantle garnet lherzolites but it does not match natural garnet lherzolites perfectly. Updates will still be needed for THERMOCALC to better match natural samples.

5.3 A revised single grain clinopyroxene geobarometer

An updated single grain clinopyroxene geobarometer was derived using natural garnet lherzolite data and a modified version of the Nimis and Taylor (2000) geobarometer, following an attempt to derive a barometer based on THERMOCALC thermodynamic data. This was calibrated through multiple linear regression of natural data using temperature calculated from Taylor's (1998) thermometer and pressure calculated from Nickel and Green's (1985), modified after Carswell and Gibb (1987), barometer as the correct temperature and pressure estimates (recommended thermometer and barometer of Nimis and Grütter 2010). The updated barometer had good agreement with the Nickel and Green (1985) barometer for the four localities used as examples. The Nimis et al. (2020) correction applied to the Nimis and Taylor (2000) barometer also has good agreement with the Nickel and Green (1985) barometer and gave similar results to the update barometer. The Sudholz et al. (2021) barometer tends to overestimate when compared to the Nickel and Green (1985) barometer as the average ΔP values ($\Delta P = P_{NG1985} - P_{SUD2021}$) for all four localities were negative and lower minimum values than the other clinopyroxene barometers.

5.4 Further work

The clear disconnect between Al, Cr and Na in experimental clinopyroxenes and natural garnet lherzolite clinopyroxenes suggests that extant experimental clinopyroxenes do not simulate

natural clinopyroxenes well. Given that Al, Cr and Na are key components of both the Nimis and Taylor (2000) and Sudholz et al. (2021) barometers. These cations need to be better constrained in future experimental work to natural cations, specifically with Na:(Al+Cr) having an ~1:1 ratio to better match natural samples. Such experiments will provide invaluable data to refine clinopyroxene based barometers.

References

Benisek A, Etzel K, Cemič L (2007) Thermodynamic mixing behavior of synthetic Ca-Tschermak–diopside pyroxene solid solutions: II. Heat of mixing and activity–composition relationships. Phys Chem Minerals 34, 747–755

Boyd FR (1973) A pyroxene geotherm. Geochimica et Cosmochimica Acta 37, 2533–2546

Brey GP, Bulatov VK, Girnis AV (2008a) Geobarometry for Peridotites: Experiments in Simple and Natural Systems from 6 to 10 GPa. Journal of Petrology 49, 3–24

Brey GP, Bulatov VK, Girnis AV, Lahaye Y (2008b). Experimental melting of carbonated peridotite at 6–10 GPa. Journal of Petrology 49, 797–821

Brey GP, Bulatov VK, Girnis AV (2009) Influence of water and fluorine on melting of carbonated peridotite at 6 and 10 GPa. Lithos 112, 249–259

Brey GP, Bulatov VK, Girnis AV (2011) Melting of K-rich carbonated peridotite at 6–10GPa and the stability of K-phases in the upper mantle. Chemical Geology 281, 333–342

Brey GP, Köhler T (1990) Geothermobarometry in Four-phase Lherzolites II. New Thermobarometers, and Practical Assessment of Existing Thermobarometers. Journal of Petrology 31, 1353–1378

Brey G, Köhler T, Nickel K (1990) Geothermobarometry in four-phase lherzolites I. Experimental results from 10 to 60 kb. Journal of Petrology 31, 1313–1352

Brey GP, Nickel KG, Kogarko L (1986) Garnet-pyroxene equilibria in the system CaO-MgO-Al_2O_3-SiO_2 (CMAS): prospects for simplified ('T-independent') lherzolite barometry and an eclogite-barometer. Contrib Mineral Petrol 92, 448–455

Cameron M, Papike JJ (1981). Structural and chemical variations in pyroxenes. American Mineralogist, 66, 1-50.

Canil D and O'Neill HSC (1996) Distribution of ferric iron in some upper mantle assemblages. J. Petrol. 37: 609–635

Carswell DA, Gibb FG (1987) Evaluation of mineral thermometers and barometers applicable to garnet lherzolite assemblages. Contrib Mineral Petrol 95, 499–511

Cohen RE, Burnham CW (1985) Energetics of ordering in aluminous pyroxenes. American Mineralogist, 70, 559-567

Cohen RE (1986) Thermodynamic solution properties of aluminous clinopyroxenes: Nonlinear least squares refinements. Geochim Cosmochim Acta, 50, 563–575

Connolly JAD (2005) Computation of phase equilibria by linear programming: A tool for geodynamic modeling and its application to subduction zone decarbonation. Earth and Planetary Science Letters 236, 524-541

De Capitani C, Petrakakis K (2010) The computation of equilibrium assemblage diagrams with Theriak/Domino software. American Mineralogist 95, 1006-1016

Gasparik T (1984) Two-pyroxene thermobarometry with new experimental data in the system CaO-MgO-Al_2O_3-SiO_2. Contrib Mineral Petrol 87, 87–97

Green ECR, Holland TJB, Powell R., White RW (2012a) Garnet and spinel lherzolite assemblages in MgO–Al_2O_3–SiO_2 and CaO–MgO–Al_2O_3–SiO_2: thermodynamic models and an experimental conflict. Journal of Metamorphic Geology 30, 561–577

Grütter HS (2009) Pyroxene xenocryst geotherms: Techniques and application. Lithos 112, 1167–1178

Harley SL (1984) The Solubility of Alumina in Orthopyroxene Coexisting with Garnet in FeO-MgO-Al_2O_3-SiO_2 and CaO-FeO-MgO-Al_2O_3-SiO_2. Journal of Petrology 25, 665–696

Hasterok D, Chapman DS (2011) Heat production and geotherms for the continental lithosphere. Earth and Planetary Science Letters, 307, 59–70

Holland TJB, Powell R (1996a) Thermodynamics of order–disorder in minerals: 1. Symmetric formalism applied to minerals of fixed composition. American Mineralogist, 81, 1413–1424

Holland TJB, Powell R (1996b) Thermodynamics of order–disorder in minerals: 2. Symmetric formalism applied to solid solutions. American Mineralogist, 81, 1425–1437

Holland TJB, Green ECR, Powell R (2018) Melting of Peridotites through to Granites: A Simple Thermodynamic Model in the System KNCFMASHTOCr. Journal of Petrology 59, 881–900

Jennings ES, Holland TJB (2015) A Simple Thermodynamic Model for Melting of Peridotite in the System NCFMASOCr. Journal of Petrology 56, 869–892

Krogh EJ (1988) The garnet-clinopyroxene Fe-Mg geothermometer – a reinterpretation of existing experimental data. Contrib Mineral Petrol 99, 44–48

Lindsley DH (1983) Pyroxene thermometry. American Mineralogist 68 : 477–493

Mather KA, Pearson DG, McKenzie D, Kjarsgaard BA, Priestley K (2011) Constraints on the depth and thermal history of cratonic lithosphere from peridotite xenoliths, xenocrysts and seismology. Lithos 125(1–2): 729–742

Miller WGR, Holland TJB, Gibson SA, (2016) Garnet and Spinel Oxybarometers: New Internally Consistent Multi-equilibria Models with Applications to the Oxidation State of the Lithospheric Mantle. J. Petrology 57, 1199–1222

Morimoto N (1988) Nomenclature of pyroxenes. In: Bulletin de Minéralogie, volume 111, 5, 535-550

Morris TF, Sage RP, Ayer JA, Crabtree DC (2002) A study in clinopyroxene composition: implications for kimberlite exploration. Geochemistry: Exploration, Environment, Analysis 2, 321–331

Nickel KG, Brey GP, Kogarko L (1985) Orthopyroxene-clinopyroxene equilibria in the system CaO-MgO-Al_2O_3-SiO_2: implications for two-pyroxene thermometry. Contrib Mineral Petrol 91, 44–53

Nickel KG, Green DH (1985) Empirical geothermobarometry for garnet peridotites and implications for the nature of the lithosphere, kimberlites and diamonds. Earth and Planetary Science Letters 73, 158–170

Nimis P (1998) Evaluation of diamond potential from the composition of peridotitic chromian diopside. Eur. J. Mineral. 10, 505–520

Nimis P (2002) The pressures and temperatures of formation of diamond based on thermobarometry of chromian diopside inclusions. The Canadian Mineralogist 40, 871–884

Nimis P, Grütter H (2010) Internally consistent geothermometers for garnet peridotites and pyroxenites. Contrib Mineral Petrol 159, 411–427

Nimis P, Preston R, Perritt SH, Chinn IL (2020) Diamond's depth distribution systematics. Lithos 376:105729

Nimis P, Taylor WR (2000) Single-clinopyroxene thermobarometry for garnet peridotites. Part I. Calibration and testing of a Cr-in-Cpx barometer and an enstatite-in-Cpx thermometer. Contrib Mineral Petrol 139, 541–554

O'Neill HStC, Wood BJ (1979) An experimental study of Fe-Mg partitioning between garnet and olivine and its calibration as a geothermometer. Contrib Mineral Petrol 70, 59–70

Pearson DG, Canil D, Shirey SB (2014) Mantle Samples Included in Volcanic Rocks, in: Treatise on Geochemistry. Elsevier, pp. 169–253

Perkins D, Newton RC (1981) The compositions of coexisting pyroxenes and garnet in the system CaO-MgO-Al_2O_3-SiO_2 at 900°–1,100°C and high pressures. Contrib Mineral Petrol 75, 291–30

Powell R, Holland TJB (1988) An internally consistent thermodynamic dataset with uncertainties and correlations: 3: application methods, worked examples and a computer program. Journal of Metamorphic Geology, 6, 173–204

Ramsay RR (1992) Geochemistry of diamond indicator minerals. PhD Thesis, University of Western Australia, Perth

Ramsay RR, Tompkins LA (1994) The geology, heavy mineral concentrate mineralogy, and diamond propectivity of the Boa Esperanca and Cana Verde pipes, Corrego D'anta, Minas Gerais, Brasil. In Fifth International Kimberlite Conference, Minas Gerais, Brazil (Vol. 1B, pp. 329-345). Minas Gerais, Brazil: Companhia de Pesquisa de Recursos Minerais, Special Publication

Read G, Grütter H, Winter S, Luckman N, Gaunt F, Thomsen F (2004) Stratigraphic relations, kimberlite emplacement and lithospheric thermal evolution, Quiricó Basin, Minas Gerais State, Brazil. Lithos 77, 803–818

Sudholz ZJ, Yaxley GM, Jaques AL, Brey GP (2021) Experimental recalibration of the Cr-in-clinopyroxene geobarometer: improved precision and reliability above 4.5 GPa. Contributions to Mineralogy and Petrology 176, 11

Takahashi E (1986) Melting of a Dry Peridotite KLB-1 up to 14 GPa: Implications on the Origin of Peridotitic Upper Mantle. Journal of Geophysical Research: Solid Earth 91, 9367–9382.

Taylor WR (1998) An experimental test of some geothermometer and geobarometer formulations for upper mantle peridotites with application to the thermobarometry of fertile lherzolite and garnet websterite. N Jahrb Mineral Abh 172, 381–408

Tomlinson EL, Holland TJB (2021) A Thermodynamic Model for the Subsolidus Evolution and Melting of Peridotite. Journal of Petrology 62, egab012

Walter MJ (1998) Melting of Garnet Peridotite and the Origin of Komatiite and Depleted Lithosphere. Journal of Petrology 39, 29-60

Woodland AB (2009) Ferric iron contents of clinopyroxene from cratonic mantle and partitioning behaviour with garnet. Lithos 112, 1143–1149

Woodland AB, Peltonen P (1999) Ferric iron contents of garnet and clinopyroxene and estimated oxygen fugacities of peridotite xenoliths from the Eastern Finland Kimberlite Province. In: Gurney, J.J., Gurney, J.M., Pasco, M.D., Richardson, S.H. (Eds.), Proceedings of the 7th Kimberlite Conference, Redroof Publishers, Cape Town, S.A., pp. 904–911

Workman RK, Hart SR (2005) Major and trace element composition of the depleted MORB mantle (DMM). Earth and Planetary Science Letters 231, 53–72

Yaxley GM (2000) Experimental study of the phase and melting relations of homogeneous basalt + peridotite mixtures and implications for the petrogenesis of flood basalts. Contributions to Mineralogy and Petrology 139, 326–338

Ziberna L, Nimis P, Kuzmin D, Malkovets VG (2016) Error sources in single-clinopyroxene thermobarometry and a mantle geotherm for the Novinka kimberlite, Yakutia. American Mineralogist 101, 2222–2232

Appendix A

The complete datasets used for Chapters 2, 3 and 4 are available through the University of Alberta UAL Dataverse as “CG Elzinga MSc thesis 2023 Supplementary Online Dataset” (https://doi.org/10.5683/SP3/RTTCPS)

Appendix B

THERMOCALC workflow example for KR4003 Bulk Composition Mineral compositions:

To use the THERMOCALC program a specific set of files need to initially be prepared. This includes a dataset file, with the most recent dataset update coming from Tomlinson and Holland (2021), represented by the file *tc-ds634*. The next step is to set up the *tc-prefs* file which is used to set the script file and script dataset, along with selecting which calcmode you want THERMOCALC to run. Calcmode is separated into calcmode 0, 1, 2 and 3 with the numbers representing a calculation preformed by THERMOCALC. These calculations are:

Calcmode 0 = Thermodynamic data listings

Calcmode 1 = Phase equilibrium calculations with solid solutions

Calcmode 2 = avPT calculations

Calcmode 3 = Phase equilibrium calculations without solid solutions

For this example, Calcmode 1 will be used as this provides mineral compositions. Once the *tc-prefs* file is set the next step is to open the scriptfile and set the axfile (the axfile is downloaded from the THERMOCALC website). The bulk composition used by THERMOCALC is set in the scriptfile. After that choose if you want to create a pseudosection and print guess form and bulk information. The next step is choosing what phases to use in the scriptfile calculation and choosing the bounds of the diagram for the pseudosection.

THERMOCALC can now be run with the phases and the PT range and increments chosen by the user (For a garnet lherzolite example the phases would be garnet, olivine, clinopyroxene and orthopyroxene). Once the phases and PT ranges and increments are chosen by the user,

THERMOCALC will output four files which are *tc-<projectname>-dr*, *tc-<projectname>-ic*, *tc-<projectname>-it* and *tc-<projectname>-o*. The *dr* file is used for drawing pseudosections, while the *ic*, *it* and *o* files are related to the calculated chemistry and activities of the mineral phases in the model. The *it* file provides the "HPx-eos" used in the calculation. This includes the cation allocation for the endmembers of the chosen phases, the formulas for endmember proportion calculations, ideal mixing activities, non-ideality interaction parameters and how to "make" endmembers that are not output by THERMOCALC. The *o* file is a record of the THERMOCALC on-screen output and user commands.

The *ic* file is the important file for the mineral chemistry of the chosen phases at a given pressure and temperature, as this is where THERMOCALC outputs the 'oxide compositions' which can be used to calculate weight percentage and cation amounts. This file also has the site fractions, modal amounts of the phases, endmember activities for the phases, thermodynamic properties for phases and the system are also output by THERMOCALC into this file.

All this information is available on the Hpx-eos and THERMOCALC website (https://hpxeosandthermocalc.org/ as of May, 2023).

Appendix C

Example of THERMOCALC thermobarometer comparisons for modelled garnet lherzolites projected on 40 mW/m^2 geotherm using THERMOCALC T and P: 1500°C and 69.4 kbar (was restricted to this PT as the other THERMOCALC PT combinations gave errors on the single grain clinopyroxene barometers due to clinopyroxene compositions):

Table C.1 Geothermobarometer results from modelled garnet lherzolites projected onto 40 mW/m^2. The original THERMOCALC input temperature and pressure were 1500°C and 69.4 kbar, respectively. None of the geothermobarometer combinations correctly calculate the THERMOCALC temperature and pressure. This is likely a result of the modelled mineral chemistry not matching natural mineral chemistry as seen with the failure of the Grütter (2009) and Ziberna et al. (2016) filters

	THERMOCALC	NT2000	SUD2021	NG1985/TA1998	BK1990
KLB-1	69.4 kbar, 1500°C	149.6 kbar, 1696°C	217.7 kbar, 1877°C	104.6 kbar, 1622°C	98.7 kbar, 1542°C
KR4003	69.4 kbar, 1500°C	97.7 kbar, 1582°C	135.9 kbar, 1685°C	95.8 kbar, 1612°C	165.2 kbar, 1736°C
Depleted Mantle	69.4 kbar, 1500°C	88.9 kbar, 1531°C	118.3 kbar, 1610°C	74.7 kbar, 1495°C	130.6 kbar, 1665°C
Grütter (2009) Filter		Failed	Failed	Failed	Failed
Ziberna (2016) Filter		Failed	Failed	Failed	Failed

Example of THERMOCALC thermobarometer comparisons for modelled garnet lherzolites projected on 45 mW/m^2 geotherm using THERMOCALC T and P: 1500°C and 55 kbar (was restricted to this PT as the other THERMOCALC PT combinations gave errors on the single grain clinopyroxene barometers due to clinopyroxene compositions):

Table C.2 Geothermobarometer results from modelled garnet lherzolites projected onto 45 mW/m^2. The original THERMOCALC input temperature and pressure were 1500°C and 55 kbar, respectively. The NG1985/Taylor appears to gives calculated results similar to the THERMOCALC PT. The other geothermobarometer combinations are not close to the THERMOCALC PT. This is likely a result of the modelled mineral chemistry not matching natural mineral chemistry as seen with the failure of the Grütter (2009) and Ziberna et al. (2016) filters

	THERMOCALC	NT2000	SUD2021	NG1985/TA1998	BK1990
KLB-1	55 kbar, 1500°C	74.6 kbar, 1531°C	100.6 kbar, 1602°C	57.1 kbar, 1459°C	66.0 kbar, 1561°C
KR4003	55 kbar, 1500°C	65.7 kbar, 1526°C	88.5 kbar, 1589°C	56.2 kbar, 1474°C	63.9 kbar, 1521°C
Depleted Mantle	55 kbar, 1500°C	62.3 kbar, 1493°C	79.6 kbar, 1540°C	52.0 kbar, 1436°C	60.4 kbar, 1481°C
Grütter (2009) Filter		Failed	Failed	Failed	Failed
Ziberna (2016) Filter		Failed	Failed	Failed	Failed

Appendix D

Calculations for THERMOCALC derived failed single grain geobarometer for the reaction:

$Mg_3Al_2Si_3O_{12}$ (pyrope) + 2 $NaCrSi_2O_6$ (kosmochlor) = $Mg_3Cr_2Si_3O_{12}$ (knorringite) + 2 $NaAlSi_2O_6$ (jadeite)

Miller et al. (2016) formula:

$\Delta G = a + bT + cP + dT^2 + eP^2 + fPT$

With a, b, c, d, e and f being constants derived form THERMOCALC

a = 22.7789

b = - 0.00329024

c = - 0.113765

d = 4.27336E-07

e = - 0.000448803

f = 0.0000155064

Equilibrium expression formula:

$\Delta G° = -RT\ln K$

lnK can be represented by the formula:

$\ln K = \ln(Cr/Al)^{garnet} - \ln(Cr/Al_{M1})^{cpx} + \ln(\gamma_{knor})^{gt} - \ln(\gamma_{py})^{gt} + 2\ln(\gamma_{jd})^{cpx} - 2\ln(\gamma_{kos})^{cpx}$

$\ln(Cr/Al)^{garnet}$ and $\ln(Cr/Al_{M1})^{cpx}$ were found to be correlated in natural samples and a formula can be derived through multiple linear regression to represent this correlation. The formula calculated was:

$\ln(Cr/Al)^{garnet} = 1.1114 \ln(Cr/Al_{M1})^{cpx} - 9.08\ Ca/(Ca+Mg+Fe) + 2.2835(Ca+Na+K) + 17.028P/T$

with an R2 value of 0.975

The lnK formula now becomes:

$\ln K = 0.1114 \ln(Cr/Al_{M1})^{cpx} - 9.08\ Ca/(Ca+Mg+Fe) + 2.2835(Ca+Na+K) + 17.028P/T + \ln(\gamma_{knor})^{gt} - \ln(\gamma_{py})^{gt} + 2\ln(\gamma_{jd})^{cpx} - 2\ln(\gamma_{kos})^{cpx}$

For the non-ideality terms $\ln(\gamma_{knor})^{gt}$, $\ln(\gamma_{py})^{gt}$, $2\ln(\gamma_{jd})^{cpx}$ and $2\ln(\gamma_{kos})^{cpx}$ the garnet endmembers ($\ln(\gamma_{knor})^{gt}$ and $\ln(\gamma_{py})^{gt}$) are assumed to be 1. This gives a value of zero ($\ln(1) = 0$) as this is a single grain clinopyroxene geobarometer.

The clinopyroxene endmembers can be calculated using the interaction energies (Table D.1) and endmember proportion formulas (Table D.2) from THERMOCALC. Since THERMOCALC does not output kosmochlor data the Al and Cr bearing endmembers output by THERMOCALC need to be used. This can be resolved using the reaction:

$NaAlSi_2O_6$ (jadeite) + $CaCrAlSiO_6$ (Cr-diopside) = $NaCrSi_2O_6$ (kosmochlor) + $CaAlAlSiO_6$ (Ca-tschermak)

$RT \ln a_{kos} - RT \ln a_{jd} = RT \ln a_{crdi} - RT \ln a_{cats} - \Delta G_R$ with $-\Delta G_R = 4.9$ kJ

(The assumption that this ΔG_R is independent of pressure and temperature may be part of why our attempt at geobarometry failed)

So, the Cr-diopside and Ca-tschermak endmembers output by THERMOCALC can be used.

Table D.1 Interaction parameters for clinopyroxene from THERMOCALC

$W_{1,2}$	$W_{crdi,cats}$	2
$W_{1,3}$	$W_{crdi,di}$	8
$W_{1,4}$	$W_{crdi,cfs}$	38.3
$W_{1,5}$	$W_{crdi,cess}$	2
$W_{1,6}$	$W_{crdi,cbuf}$	6
$W_{1,7}$	$W_{crdi,cen}$	52.3
$W_{1,8}$	$W_{crdi,cfm}$	40.3
$W_{1,9}$	$W_{crdi,jd}$	3
$W_{1,10}$	$W_{crdi,kjd}$	3
$W_{2,3}$	$W_{cats,di}$	13 – 0.06 P
$W_{2,4}$	$W_{cats,cfs}$	25 – 0.1 P
$W_{2,5}$	$W_{cats,cess}$	2
$W_{2,6}$	$W_{cats,cbuf}$	6
$W_{2,7}$	$W_{cats,cen}$	45.2 – 0.35 P
$W_{2,8}$	$W_{cats,cfm}$	27 – 0.1 P
$W_{2,9}$	$W_{cats,jd}$	6
$W_{2,10}$	$W_{cats,kjd}$	6
For the $RT \ln \gamma_{crdi} - RT \ln \gamma_{cats}$ *expression:*		
$W_{1,2}$	$W_{crdi,cats}$	2
$W_{1,3} - W_{2,3}$	$W_{crdi,di} - W_{cats,di}$	–5 + 0.06 P
$W_{1,4} - W_{2,4}$	$W_{crdi,cfs} - W_{cats,cfs}$	13.3 + 0.1 P
$W_{1,5} - W_{2,5}$	$W_{crdi,cess} - W_{cats,cess}$	0
$W_{1,6} - W_{2,6}$	$W_{crdi,cbuf} - W_{cats,cbuf}$	0
$W_{1,7} - W_{2,7}$	$W_{crdi,cen} - W_{cats,cen}$	7.1 + 0.35 P
$W_{1,8} - W_{2,8}$	$W_{crdi,cfm} - W_{cats,cfm}$	13.3 + 0.1 P
$W_{1,9} - W_{2,9}$	$W_{crdi,jd} - W_{cats,jd}$	-3
$W_{1,10} - W_{2,10}$	$W_{crdi,kjd} - W_{cats,kjd}$	-3

Table D.2 Expressions for endmember proportion in terms of cations/formula unit, modified from THERMOCALC

p_1	p_{crdi}	Cr
p_2	p_{cats}	0.5*(Al – Na – K – Cr – Fe^{3+} – 2 Ti)
p_3	p_{di}	Ca – 0.5*(Al + Cr + Fe^{3+} + 2Ti – Na – K)
p_4	p_{cfs}	[Fe/(Fe + Mg)][1 – 0.5*(K + Na + Al + Cr + Fe^{3+})]
p_5	p_{cess}	Fe^{3+}
p_6	p_{cbuf}	2 Ti
p_7	p_{cen}	[1 – Ca – Na – K][Mg/(Fe + Mg)]
p_8	p_{cfm}	[Fe/(Fe + Mg)][0.5*(Al + Cr + Fe^{3+} – Na – K) – Ca]
p_9	p_{jd}	Na
p_{10}	p_{kjd}	K

Using the cats and crdi endmembers from THERMOCALC we can calculate the non-ideal terms as:

$2(p_{cats} - p_{crdi}) + p_{di}(-5 + 0.06\ P) + p_{cfs}(13.3 + 0.1\ P) + p_{cen}(7.1 + 0.35\ P) + p_{cfm}(13.3 + 0.1\ P) - 3(p_{jd} + p_{kjd})$

The lnK formula is now:

$\ln K = 0.1114\ \ln(Cr/Al_{M1})^{cpx} - 9.08\ Ca/(Ca+Mg+Fe) + 2.2835(Ca+Na+K) + 17.028P/T) + 2(p_{cats} - p_{crdi}) + p_{di}(-5 + 0.06\ P) + p_{cfs}(13.3 + 0.1\ P) + p_{cen}(7.1 + 0.35\ P) + p_{cfm}(13.3 + 0.1\ P) - 3(p_{jd} + p_{kjd})$

substituting in the Miller et al. (2016) formula the equation becomes:

$a + bT + cP + dT^2 + eP^2 + fPT = -RT\ln K$

Rearrange the formula to solve for zero.

$a + bT + cP + dT^2 + eP^2 + fPT + RT\ln K = 0$

Substituting in all the known values gives the formula:

$0 = 22.7789 + -0.00329024*T + - 0.113765*P + 4.27336E\text{-}07*T^2 + -0.000448803*P^2 + 0.0000155064*PT + RT[0.1114\ \ln(Cr/Al_{M1})^{cpx} - 9.08\ Ca/(Ca+Mg+Fe) + 2.2835(Ca+Na+K) + 17.028P/T) + 2(p_{cats} - p_{crdi}) + p_{di}(-5 + 0.06\ P) + p_{cfs}(13.3 + 0.1\ P) + p_{cen}(7.1 + 0.35\ P) + p_{cfm}(13.3 + 0.1\ P) - 3(p_{jd} + p_{kjd})]$

Using the quadratic equation pressure can be solved for. The general form of the quadratic equation is:

$ax^2 + bx + c = 0$

$$x = \frac{-b \pm \sqrt{b^2 - 4ac}}{2a}$$

with x being equal to pressure. For the other variables a, b and c those are equal to:

$a = -4.48803E\text{-}4$

$b = -0.00329024*T - 0.113765 + 17.028R + RT[0.06p_{di} + 0.1p_{cfs} + 0.35p_{cen} + 0.1p_{cfm}]$

$c = 22.7789 + -0.00329024*T + 4.27336E\text{-}07*T^2 + RT[0.1114 \ln(Cr/Al_{M1})^{cpx} - 9.08 Ca/(Ca+Mg+Fe) + 2.2835(Ca+Na+K) + 2(p_{cats} - p_{crdi}) - 5p_{di} + 13.3p_{cfs} + 7.1p_{cen} + 13.3p_{cfm} - 3(p_{jd} + p_{kjd})$